Alma Mater Studiorum – Università di Bologna

DOTTORATO DI RICERCA IN

MECCANICA E
SCIENZE AVANZATE DELL'INGEGNERIA

Ciclo XXXII

Settore Concorsuale: 09/G2

Settore Scientifico disciplinare: ING-IND/34 BIOINGEGNERIA INDUSTRIALE

DEVELOPMENT AND APPLICATION OF METHODS FOR THE BIOMECHANICAL CHARACTERIZATION OF SPINE LIGAMENTS AND INTERVERTEBRAL DISCS

Presentata da: **Maria Luisa Ruspi**

Coordinatore Dottorato

Marco Carricato

Supervisore

Luca Cristofolini

Esame finale anno 2020

A chi non si è mai arreso
e a chi non ha mai smesso
di sognare

Toti

Abstract

In the last century, technology had a great evolution with a speed that can equal or even exceed the progress made over millions of years in the "Homo" story. At the same time the way of life of the population has radically changed, resulting in a style typical of "*Homo Sedentarius*". Excessive use of the car, the increase of technology (elevators, escalators, appliances, remote control, cordless phone), too many hours in front of the television or computer reduced time spent in outdoor activities. This lifestyle and the increase in human longevity has led to an increase in health problems and consequently to have an increasing need for knowledge of the human body to improve health care.

The spine is one of the major organs subject to trauma or genetic problems. Today 30% of people suffer from back pain. Every day a large number of surgical interventions on the spine are performed to treat those patients with severe spinal deformities (about 50,000 a year in Italy), such as scoliosis or kyphosis. From a statistical analysis, the percentage of failures for this type of interventions is around 25-30%.

In literature there are many studies which investigate the biomechanics of the spine from different points of view. *In vivo* tests allow the analysis of the movement considering the human motion in its complex when a patient or a healthy subject is performing different daily motor tasks (such as walking, walking up/down stairs, standing to sitting position, …). In silico tests are useful to simulate different loading scenarios and pathologies analyzing how the spine acts under the influence of forces and moments. *In vitro* tests allow measuring the stiffness and range of motion of spine and allow the test of new spinal devices investigating what happen: at tissue-level to elucidate the rheological properties, at organ-level to study the structural properties and at spinal level to investigate the biomechanical function.

The aim of my PhD thesis was the improvement of the knowledge of the strain distribution on biological tissues, in particular on ligaments and intervertebral discs of the human spine in the healthy conditions. The results obtained could help clinicians to develop new surgical procedures and the development of new prosthesis devices.

The first part of this thesis was the improvement of the methodologies used to measure the strain distribution, simultaneously on hard tissues (vertebrae) and soft tissues (ligaments and intervertebral discs), by the use of Digital Image Correlation (DIC). In this way the interaction between different tissues of the spine can be analyzed in detail simulating real load conditions.

The second part of the research was to study in deep the biomechanical behaviour of the intervertebral discs and of the different ligaments on untreated and treated spine. The disc acts as a shock absorber for the spine, reducing shocks and impacts. The disc tends to stiffen as the loading rate increases but the loading rate does not affect the way the disc is deformed.

The supraspinous and interspinous ligament were studied analysing how they were deformed under different loading conditions. These ligaments limited the movement of the spine during flexion

reducing in this way the overload on the intervertebral disc; conversely these ligaments did not give significant mechanical resistance during extension and lateral bending.

Another ligament which was investigated in depth was the anterior longitudinal ligament. This ligament limited mainly the extension of the spine reducing the range of motion of the column; during flexion the ligament limited also the bulging of the disc. The anterior longitudinal ligament did not offer great mechanical strength during lateral bending and axial torsion. Furthermore, the anterior longitudinal ligament, unlike other ligaments (such as the ligament of the knee or of the ankle) does not intervene limiting the movement only when large range of motion are reached by the joint, but intervenes immediately by offering mechanical resistance to the column mainly during flexion and extension.

Summarizing, the study underlines the necessity of using a full-field strain analysis to enhance the knowledge of the biomechanics of the spine and the interaction between different types of tissue. Furthermore, the results reported in this thesis could be useful also to build better multibody spine models and to include more realistic properties in finite element models. These results could be a starting point for future works in which the effect of different surgical procedures and the use of new surgical devices could be investigated.

Summary

Chapter 1

Background

1.1 Biomechanical function of the spine

The spine is one of the most complex parts of the skeleton.[1, 2] The principal function of the spine is to support and maintain the upright position of the body during the daily life. Furthermore, the spine has also the role of protecting the spinal cord and nerves and, thanks to the presence of intervertebral discs, can reduce the stresses and the impacts to which the body is subjected (for example during walk, up and down stairs, running, …).[3]
The spine must also allow the movements of the trunk which happen on different planes: on sagittal plane (flexion-extension movement), on frontal plane (right-left lateral bending) and on transverse plane (clockwise-anticlockwise axial torsion) (Fig.1.1).[4, 5]

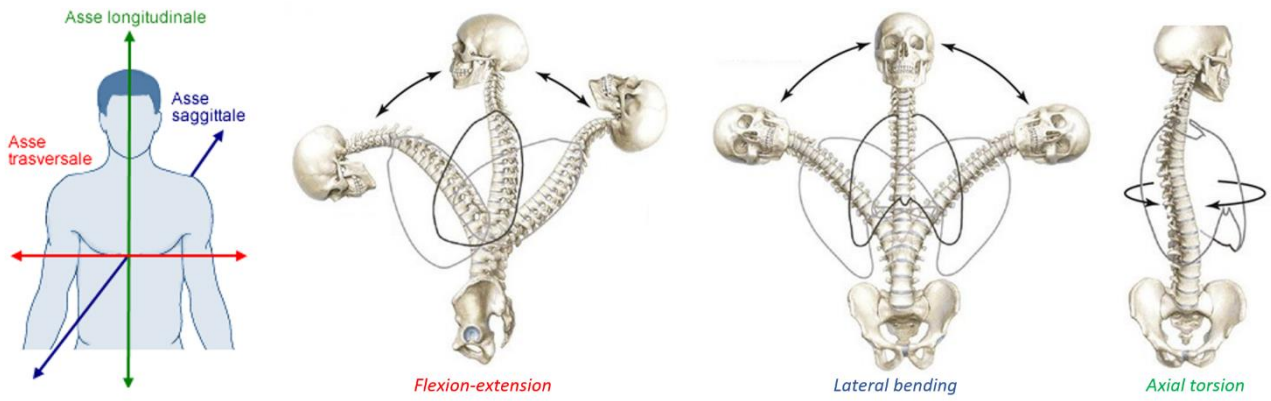

Fig. 1.1 - The axes of human body: sagittal, longitudinal and transverse axes and the principal movements of the spine. (Image from: https://www.my-personaltrainer.it/anatomia/assi-e-piani-corpo-umano.htm)

1.2 Anatomy of the spine

The spine consists of 33-34 vertebrae with various sizes and shapes. The spine is divided in four different segments: cervical spine (C1-C7), thoracic spine (T1-T12), lumbar spine (L1-L5) and sacrum (three-five fused coccyx vertebrae) (Fig.1.2).[6] The spine is not a straight structure but has a physiological curvature: lordosis is the normal inward curvature of the lumbar and cervical regions of the human spine while kyphosis is the normal outward (convex) curvature in the thoracic

and sacral regions.[6] Thanks to these curvatures, the spine is able to support a weight ten times greater than a completely straight column.
The column consists of an alternation of vertebrae and intervertebral discs. The vertebra consists of a thick layer of cortical bone which surrounds the structure, while in its interior there is the trabecular bone.

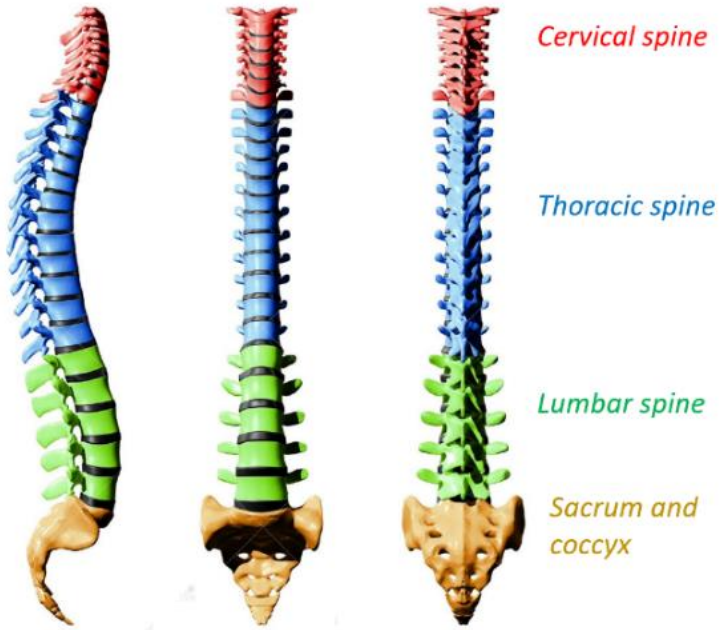

Fig 1.2 - The physiological curvature of the human spine with the different regions (cervical, thoracic, lumbar, sacrum and coccyx spine (Image from: http://www.osteopatasiracusa.net/2017/06/29/1572/)

The anterior side of the vertebra is connected with the posterior side by two structures called pedicles. In the posterior side there are the transverse processes, the lamina and the spinous process (Fig.1.3). Between the anterior body of the vertebra and the posterior arch there is the vertebral foramen where the spinal cord is placed.[6]
Between the anterior bodies of two contiguous vertebrae, there is the intervertebral disc (Fig.1.3). This is composed of the nucleus pulposus and the anulus fibrosus. The nucleus pulposus consists of proteoglycans and collagens. It acts as a shock absorber for axial forces and as a semifluid ball during flexion, extension, rotation, and lateral bending of the vertebral column. The anulus fibrosus consists of several layers of fibrocartilage that surround the internal gelatinous nucleus pulposus. This arrangement provides very strong bands between adjacent vertebrae while allowing some degrees of movement of the vertebrae. The vertebrae and intervertebral discs are connected by the endplates, made of hyaline cartilage. The endplates contain the discs and provide anchorage to the collagen fibers.[7]
Finally, ligaments and tendons are fibrous bands of connective tissue which are attached to bone (Fig.1.3). Ligaments connect two or more bones together and help to stabilize joints while tendons link muscle to bone.[8] There are ligaments which connect two contiguous vertebrae (such as supraspinous, interspinous ligaments and ligamentum flavum) and other ligaments that connect more vertebrae covering the entire spine (anterior and posterior longitudinal ligaments). The system of ligaments, tendons and muscles contribute to protect the spine from injuries due to hyperextension and hyperflexion (excessive movements).[8]

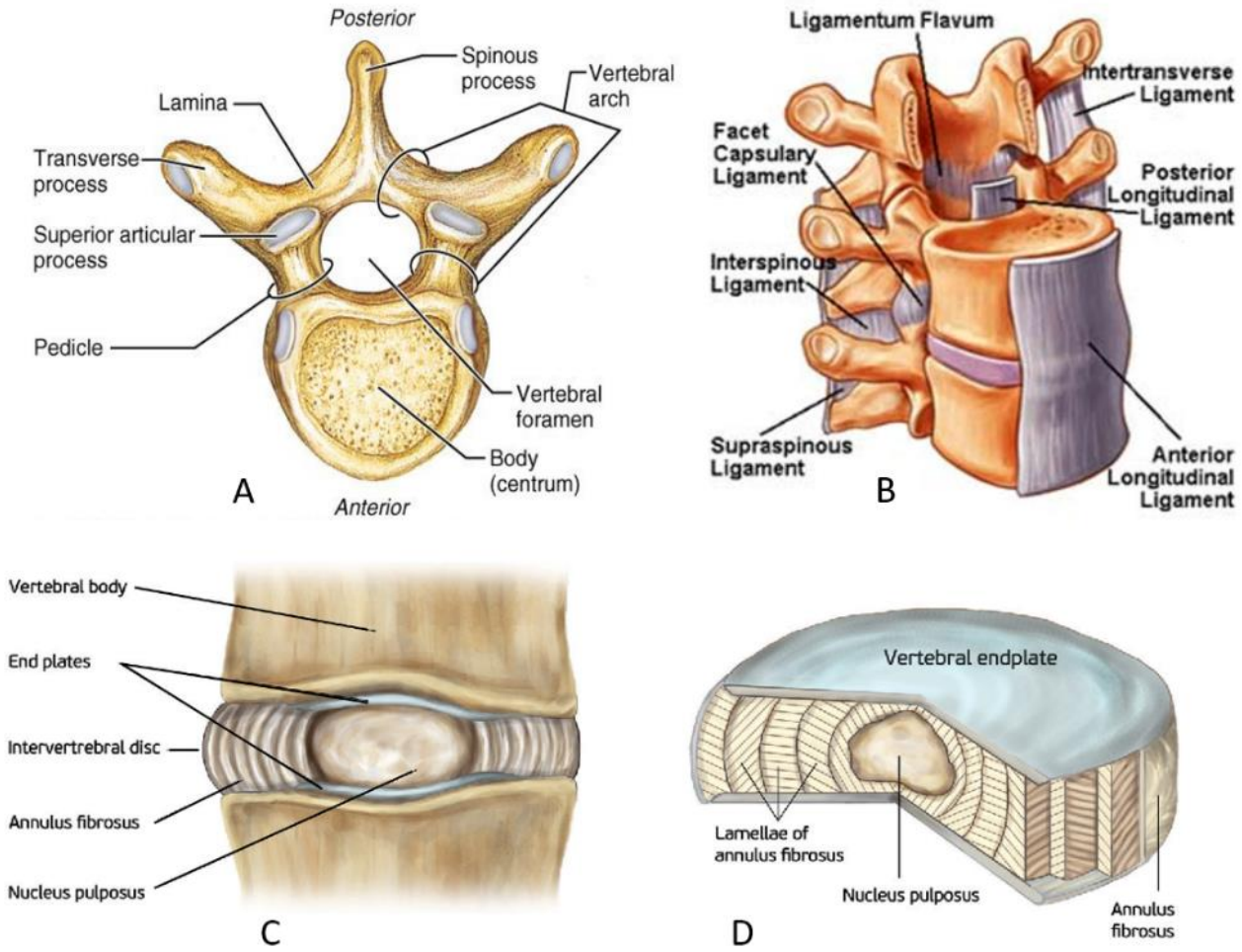

Fig. 1.3 - A: The anatomy of a vertebra. B: The ligaments of the human spine. C and D: The anatomy of intervertebral disc (Image from: https: //www.kinesiopatia.it/glossario/apofisi-spinosa-vertebrale/, https://www.spineuniverse.com/anatomy/ligaments, https://www.semanticscholar.org/paper/The-biology-behind-the-human-intervertebral-disc-Tomaszewski-Saganiak/ccdcee0a3c16c042c1b4265782db6dea68c663d9)

1.3 Pathologies of the spine

Today 30% of people suffer from back pain.[9] The problems related to the spine can be originated by different causes: postural balance, impacts, trauma or can have genetic origin.
Postural balance is very important especially in the recent years when people's lifestyle has changed becoming much more sedentary. This could cause changes in the physiological curvature of the spine generating pain. In these cases a postural rehabilitation program could benefit the individual. Back injuries are very frequent, causing fractures of the vertebrae (especially in patients with osteoporosis). In these cases the patients could be operated injecting cement into the vertebra to restore the shape

and the initial size of the vertebra. The problems with genetic origin are also widespread and can cause deformity of the spine in the pre-pubertal period (9-10 years). These abnormal curvatures of the spine (especially scoliosis) can lead to paralysis if not treated soon.

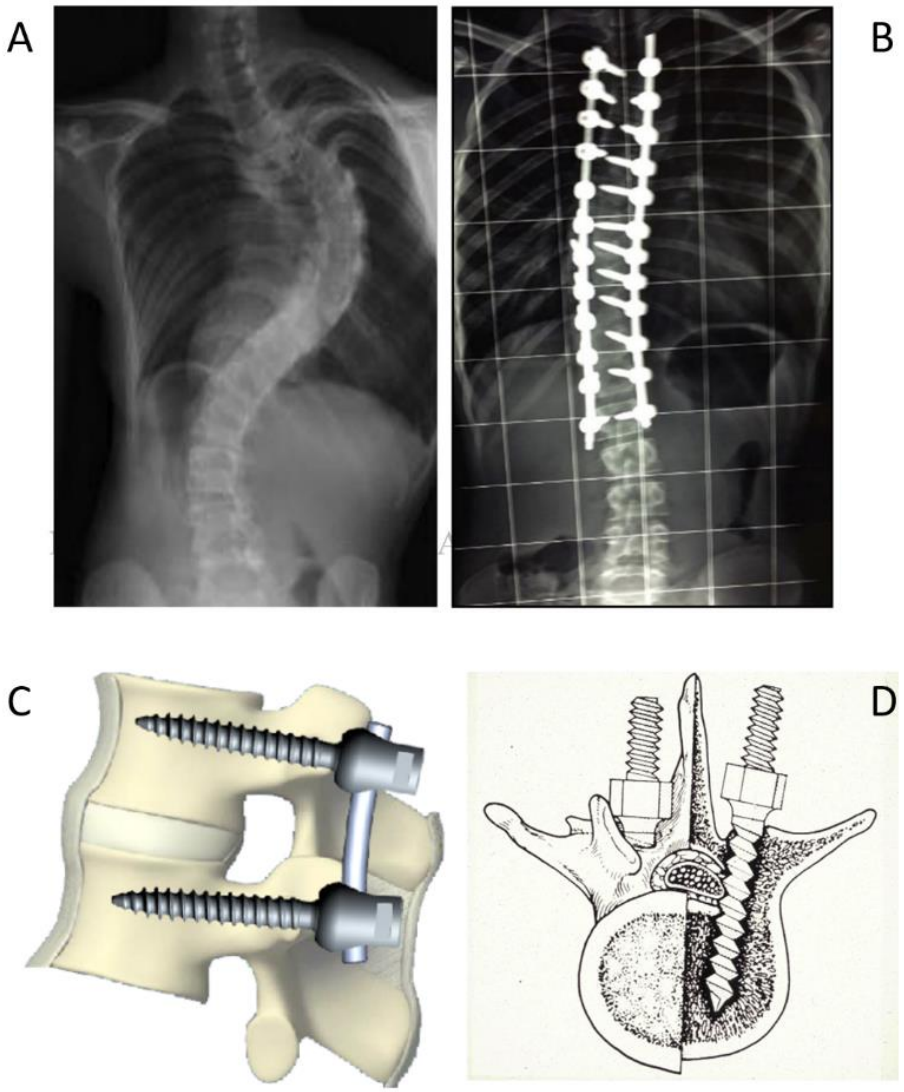

Fig. 1.4 - A: a radiography of a spine with scoliosis. B: A spine treated with rods and pedicle screws. C and D: Images of vertebrae with two pedicle screws and the rod. (Image from: https://mmcneuro.wordpress.com/2013/02/28/making-sure-pedicle-screws-are-correctly-placed-during-spine-surgery/)

Other types of problems can be associated with tumours and the spine is also the most common site for bone metastases (50% of osseous metastases).[10] In cases of vertebral metastases, the clinician is faced with a multifactorial problem which involves neurologic, oncologic, mechanical, and systemic considerations. In this framework, the risk of spine failure related to mechanical instability plays a fundamental role. In addition there could be also problems related to postoperative complications such as infections, septic loosening or pseudoarthrosis.
Every day a large number of surgical interventions are performed to treat those patients with severe spinal deformities (about 50,000 a year in Italy), such as scoliosis (a sideways curvature of the spine) or kyphosis. From a statistical analysis, the percentage of failures for this type of interventions is around 25-30%.[11] This means that the patient is forced to return to the surgery to be re-operated again and this event occurs half the time within one year from the first operation. The treated pathologies and the relative interventions concern, in 50% of the cases, individuals with age under 60 with a significant percentage of individuals in childhood or adolescence.[12, 13] To treat spinal deformities, the

surgeons use a fixation device which consists of screws and rods (Fig.1.4). For certain types of interventions, even hooks are used to fix bony parts of the vertebrae after an osteotomy has been performed. These devices fix the spine to give it the right physiological curvature but avoid any type of movement.
The failures of the fixation system can be divided into three categories (Fig.1.5):

1. *Rupture of the rod*: the rod, which connects the vertebrae, is broken.[14, 15] Sometimes, after this rupture, during the re-intervention, the broken rod is replaced with a new element or the surgeon tries to further stiffen the affected column segment by adding a second rod. The result of this further stiffening in many cases causes the double bars to break again.
2. *Pull-out of the pedicle screws from the vertebra*: in this case there is no rupture of the prosthetic system but there is a pull-out of the screw from the peduncle of the vertebra.[11, 15] As previous, the patient must undergo a new surgical procedure to restore the correct position of the screws.
3. *Proximal Junctional Kyphosis (PJK)*: also in this case, the system does not break, but instead there is a "collapse" of the vertebral column starting from the first non-instrumented vertebra adjacent to the last instrumented one.[16-19] Following this failure, the surgeon tends to extend the fixation system even to the "collapsed" vertebra but in many cases the result is that the problem is not solved but is only transferred to the next vertebra.

There are not only the mechanical failures related to the instrumentation used, but also other types postoperative complications such as infections, septic loosening or pseudoarthrosis.

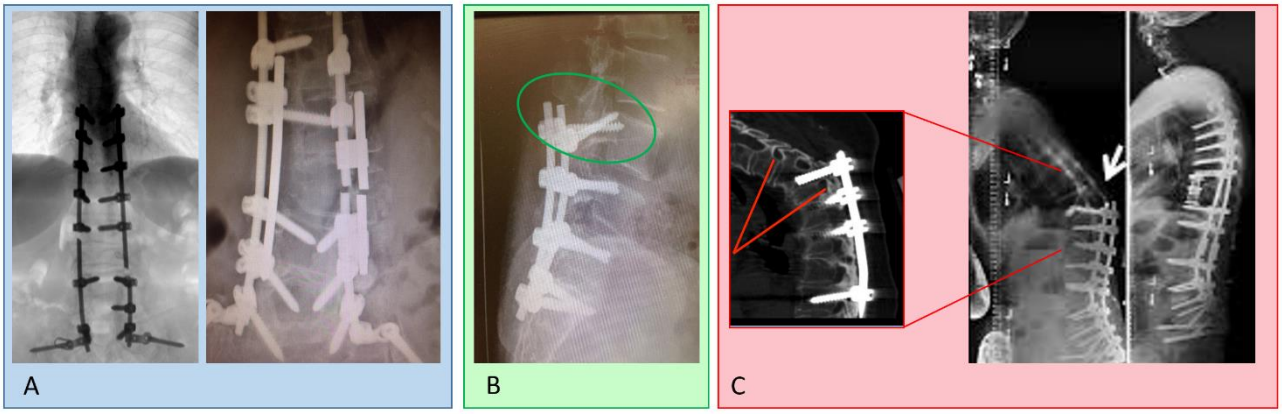

Fig. 1.5 - A: The rupture of a single or double rods. B: The pull-out of the screw from the vertebral body. C: The Proximal Junction Kyphosis. (Images from: https://med.virginia.edu/neurosurgery/services/spine-surgery/treatment/minimally-invasive-spine-surgery/, https://neupsykey.com/proximal-and-distal-junctional-fixation-techniques/)

1.4 Aim

The aim of my project is the study of the spinal column in order to improve the knowledge about this organ to elucidate the role of the different elements (vertebrae, intervertebral disc, ligaments). In order to achieve this broad aim, this PhD project included both a methodological part, where the methods were fine-tuned and validated, and a more applicative one, where the methods were deployed to assess the specific biomechanical behaviour of the different parts of the spine.
I have optimized the technique of the DIC to be able to study displacements and strains simultaneously on hard (vertebrae) and soft tissues (intervertebral discs and ligaments). In this way, the entire spine can be investigated in its complex without separating some elements from the rest of the structure, preserving in this way the functionality of the organ. After a preliminary part of the research in which I tuned the tool, I have investigated the spine concentrating the attention mainly on

two different types of tissues: intervertebral discs and ligaments. I studied their biomechanical role measuring the superficial distribution of strain when different loading conditions were simulated.
In particular the aims of the present study were:

1. a review of literature about:
    a. the methods used for testing the spine and the differences between different types of specimens *(Chapter 2)*: the functionality of the spine can be investigated using different approaches. *In vivo* assessment allows the analysis of the movement when a patient or a healthy subject is performing different daily motor tasks but does not allow to simulate the effects of specific injuries or pathologies. *In vitro* tests allow to study the biomechanics of specific segments of a body simulating realistic loading and boundary conditions, different injuries, and varying damage in a controlled manner, thus allowing to measure the effect of selected defects or investigating the effects of different implants and surgical techniques. Numerical models can be built with different strategies and allow the analysis of mechanical systems (such as the spine) when moving under the influence of forces and moments.
    b. the biomechanical study on intact and lesioned ligaments and on osteotomy surgical procedures *(Chapter 3)*: the stability of the column is granted mainly by the posterior structures of the vertebrae. In case of ligament damage or osteotomies, the stability of the spine is compromised and the instability firstly leads to pain and subsequently to degeneration and deformity. A biomechanical analysis of the lesions of the spine ligament and vertebral bone and their effects on spine stability may help surgeons improve those invasive surgical techniques, which involve partial or complete damage of the spine ligaments.

2. the use of Digital Image Correlation on biological tissues *(Chapter 4, Chapter 5)*: the feasibility and the potential of using Digital Image Correlation tool to measure the strain distribution simultaneously on hard tissues (vertebrae) and soft tissues (intervertebral discs and ligaments) of the spine were explored.

3. how the distribution of strain on the disc changed with different loading rates and with or without a conditioning *(Chapter 6)*: the mechanical properties of the intervertebral discs significantly depend on loading rate and hydration. What is missing is how the deformation trend of the anulus fibrosus changes at different loading rates and the effect of conditioning. By the use of Digital Image Correlation, the strain distribution on the surface of intervertebral discs was measured in order to understand how the kinematics of the disc could change.

4. the role of the anterior longitudinal ligament *(Chapter 7):* the anterior longitudinal ligament (ALL) is fundamental in constraining motions especially in the sagittal plane and confines the intervertebral discs, preventing herniation. Digital image Correlation was used to investigate in depth the biomechanical function of the ALL in front of the vertebrae and in front of the intervertebral discs, measuring the strain distribution in the ALL for different directions of motions (flexion-extension, lateral bending and torsion) and understanding how the strain distribution changes through the progression of the loading.

5. the non-linear behaviour of the anterior longitudinal ligament *(Chapter 8):* while the non-linear behaviour of spine segments has been extensively investigated in the past, the behavior of the ALL and its contribution during spinal flexion and extension has never been studied considering the spine as a whole. The strain distribution on the ALL in situ during flexion-extension was measured comparing the strain on specific regions of interest of the ALL in front of the vertebra and the intervertebral disc and analyzing the non-linear relationship between the measured strain and the imposed rotation and the resultant moment.

Chapter 2

Tools for the biomechanical investigation of the spine

Adapted from the manuscript (first part)

In vitro **experimental studies and numerical modeling to investigate the biomechanical effects of surgical interventions on the spine** [20]

Maria Luisa Ruspi, MEng[1], Mohammadreza Chehrassan, MD[2], Cesare Faldini, MD[2], Luca Cristofolini, PhD.[1]

[1] Department of Industrial Engineering, School of Engineering and Architecture, Alma Mater Studiorum - Università di Bologna, Bologna , Italy
[2] First Orthopaedic and Traumatologic Clinic, Rizzoli Orthopaedic Institute, Bologna, Italy

The authors wish to thank Critical Reviews™ for providing the permissions to re-use the manuscript titled *"In vitro experimental studies and numerical modeling to investigate the biomechanical effects of surgical interventions on the spine"* in the present Ph.D thesis.

Published in: Critical Reviews™ in Biomedical Engineering, 2019, 47: 295-322

2.1 Introduction

The spine is subject to several pathologies due to traumas, deformities, tumors and other degenerative processes. These pathologies may be localized in a single vertebra or extended to a segment of spine and can impact both hard and soft tissues. Generally, the aim of spine surgery is to relieve pain, restore mechanical stability, prevent or reduce neurological damage and restore the physiological functionality of the spine. To achieve these purposes, the use of screws and rods is mandatory in most cases.[21] However, post-operative failures like rod breakage, screw pull-out or Proximal or Distal Junctional Kyphosis (PJK or DJK) may occur.[18,11] The reason of the high number of failures relates to the biomechanical function of the different substructures of the spine (ligaments, facets joints, muscles, etc.), which may be partially or completely removed or damaged during the surgery. Although extensive pre-clinical and clinical research has focused on such failures, there is still a lack of understanding and limited consensus on the causes leading to such failures.
Very briefly: the vertebrae consist of a vertebral body, connected to the adjacent vertebrae by the intervertebral discs (IVD), and of a posterior arch, wrapping the spinal cord (Fig. 2.1). The spinous and transverse processes are connected by ligaments constraining motions and contributing to spinal stability. Adjacent vertebrae are also connected at the facet joints, which constrain motion in extension. The aim of the present review is to provide an overview of the biomechanical studies on the different structures of the spine. The first section of this review provides an overview of the different tools and methods of investigation. The second section summarizes the main biomechanical findings of such studies.

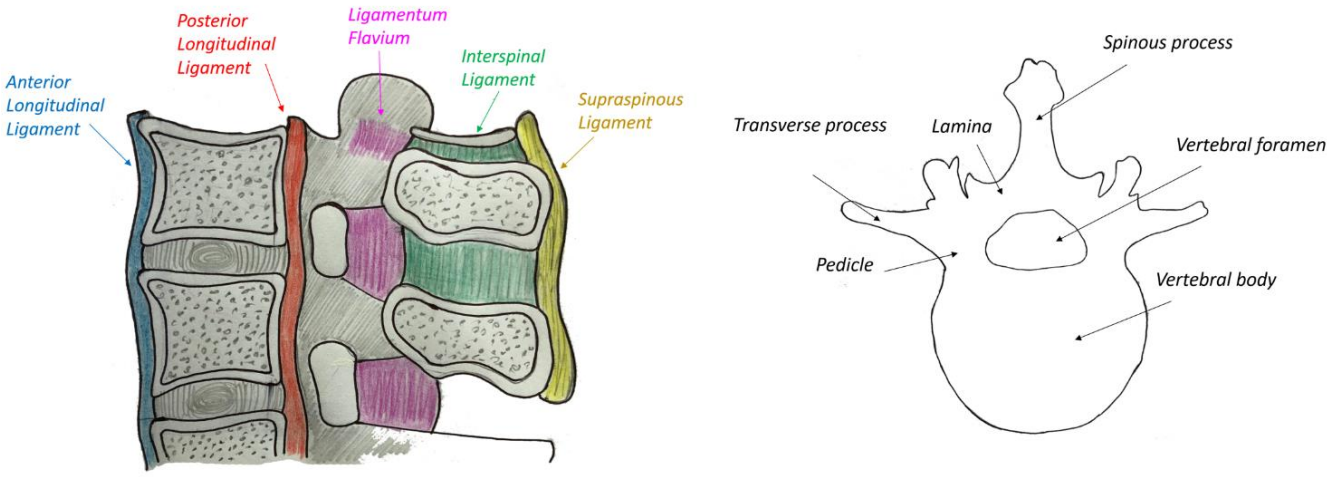

Fig. 2.1 - Anatomy of the spine (left, sagittal section showing the main ligaments) and of the vertebra (right, showing the anatomical parts of the vertebral body and of the posterior part)

2.2 Methods

2.2.1 Search strategy

A systematic search (Fig. 2.2) using PubMed, OVID-MEDLINE and Google Scholar databases was performed to identify papers relevant to the biomechanical role of spinal ligaments, facets and lamina, and to the methods of *in vitro* and numerical investigation up to 20 December 2017. The initial search terms were "spine" in combination with "ligaments", "anterior longitudinal ligament", "posterior longitudinal ligament", "interspinous ligament", "supraspinous ligament", "flavum ligament",

"capsular ligament", "intertransverse ligament" (and the corresponding Latin versions), "lamina", "facet", "facetectomy", "laminectomy", "laminoplasty", "laminotomy", "range of motion", "instantaneous axis of rotation", "stiffness", "stress, strain", "muscles". Moreover, the list of citations from the different papers was scanned for additional papers missed from the database search.

2.2.2 Inclusion-exclusion criteria and data extraction

After this search, the titles and abstracts were examined, and all the truly relevant papers underwent thorough text review. Inclusion criteria were manuscript in English, subjected to peer-reviewing, focusing on the human or animal spine, reporting *in vivo*, *in vitro* or numerical biomechanical studies. Numerical models completely lacking of validation were excluded.
We performed data extraction for the following aspects: type of investigation method (*in vivo*, *in vitro* or numerical), type of spine specimen (animal vs. human), type of measurement method (e.g. stereophotogrammetry or spine tester), type of loading (e.g. flexion, lateral bending etc.), spine segment under investigation (cervical, thoracic or lumbar tract) and measured quantities (e.g. range of motion or stiffness or failure load).

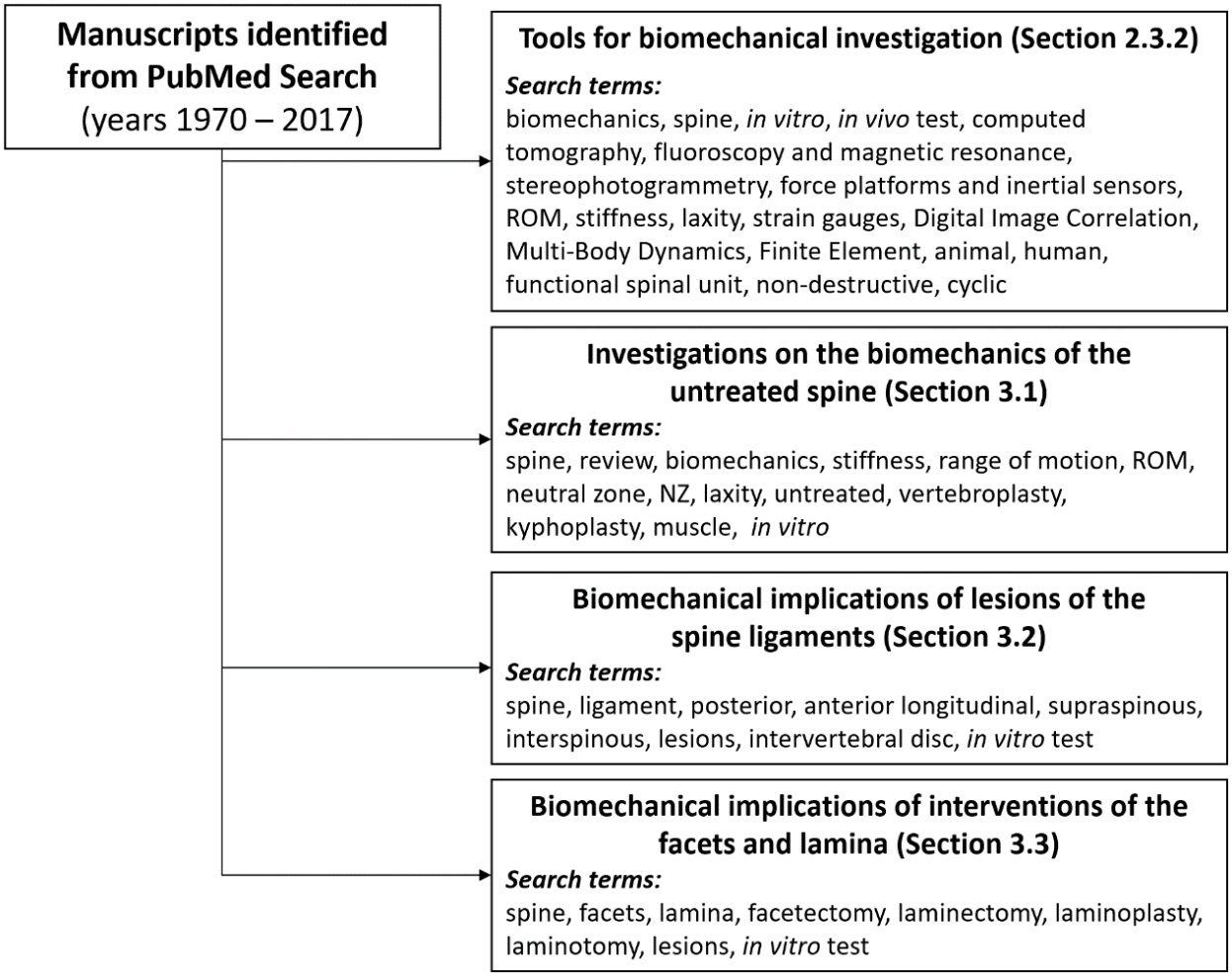

Fig. 2.2 - Outline of the search strategy and search terms adopted for the different sections of this review

2.3 Results

2.3.1 Articles selection

A total of over 300 potentially relevant papers were considered in the initial extensive systematic literature search. After selection, 66 documents satisfied the inclusion criteria: 35 focused on the different methods of biomechanical investigation, 15 papers dealt with the effects of surgical interventions on the ligaments, and 16 papers with interventions on the facets and lamina.

2.3.2 Tools for biomechanical investigation

The functionality of the spine can be investigated using different approaches (Fig. 2.3).
In vivo assessment allows the analysis of the movement when a patient or a healthy subject is performing different daily motor tasks (such as walking, walking up/down stairs, standing to sitting position, …) considering the human motion in its complex. Both the natural condition, and the effects of postural problems, surgical corrections, rehabilitation and tissue adaptations can be investigated. *In vivo* investigation does not allow to simulate the effects of specific injuries or pathologies and cannot compare the effects of different possible types of surgery on the same individual.[22]
In order to analyse the range of motion (ROM) and to estimate kinematics trajectories, different non-invasive tools are available (such as stereophotogrammetry, force platforms and inertial sensors). However, due to the unavoidable soft tissue artefacts[23,24,25], such movement analysis tools are suitable only to measure relative motions of large segments (e.g. thoracic area respect to sacral area).

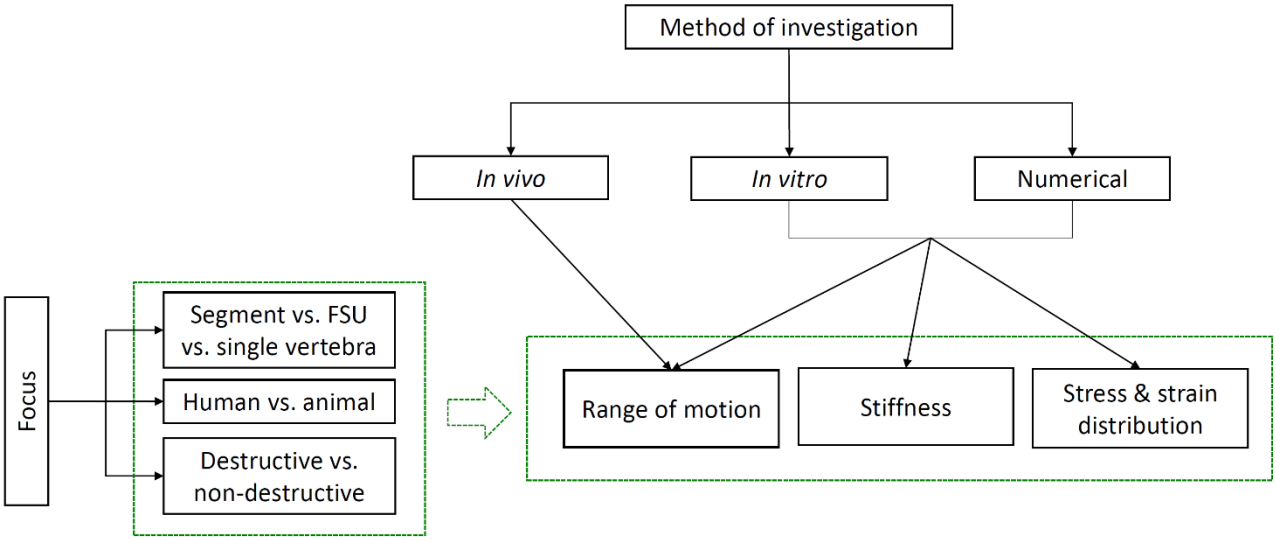

Fig. 2.3 - Possible approaches to investigate the biomechanics of the spine, including different investigation tools, different type of specimen, and different kinds of simulation

Conversely, such *in vivo* tools cannot address in detail inter-vertebral motions, which are small compared to the measurement uncertainties.
Imaging techniques (plane radiography, x-ray computed tomography (CT), fluoroscopy and magnetic resonance) can provide information on the internal anatomical structures, the condition of an implant and possible implant migrations. Such imaging techniques allow to measure the motions of individual structures of the spinal structure.[26] However, the use of these imaging tools is constrained by their impact on the patients (in terms of radiation exposure) and by their cost. In this review the *in vivo*

investigations are not considered in detail because reviews on this topic have been published recently.[27,28]

One of the most critical points for *in vitro* biomechanical testing is that the specimen ideally should have the same anatomy, mechanical properties etc. as the human spine. For this reason, fresh spines from human donors are definitely the most fidelic model. However, animal specimens are generally easier to obtain. Porcine and sheep specimens are most similar to human in terms of anatomical parameters for vertebrae, while mouse and rat lumbar discs and mouse tail discs are the closest representation of the human lumbar intervertebral disc geometry (Table 2.1).[28,29] On the other hand, the use of animal models raises some concerns as their anatomy is different because of the specific posture (quadruped vs. bipedal) leading to a different biomechanical loading.[29,30] For these reasons, animal specimens are suited only for preliminary tests, but clinically relevant conclusions and guidelines cannot be based on animal models.

Table 2.1 - Outline of the search strategy and search terms adopted for the different sections of this review

		Vertebral body						***Pedicle***	
		upper width	lower width	upper depth	lower depth	anterior height	posterior height	width	height
Cervical	baboon	similar	similar	similar	similar	similar	different	similar	similar
	sheep	different	different	different	different	different	different	similar	different
Thoracic	sheep	similar	similar	different	different	similar	similar	similar in T1-T4, different in T4-T12	similar
	deer	different	different	different	different	different	similar	similar	different in T1-T9, similar in T10-T12
	porcine	similar	similar	similar	similar	similar	similar	similar	similar
Lumbar	sheep	similar	similar	similar	similar	similar	similar	similar	different
	deer	similar	similar	similar	similar	the highest is at L2	similar	similar	different
	porcine	similar	similar	similar	similar	similar	similar	different	similar

When designing an *in vitro* test, the choice of the type of specimen depends on the problem under investigation.[31,32,33] The specimen can consist of multi-segmental spinal unit (composed by a series of adjacent vertebrae and interconnecting soft tissues), a set of three adjacent vertebrae, a Functional Spinal Unit (FSU, consisting of two adjacent vertebrae with the respective intervertebral disc and all the interconnecting ligaments), or a single vertebra.

In vitro tests allow to study the biomechanics of specific segments of a body simulating realistic loading and boundary conditions (including trauma), different types of injuries, different extent of damage in a controlled manner, thus allowing to measure the effect of selected types of defects or investigating the effects of different implants and surgical techniques. These tests are performed either reproducing non-destructive cyclic movements, or imposing destructive conditions until

failure.[34,35] While complex multiaxial simulations can be used to replicate physiological loading conditions, sometimes simplified loading conditions are preferred as they allow better control and reproducibility of the test conditions.
In order to measure the stiffness, laxity and ROM[36,37] of a spine segment, different types of motor tasks are simulated. To quantify the local magnitude of strain, strain gauges allow provide great measurement precision at selected points on the surface of the specimen (but can be applied only to hard tissue).[38] Digital Image Correlation (DIC) is a recent tool that allows contact-less and full-field measurement of the displacements and of the distribution of strain on the specimen surface when it is prepared with a suitable speckle pattern.[39] The main limitation of DIC is that it yields relatively noisy results on the measured strains, if the method is not properly optimized.[34,40] DIC can be applied to *in vitro* testing of hard tissue, such as vertebrae affected by metastases.[10] The authors developed a method to apply the pattern also to soft tissue, so as to investigate the strain distribution in the intervertebral discs, in the ligaments and in the vertebra at the same time and soft tissue.[41]
A limitation of *in vitro* tests is the impossibility of investigating the effects of tissue adaptation (bone remodeling, modifications of soft tissues etc.) in the period following surgeries or injuries.
Numerical simulations became more powerful and better reliable in the past two decades. Numerical models can be built with different strategies, depending on the research question.[42,43] A Multi-Body Dynamics (MBD) system consists of solid bodies (or links) that are connected to each other by joints, which restrict their relative motion. MBD allows analyzing how a mechanical system (such as the spine) moves under the influence of forces and moments.[44,45,46,47] Conversely, to investigate the distribution of stress within an organ, Finite Element (FE) models can be used (Fig. 2.3).[48,49,50, 51] Since numerical models incorporate a number of assumptions and simplifications, their closeness to reality cannot be taken for granted.[52] For this reason, numerical models need a validation to confirm that the reliability of the outputs.[53-55] While most experimental techniques allow measuring the state of stress/strain only on the exposed surface of the specimen, FE modelling enables to estimate the state of stress/strain inside the structure too.
A synergistic use of experimental and numerical approaches allows building more complete information and increases the reliability of the conclusions.

Chapter 3

A review of the investigations on the biomechanics of the untreated and treated spine

Adapted from the manuscript (second part)

In vitro experimental studies and numerical modeling to investigate the biomechanical effects of surgical interventions on the spine [20]

Maria Luisa Ruspi, MEng[1], Mohammadreza Chehrassan, MD[2], Cesare Faldini, MD[2], Luca Cristofolini, PhD. [1]

[1] *Department of Industrial Engineering, School of Engineering and Architecture, Alma Mater Studiorum - Università di Bologna, Bologna , Italy*
[2] *First Orthopaedic and Traumatologic Clinic, Rizzoli Orthopaedic Institute, Bologna, Italy*

The authors wish to thank Critical Reviews™ for providing the permissions to re-use the manuscript titled *"In vitro experimental studies and numerical modeling to investigate the biomechanical effects of surgical interventions on the spine"* in the present Ph.D thesis.

Published in: Critical Reviews™ in Biomedical Engineering, 2019, 47: 295-322

3.1 Investigations on the biomechanics of the untreated spine

Research on the biomechanics of the natural spine may develop important insights on the etiology of diseases affecting the spine. This understanding can provide crucial information on the interaction between adverse mechanical loading and unfavorable biochemical environment, which can trigger the degeneration of spine substructures including intervertebral disc, ligaments, join facets and bony structures (Fig. 3.1), (Tables 3.1 and 3.2).[3]

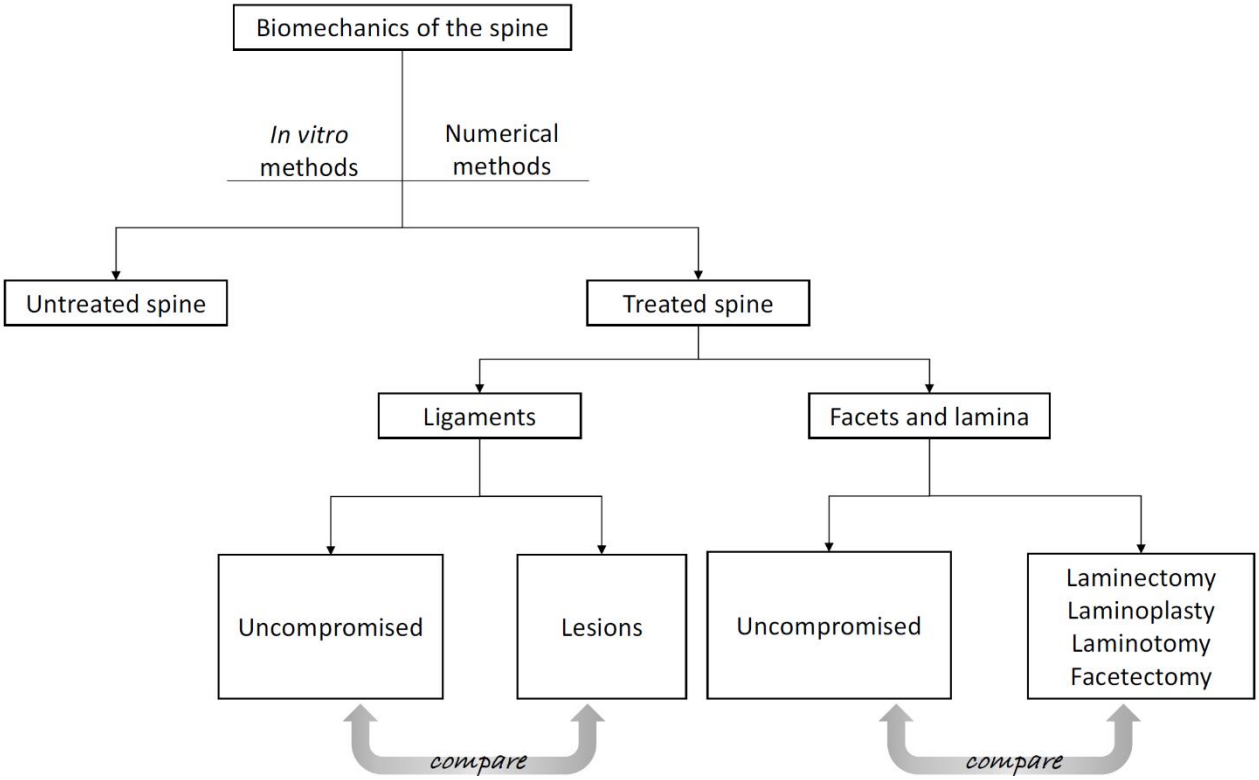

Fig. 3.1 - Overview of the conditions under which the biomechanics of the spine must be investigated

The review of White *et al.*[1] describes the spinal kinematics and gives information about the ROM for different directions, at all levels from Occiput-C1 to L5-S1. The thoracolumbar region of the human spine (from T1 to L4) was investigated by Busscher *et al.*[33] whose study addressed the ROM, neutral zone and stiffness. Panjabi *et al.*[56] investigated the elastic physical properties of each lumbar intervertebral level from L1 to S1. The motions were reported in the form of a set of six load-displacement curves (intervertebral rotations and translations). The consequences of the contraction of spinal muscles due to the loads acting on the spine was studied in human cadaveric lumbar specimens by Quint *et al.*[57] The action of the intersegmental agonist and antagonist muscles biomechanically increased the stiffness of the intervertebral joints in axial torsion and lateral bending; conversely, the muscles could destabilize the segment in flexion.
Wilcox *et al.*[58] provided an extensive review concerning the biomechanics of vertebroplasty and kyphoplasty (covering both with *in vitro* tests and FE models). More recently, a review was published concerning the loading conditions imposed to the cements for vertebroplasty and kyphoplasty.[59] An overview of the studies (*in vitro* tests and FE models) conducted and their contribution to understand the biomechanics and the functionality of the intervertebral disc (IVD) was described in Newell *et al.*[7]
An extensive overview on the evaluation of the spine biomechanics in the untreated condition was recently published by Oxland.[60] This review covers the studies using human materials, both *in vivo*

and *in vitro*, including numerical models and animal experimentations when other data were not available.

3.2 Biomechanical implications of lesions of the spine ligaments

3.2.1 Biomechanics of uncompromised spine ligaments

The natural biomechanical role of ligaments is to provide stability and prevent hyper-extension or hyper-flexion or excessive rotation.[61] One way to elucidate the function of the spine ligaments is to subject them to mechanical testing either individually, or as part of a spine segment (Fig. 3.1), (Tables 3.1 and 3.2). Due to the complex nature and role of the ligaments, a multiscale approach (i.e. spanning different dimensional levels) is necessary, to elucidate the rheological properties at tissue-level, the structural properties at the organ-level, and their biomechanical function at spine level. Hukins *et al.*[62] used polarized light microscopy, scanning electron microscopy and x-ray diffraction to evaluate the organization of the collagen in ligaments, and to link the microstructure of the ligaments to their mechanical properties. According to Hukins *et al.*, the longitudinal ligaments constrain bending of the spine in a sagittal plane: the posterior and anterior ligaments limit respectively flexion and extension. During these movements, they reinforce the action of the anulus fibrosus of the intervertebral disc. Furthermore, they found a stress relaxation of about 50% within one minute, due to the viscoelasticity of ligaments. The mechanical test performed by Dickey *et al.*[63] addressed the importance of the micro-structure of the ligaments in terms of arrangement of the fibers. They showed that the collagen fibers in the interspinous ligament form a complex spatial network, which provides optimal resistance to spinal flexion when intact; partial lesions of the ligament compromised the interaction between fibers, significantly reducing the residual stiffness and strength. Among the studies addressing the geometry and mechanical properties of the ligaments, Yoganandan *et al.*[64] measured the lengths and the cross-sectional areas of the different ligaments using computed tomography and a cryomicrotome. Grimes *et al.*[65] studied segments of human lumbar spines, cutting some of them into sagittal sections for a qualitative description of the intraforaminal ligamentous structures, while others were used for biomechanical tests to failure to evaluate the strength of nerve roots with ligamentous attachments.
Yoganandan *et al.*[66] provided an extensive review of the numerical studies addressing the responses and contributions of the soft tissue structures (ligaments, intervertebral disc and zygapophysial joints) of the human neck, including their functional mechanical role, geometry (such as the length and cross-sectional areas), and material properties (such as force-displacement and stress-strain responses). These properties were described for all components; modelling approaches were discussed for each soft tissue structure.

3.2.2 Lesions of spine ligaments

In case of ligament damage, the stability of the spine is compromised either at a single level or involving a longer spine segment. Instability firstly leads to pain and subsequently to degeneration and deformity.[67] A biomechanical analysis of the lesions of the spine ligament and an *in vitro* and/or numerical evaluation of their effects on spine stability may help surgeons improve those invasive surgical techniques, which involve partial or complete damage of the spine ligaments. This can help preventing iatrogenic lesions, which may trigger failure of the treatment (Tables 3.1 and 3.2).
Some studies analyze the behaviour of a specific FSU, while others take into account a segment of three or more vertebrae. Many ligaments (such as the anterior and posterior longitudinal ligaments and supraspinous ligament) extend across several vertebrae, forming a continuous structure.

Published in: Critical Reviews™ in Biomedical Engineering, 2019, 47: 295-322

Therefore an *in vitro* multisegmental vertebral unit represents the *in vivo* condition more closely than shorter segments (Fig. 3.1).[68]
For instance, Hindle *et al.*[69] tested human lumbar FSUs in order to understand the function of the interspinous and supraspinous ligaments during flexion and extension. This test was performed applying a force, varying the distance between the instant axis of rotation (IAR) and the center of the ligaments. They showed the contribution of the supraspinous and interspinous ligaments to the stiffness of the FSU; the stiffness decreased with the number of resected ligaments. Furthermore, this test showed that the stiffness increased for higher strain rates.
One of the first studies addressing the effect of the different ligaments was performed on a porcine model by Gillespie *et al.*[70] In order to understand the contribution of the individual posterior spinal ligaments, Gillespie *et al.* analyzed segments of porcine lumbar spine in flexion-extension, applying sequences of ligament resections. For the extension test, not all the resections showed significant differences about the functionality of the spine. Conversely, during flexion test, each sequential resection reduced peak moment and stiffness increasing the laxity zone. The ligamentum flavum gave the largest contribution to resisting flexion movement.
Panjabi *et al.*[71] analysed the effect of the different ligaments on the stability of human spine. They tested thoracic FSUs in flexion-extension *in vitro*, while an anterior pull was applied to the proximal vertebra. The tests were performed until failure, with a progressive resection of all the ligaments in two different sequences: from the most anterior to the most posterior one, and vice-versa. The FSUs were less stable in flexion for the sequence of posterior to anterior resection, while it was less stable in extension when the anterior injury was simulated. The ligament affecting more significantly the stability in flexion was the posterior longitudinal ligament, while resection of the anterior longitudinal ligament affected more significantly stability in extension.
Panjabi *et al.*[72] investigated the effect of whiplash on the human cervical spine. The spine was stabilized by a system of cables attached to the different vertebrae to simulate the stabilization and compression deriving from the muscles force. In order to understand the contribution of each ligament to constraining spine motion, a marker was attached to each vertebra to measure the inter-vertebral motion. This test demonstrated that the supraspinous, interspinous ligaments and the ligamentum flavum had the greatest risk of injury during rapid antero-posterior loading due to whiplash.
Brolin *et al.*[73] studied the human cervical spine, using a subject-specific FE model obtained from CT scans. The ligaments were modelled with nonlinear springs and required some simplifications (such as the lack of interactions between ligaments) which can cause a softer response compared to *in vitro* experiments on a real spine segment. They showed how ligament sprains compromise the stiffness and stability of the cervical spine. A FE model of the cervical spine was used also by Ng *et al.*[74] in order to evaluate the effect of different injuries (simulating complete removal of the ligaments, of the facets, and of the disc nucleus) on the stability for compression, anterior-posterior shear and sagittal movements. Another study[50] demonstrated how the lesions of ligaments, facets and disc nucleus affected cervical spine stability in terms of sagittal rotational movement or redistribution of load under axial compression, flexion and extension.
The main limitation of the FE models is that in many cases their adherence with the physical reality is not assessed, or is only assessed in qualitative terms. One of the FE models most extensively validated was describe by Guan *et al.*[75] They developed a model of the lumbosacral region and validated its nonlinear response by comparison against *in vitro* tests of the same subject, for different loading conditions, for each motion segment (L4-L5 and L4-S1) and with increasing loads. This study allowed evaluating the non-linearity of the different parts of lumbosacral region and how the internal load transfer and stresses affected spine stability.
While the biomechanical studies summarized above suggest that the lesions of the spine ligaments compromise stability and can result in disc overloading, their impact in a clinical context is more difficult to assess as iatrogenic damage to the ligaments is typically associated to very invasive surgeries such as fusion. In all cases, these findings indicate that surgeons should strive to improve such invasive surgical techniques, so as to minimize ligament damage.

3.3 Biomechanical implications of interventions of the facets and lamina

Lumbar stenosis is one of the most common diseases of the spine in the geriatric population.[76] The stenosis is defined as a narrowing of the spinal canal and is caused by the overgrowth and degeneration of the joints between vertebral segments. This can lead to a compression of nerve roots traveling through the lumbar spine to the lower back and legs.[76] The pathophysiology of lumbar stenosis is complex and multifactorial, but generally the compression of neural elements is due to a combination of degenerative changes (such as ligamentum flavum hypertrophy, bulging of the intervertebral disc, and facet thickening with arthropathy). For patients over the age of 65, lumbar stenosis is usually treated through surgical interventions.[76] The surgery typically consists of muscle dissections and an extensive resection of posterior spinal elements such as the interspinous ligaments, spinous processes, bilateral laminae, portions of the facet joints and capsule and the ligamentum flavum. These interventions involve different types of bony resections:

- *Laminectomy*: the creation of space by removing the lamina (a portion of the vertebral bone that covers the spinal canal). This resection enlarges the spinal canal to relieve pressure on the spinal cord or nerves. This is a major spinal treatment used only when more-conservative treatments (such as medication, physical therapy or injections) have failed to relieve symptoms. Laminectomy may also be recommended if symptoms are severe or worsening dramatically.
- *Hemilaminectomy*: the removal of only a part of the lamina and only a portion of the facet joint to allow more room for the lumbar nerve.
- *Laminotomy*: the removal of part of the lamina of a vertebra arch in order to relieve pressure in the vertebral canal. A laminotomy is less invasive than laminectomy because it leaves more ligaments and muscles attached to vertebral column intact and it requires removing less bone from the vertebra. As a result, laminotomies typically have a faster recovery time and result in fewer postoperative complications.
- *Laminoplasty*: the removal of the lamina on both sides of the affected vertebrae and then "swinging" the freed flap of bone open thus relieving the pressure on the spinal cord. The spinous processes may be removed to allow the lamina bone flap to be swung open. The bone flap is then propped open using small wedges or pieces of bone such that the enlarged spinal canal will remain in place.
- *Facetectomy*: the removal of one (unilateral) or both (bilateral) of the facet joints on a set of vertebrae in the spine. Facet joints, which are found in between the vertebrae and discs of the spine, give us the ability to bend, twist, and stand up. With age and wear and tear, or sudden trauma, these joints can become worn and rub against or pinch spinal nerves.

3.3.1 Biomechanics of facets and lamina

The stability of the column is granted mainly by the posterior structures of the vertebrae (posterior and transverse processes, facet joints and laminae). The lamina is the part of the vertebra that connects the spinous process with the transverse process permitting the distribution of the forces within the upper and lower facets of the vertebrae. The spinous and transverse processes are the site of insertion of muscles, which connect contiguous vertebrae limiting movement mostly in flexion-extension. The pedicles are bridges connecting the posterior structures with the anterior part of the vertebra

transmitting tension and bending forces to the vertebral body. The facet joints assure the stability of the spine during all the movements.
Facet joint degeneration is part of a degenerative cascade and is normally a consequence of problems of other structures such as intervertebral disc degeneration, vertebral bone lesions or ligament defects.[77] Therefore, it is necessary to investigate the facet joint as a separate substructure of the spine, to elucidate its role in spine stability and biomechanics (Fig. 3.2), (Tables 3.1 and 3.2). A schematic of the different surgical interventions on the posterior structures of the vertebra is reported in Fig. 3.2.

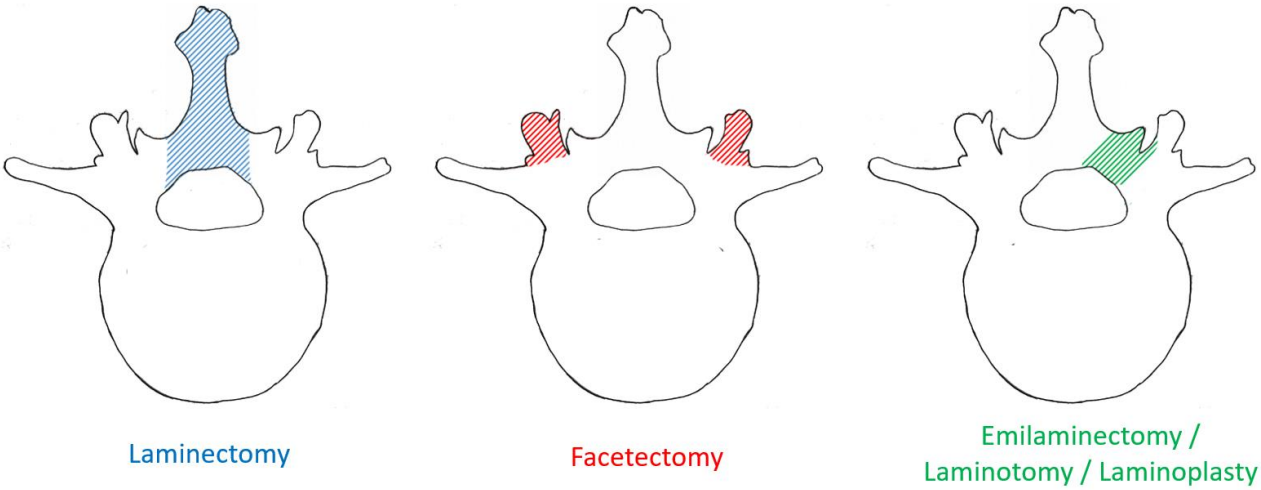

Fig. 3.2 - Schematic representation of the different surgical interventions on the posterior structures.

A number of studies have addressed the biomechanics of multi-segmental spinal units with uncompromised facets and laminae. Shah *et al.*[78] tested cadaveric lumbar spine segments (L3-L5) applying a pure axial compression, an anteriorly offset force (simulating flexion) and a posteriorly offset force (simulating extension). The strain on the surface of the central vertebra of the segment (L4) was measured using 17 rosette strain gauges placed on the anterolateral and posterolateral parts of the upper and lower vertebral rims, at the bases of the pedicles, on the posterior side of the vertebral body (i.e. on the lamina) and in both pars interarticularis. With a pure compression the maximal compressive strain was found near the bases of the pedicles and on both surfaces of the pars interarticularis. During extension, both compressive and tensile strains increased on both surfaces of the pars interarticularis, suggesting that stress fractures and spondylolisthesis could be caused by hyperextension. A similar *in vitro* study was conducted by Hongo *et al.*[79] on segments of three thoraco-lumbar vertebrae (focusing on T10, L1 and L4) subjected to pure axial compression. Eleven rosette strain gauges were applied at the upper, middle and lower vertebral surfaces of the anterior, anterolateral and posterolateral sites of the posterior surface of the lamina. Similar to Shan *et al.*, the highest tensile and compressive strains were found at the base of pedicle, both in the thoracic and lumbar vertebrae. In addition, shear strains in the vertebral body were significantly higher than in the lamina. Teo *et al.*[50] developed a validated FE model of the human lower cervical spine. This model predicted that ligaments, facets and disc nucleus have are equally important in granting stability and in redistributing the loads in flexion and extension.

3.3.2 Lesions of the facets and lamina

Segment laminectomy has been recognized as a risk factor for the development of adjacent level disease[80] and has extensively been investigated (Fig. 3.1 and 3.2), (Tables 3.1 and 3.2). Cardoso *et al.*[81] assessed the acute biomechanical effects of proximal facet violation and subsequent

laminectomy in lumbar-sacral cadaveric specimens. Biomechanical tests were performed under axial rotation, flexion-extension and lateral bending. Their found a significant progressive torsional instability depending on the facet disruption; a complete laminectomy at the cephalad level destabilized the proximal adjacent segment in flexion-extension. Quint *et al.*[82] investigated the effects of agonist and antagonist intersegmental lumbar muscles acting on FSUs in different conditions: intact, unstable due to laminectomy, and instrumentally stabilized. The *in vitro* tests with or without simulation of co-activation of the muscles showed significantly larger ROM for the FSU after laminectomy compared to the intact. The co-contraction of the muscles contributed to increase stability under bending and axial rotation, while a slight increase was noted in the ROM during flexion. Baisden *et al.*[83] compared the laminectomy and open-door laminoplasty *in vitro* on goat spines. Laminoplasty was superior to laminectomy in maintaining cervical alignment and preventing postoperative spinal deformities. A validated three-dimensional FE model (C2-T1) was modified to compare the multidirectional flexibility of the cervical spine in response to a plate-only open door laminoplasty, a double-door laminoplasty and a laminectomy at level C3-C6. They demonstrated that laminectomy increased flexion but with a risk of kyphosis and increased disc stresses in the adjacent segments. A limitation of this study was the absence of muscles, which contribute to spinal stability. The effects of bilateral laminotomy and full laminectomies on the ROM were investigated by Tai *et al.*[84] on porcine lumbar segments (L4-L5) under flexion-extension. They found that the integrity of the posterior complex played an important role on the postoperative spinal stability in decompressive surgery. Intervertebral displacement following laminectomy was significantly greater than in the intact spine or after bilateral laminotomy. The consequences of bilateral laminotomy and full laminectomies on the range of motion and stiffness of lumbar segments (L1-L5) were analyzed by Lee *et al.*[85] on cadaveric human spines. This study showed a greater increase of ROM in flexion-extension after laminectomy than after bilateral laminotomy. Therefore, laminectomy could cause worse hypermobility and potential instability. These effects were observed for flexion-extension, but not for axial rotation or lateral bending.

The impact of different surgical procedures on the cervical spine was addressed by Xie *et al.* using a nonlinear FE model. They compared the ROM of the different FSU (C1-C2, C2-C3, C3-C4, C4-C5, C5-C6 and C6-C7) in the intact condition and simulating unilateral multilevel interlaminar fenestration (UMIF), multilevel hemilaminectomy (MHL) and multilevel laminectomy (ML). UMIF and MHL better preserved the flexion mobility, with low-risk of post-operative spinal instability, and caused less increase of stress in the anulus compared to ML, thus reducing the risk of postoperative disc degeneration. A limitation of this study was the absence of the muscle effect on stability: while during laminectomy the bilateral extensor muscle is dissected from the lamina and spinous process, UMIF and MHL preserve the contralateral muscle. In order to measure the destabilizing effects of multiple consecutive lateral and bilateral hemilaminectomies, Corse *et al.*[68] conducted an *in vitro* test on canine lumbar spines. Postoperative stability in flexion and extension decreased while the ROM and the stiffness were not significantly different from the intact condition.

In order to investigate the destabilizing effects of resections, thoracic human segments were subjected to anterior-to-posterior and posterior-to-anterior sequential resections on different FSUs with intact costovertebral joints by Oda *et al.*[86] They showed that the rib head joints provided stability in the sagittal, coronal and transverse planes. The lateral portion of the facet joints played an important role in providing stability and helped in minimizing postoperative kyphotic deformity and segmental instability.

A nonlinear-FE model of the cervical spine was developed by Hong-Wan *et al.*[87] and adapted to replicate ten surgically altered models simulating laminectomy and facetectomy. Laminectomy did not cause any significant increase in intersegmental motions under lateral bending and axial rotation; extending the surgical procedures to unilateral and bilateral facetectomy increased only slightly the intersegmental motions. The effect of facetectomy on a L2-L3 segment was studied by Lee *et al.*[88] using an FE model. They showed that facetectomy significantly affected extension because it altered the ROM and flexibility, while it did not affect flexion significantly. Similar results were described

by Teo *et al.*[89] Their numerical model also highlighted the alteration of translational shear displacement of the motion segment. Zander *et al.*[90] used a validated numerical model to investigate the effects of several types of interventions (laminectomies, hemilaminectomies, facetectomies and hemifacetectomies). They investigated different loading conditions, both simplified (pure moments) and replicating specific motor tasks (standing and forward bending). Facetectomy influenced the mechanical behaviour of the lumbar sacral spine segment during loading in axial rotation, while the resection of additional parts did not further increase intersegmental rotation.
To summarize, these studies have shown that surgical interventions of decompression, with the removal of soft tissues and facets joints, could lead to iatrogenic instability altering the physiological load transfer. The removal of laminae does not produce immediate instability, but a progressive deformation of the spine: the weight and the muscular pull overstretch the remaining ligaments modifying the postural balance. Laminectomy can cause problems regarding the stability, but if alone, is not usually associated with a significant postoperative incidence of kyphosis. Furthermore, during these types of interventions, there is also the risk of damaging the spinal nerves which run in the vertebral foramen near the lamina[91].
After these interventions on facets and laminae, the surgeons usually stabilize the spine using different types of instrumentation and fixing different levels of the spine. The biomechanical effects of spinal instrumentations has been reviewed by others[15, 92-94,93,15] and is not included in the present review.

3.4 Conclusions

Local or generalized degeneration and instability can occur when the integrity of its substructures is compromised. Spinal dysfunction is investigated considering each structure separately, single FSU or the spine as a whole. Analysis of normal structure under controlled laboratory environment or dedicated numerical models can provide useful information to understand the role of each structure in spine stability. Unfavorable mechanical loading conditions, inappropriate surgical techniques and impaired hardware applications can be studied to evaluate their responsibility for the degradation process. This review has shown that systematic knowledge has been gathered about the untreated spine, while the understanding about the role of the different ligaments and about the effect of lesions of facets and lamina is limited.
This review has shown that most invasive surgical interventions performed on the intervertebral ligaments, facet joints and lamina to reduce compression of the spinal cord and/or nerve roots compromise spinal stability (especially in the sagittal plane). This can determine mid-term and long-term complications and degeneration requiring furthermore invasive corrective surgery.
Several techniques have been developed for the evaluation of FSU biomechanics and functionality including different *in vitro* techniques. While the structural behaviour of entire spine segments and local deformations in bone (e.g. measured with strain gauges), are well documented, new techniques as DIC are promising to analyze not only the hard tissues, but also the soft tissues (intervertebral discs, ligaments). This will help to better understand the role of these structures, and what occurs when they are damaged or removed during surgery. To complement *in vitro* biomechanical tests and overcome their limitations, properly developed and validated numerical models of the human spine will be extremely important.

Table. 3.1 - Possible approaches to investigate the biomechanics of the spine, including different investigation tools, different type of specimen, and different kinds of simulation

Reference	Origin	Segment	Type of study	Loading condition	Focus	Type of lesion	Measured quantity
Investigations on biomechanics of the untreated spine							
[58]	human	review covering different types of segment ad different conditions					
[60]	human	review covering different types of segment and different conditions					
[59]	human	review covering different types of segment and different conditions					
[7]	human	review covering different types of segment and different conditions					
[1]	human	occiput - S1	*in vitro*	FE, LB, AR	intact	none	ROM, IAR,
[33]	human	T1-L4	*in vitro*	FE, LB, AR	intact	none	ROM, NZ, stiffness
[56]	human	L1-S	*in vitro*	FE, LB, AR	intact	none	ROM
[57]	human	L2-S	*in vitro*	FE, LB, AR	intact	none	ROM
Biomechanics of uncompromised spine ligaments							
[66]	human	review covering different types of segment ad different conditions					
[64]	human	C2-T1	*in vitro*	tensile	ALL, PLL, ISL, LF	uncompromised	stress, strain, stiffness, energy
[61]	human	T12-S	*in vitro*	tensile	ALL, PLL, ISL, SSL, LF	none	ROM, stiffness, stress, strain, energy
[48]	human	lumbar	*in vitro*	tensile	ALL, PLL, ISL, SSL	none	organization of collagen, stiffness
[63]	porcine and human	lumbar	*in vitro*	tensile	ISL	different cuts of the collagen fiber network	ROM
[65]	human	L3-L5	*in vitro*	axial traction	intraforaminal ligamentous structures	uncompromised	load force

Published in: Critical Reviews™ in Biomedical Engineering, 2019, 47: 295-322

Lesions of ligaments							
[50]	human	C4-C6	FEM	FE	ALL, PLL, ISL, SSL, LF, CL	lesions	ROM
[74]	human	C4-C6	FEM	compression, anterior-posterior shear, LB	ALL, PLL, ISL, SSL, LF, CL	injury simulation	ROM
[72]	human	C1-T1	*in vitro*	frontal impact simulation	PLL, ISL, SSL, LF, CL	none	strain
[73]	human	C1-C3	FEM	FE, LB, AR	ALL, PLL, LF, CL, AAOM, alar ligament, apical ligament	none	ROM
[71]	human	T11-T2	*in vitro*	FE	ALL, PLL, ISL, LF	progressive resection of all the ligaments (from the most anterior to the most posterior one, and vice-versa)	ROM
[67]	human	T11-L3	*in vitro*	FE, LB, AR	ISL, SSL, LF	sequential transection of the posterior ligamentous complex	ROM, NZ,
[69]	human	L2-L5	*in vitro*	FE	ISL, SSL	resections of ligaments	ROM, IAR
[70]	porcine	L4-L5	*in vitro*	FE	ISL, SSL, LF	sequence of ligaments resections	ROM, stiffness, laxity zone
[75]	human	L4-S1	FEM	FE, LB	ALL, PLL, ISL, SSL, LF, CL, IL	none	ROM
Biomechanics of facets and lamina							
[50]	human	cervical	FEM	FE	intact	none	ROM
[79]	human	T10-L1-L4	*in vitro*	compression	intact	none	strain
[78]	human	L4-L5	*in vitro*	FE	intact	none	strain
Lesions of the facets and lamina							
[83]	goat	C3-C5	*in vitro*	FE, LB, AR	laminectomy, laminoplasty	none	ROM, stiffness

[72]	human	C2-C7	FEM	FE, LB, AR	laminectomy and unilateral/bilateral facetectomy	none	ROM
[95]	human	C2-C7	FEM	FE, LB, AR	laminectomy, hemilaminectomy	none	ROM
[68]	canine	T12-L7	*in vitro*	4-point bending	multiple hemilaminectomies	none	ROM, NZ, stability
[86]	human	T3-T9	*in vitro*	FE, LB, AR	anterior to posterior and posterior to anterior sequence of resections	none	ROM
[82]	human	L2-S2	*in vitro*	FE, LB, AR	laminectomy	none	ROM, NZ
[74]	human	L2-S1	FEM	FE, LB, AR	left/bilateral hemifacetectomy, left hemilaminectomy, bilateral laminectomy, two-level laminectomy	none	ROM, stress
[79]	human	L2-L3	FEM	FE, LB, AR, anterior and posterior shear load	laminectomy, facetectomy	none	anulus stress, ROM
[75]	human	L2-L3	FEM	compression, tension, anterior and posterior shear pression	facetectomy	none	flexibility, ROM
[84]	porcine	L4-L5	*in vitro*	FE	bilateral laminotomy, laminectomy	none	ROM
[81]	human	L3-S1	*in vitro*	FE, LB, AR	laminectomy	none	ROM
[85]	human	L1-L5	*in vitro*	FE	laminectomy, laminotomy	none	ROM

LEGEND OF TABLE 3.1:

Loading condition:
FE = flexion-extension
LB = lateral bending
AR = axial rotation

Ligaments:
PLL = posterior longitudinal ligament
ALL = anterior longitudinal ligament
ISL = interspinous ligament
SSL = supraspinous ligament
LF = ligamentum flavum
CL = Capsular ligament
IL = intertransverse ligament
AAOM = anterior atlantoaxial ligament

Measured quantity:
ROM = range of motion
IAR = instantaneous axis of rotation
NZ = neutral zone

Table 3.2 - Overview of the conditions under which the biomechanics of the spine must be investigated

Measured quantity	Author	Type of study	Segment	Flexion-extension	Lateral bending	Axial rotation
ROM, IAR,	[1]	human, *in vitro*	cervical, thoracic, lumbar	cervical: 8°-17° thoracic:4°-12° lumbar: 12°-20°	cervical: 0°-11° thoracic: 6°-9° lumbar: 3°-10°	cervical: 0°-47° thoracic: 2°-9° lumbar: 2°-5°
stiffness, strength	[58]	human, *in vitro* & FEM	cervical, thoracic, lumbar	for individual vertebra, vertebroplasty appears to increase or return strength to the pre-fracture level, whereas the stiffness is not always restored		
				for multiple -vertebra segments, the strength of the unit as a whole appears to decrease, with failure occurring in the non-augmented vertebrae		
ROM, stiffness, NZ, stress	[60]	review covering: human, *in vitro* & FEM	cervical, thoracic, lumbar	Focus on the recent progress in spine biomechanics. Topics addressed include the whole spine, the FSU and the individual components of the spine (e.g. vertebra, IVD, spinal ligaments)		
fatigue, creep	[47]	review covering human, *in vitro* & FEM	cervical, thoracic, lumbar	Focus on the tests parameters and acceptance criteria (number of cycles, duration in time, stress levels, acceptable amount of creep) for possible tests specifically relevant to cements for spinal applications		
ROM, NZ	[7]	review covering: human, *in vitro* & FEM	cervical, thoracic, lumbar	Overview of the techniques and results obtained by studies that have attempted to characterize mechanically the IVD		
ROM	[56]	human, *in vitro*	lumbar	flexion: motion at caudal lumbar levels significantly greater than at cephalic levels	the main motion is greater between the L2-L3	similar motions between L4-L5 and L5-S1
				extension: the largest motions are at the level between the L5-S1		
ROM	[57]	human, *in vitro*	lumbar	coactivation of muscles causes a 13% increase of the sagittal ROM	coactivation of muscles causes a 20% decrease in ROM (significant increase in stability)	

ROM, NZ, NZ stiffness	33	human, *in vitro*	lumbar	highest ROM and NZ and lowest NZ stiffness values at T1-T4 and L1-L4 regions	ROM and NZ decreased NZ stiffness increased from high to low vertebral levels

LEGEND OF TABLE 3.2:
IVD = intervertebral disc

Measured quantity:
ROM = range of motion
IAR = instantaneous axis of rotation
NZ = neutral zone

Chapter 4

Digital Image Correlation

In order to investigate the biomechanics of biological specimens (such as biological tissues, organs or their interactions with devices), the measurement of displacement and strain is a very import task during the experimental tests (Fig. 4.1). With testing machines, loads and displacements are recorded at the extremities of the specimen but there is a lack of information on what happens on the surface of the specimen. This is extremely important especially if the specimen, like all biological tissues, are inhomogeneous and anisotropic.

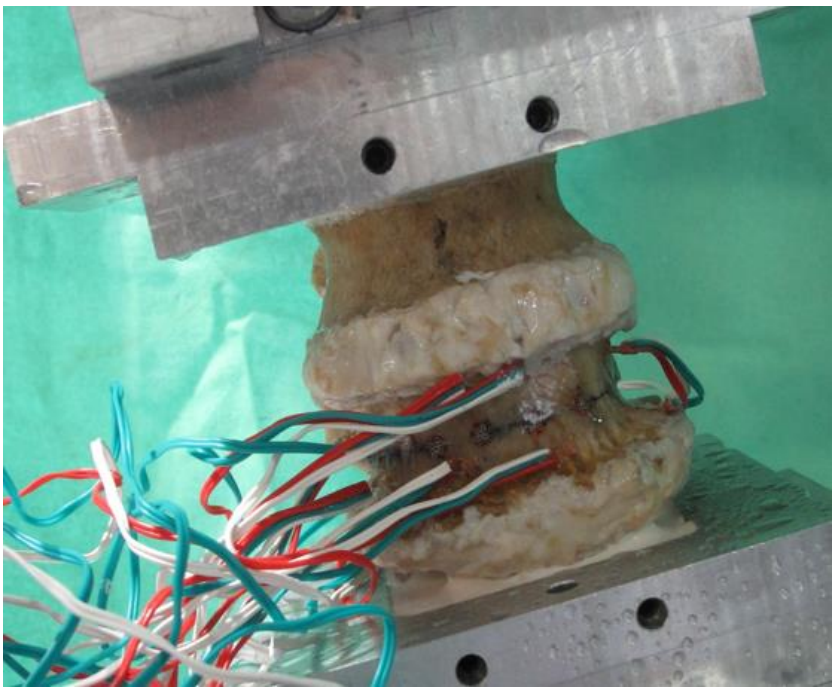

Fig. 4.1 - Measurement of the strain on a vertebra using strain gauges[38]

Strain gauges allow to measure with great precision the deformation in the point of application but nothing is known in the adjacent points. So, if a specimen is not homogeneous and therefore one part is deformed more than another, the results obtained depend too much on the positioning of the strain gauges. Some authors have applied strain gauges on bone tissues (vertebrae or femur) to measure the deformation during the application of the load but, if the specimen is not rigid enough (such as intervertebral discs or ligaments), the strain gauge can alter the tissue reinforcing it. Therefore, in this case, what is measured is not the deformation of the tissue but the reinforcing effect of the strain gauge. Moreover, the application of strain gauges on a hydrated surface is not so simple.

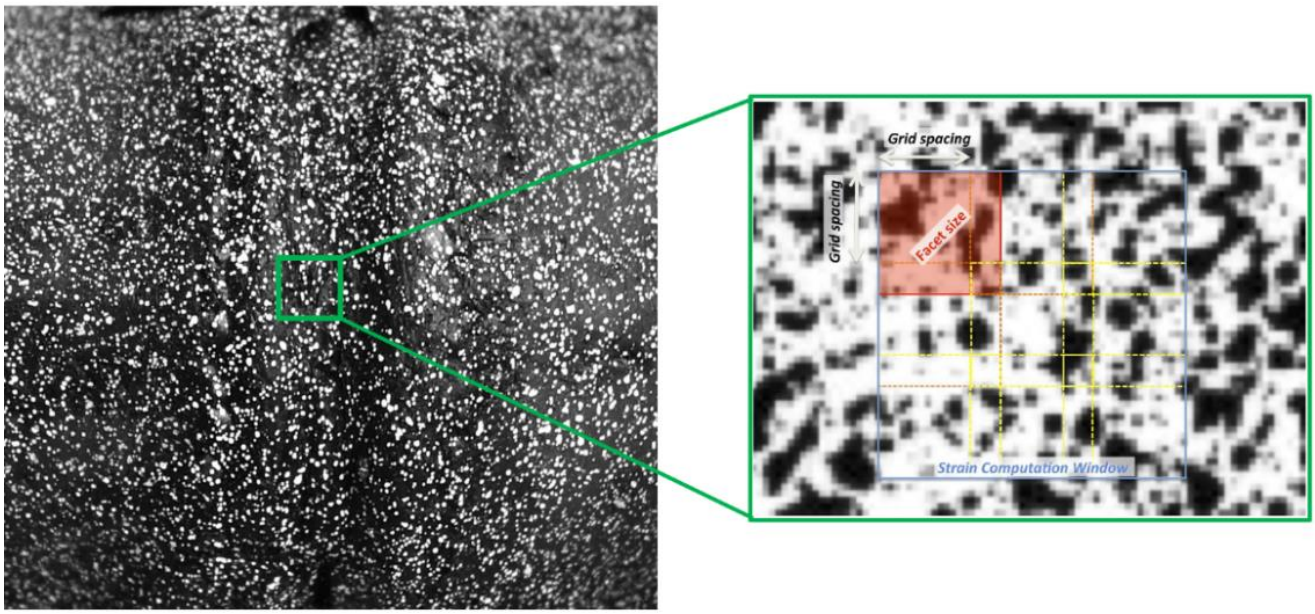

Fig. 4.2 - The white-on-black speckle pattern on the surface on a vertebra with the identification of the facet size and grid spacing[96]

DIC allows to obtain a measurement of displacement and strain in a full-field and contact-less way (not limited to a few points and furthermore the surface of the specimen is not altered by the use of the tool which could modify the biomechanical behavior). Different images are acquired using one (2D version) or more (3D version) cameras and compare in order to calculate the relative displacements and, by a derivation, the deformations. Usually the first images (called reference image) is taken when the specimen is in unload condition while the following images are taken when the specimen is subjected to the application of loads. To compare the different images, the software of the DIC divides the acquired images into sub-images, called facets of M×N pixels. Each facet is summarized by the information about the pattern and its location in space. The correlation algorithm identifies the best-matching region at different loading steps. At first, the displacements have been computed for each facet and subsequently, deriving the displacement, the strain field is computed. To allow this, the surface of the specimen must have a random pattern (Fig. 4.2). Sometimes the surface of some tissues presents a natural random pattern due to an intrinsic texture or inhomogeneity (such as the surface of heart). In other cases (such as for vertebra, intervertebral discs or ligaments) an optimized pattern must be prepared with some requirements:

1. Random distribution, in order to make each area of the surface of the specimen univocally identifiable
2. High contrast, to allow the image correlation algorithm works effectively
3. Black/white or white/black ratio of 50:50, to avoid regions that cannot be properly recognized
4. Roughness should be kept at minimum, in order to avoid alteration of the surface geometry
5. Probably the most important issue in biomechanical applications is the size of the speckle dots (in relation to the specimen size), in order to optimally exploit the resolution of the camera

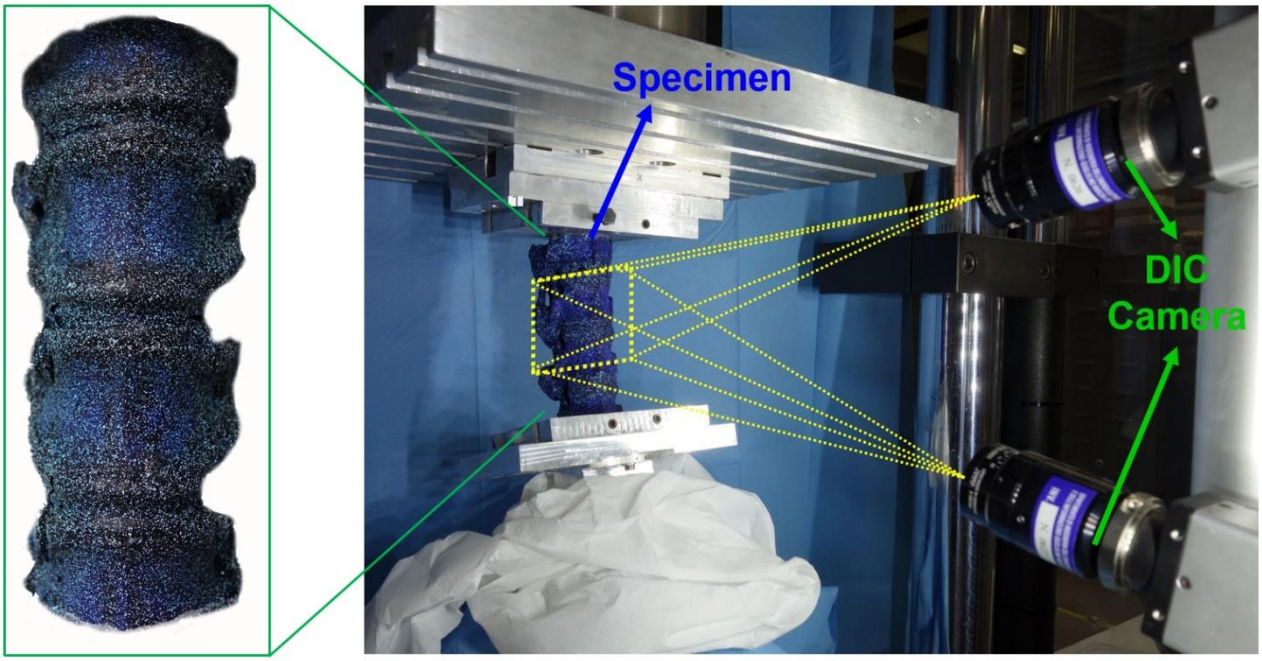

Fig. 4.3 - The setup of a test with the Digital Image Correlation. On the right there are the two DIC-cameras that have the same field of view of the specimen. On the left there is the anterior side of the specimen with the application of the speckle patter for the DIC analysis

For all the tests that I performed on the spine, the pattern used was white-on-dark (Fig. 4.3). The white speckle pattern is painted using an airbrush airgun changing the air pressure and the airflow according to the desired size of the dots.[41] Like all measurement techniques, also DIC is affected by measurement errors. These errors could be divided in systematic errors and random errors. The systematic error is generally negligible (in the order of 0.02 pixel size and few microstrain).[41, 97] The random errors are more critical than systematic errors: after the optimization of all parameters the errors can decrease below 100 microstrain.[41, 97] If all parameters of DIC are not optimized, errors of few thousands of strain (2000/3000 με) could be recorded and therefore the measurements that are carried out may be inconsistent with the real deformations.[96, 98] Errors are minor on displacement measures, while they increase on deformation measures due to the derivation process.[96]

Chapter 5

Application of Digital Image Correlation on hard and soft tissues simultaneously

From the manuscript

Full-field *in vitro* investigation of hard and soft tissue strain in the spine by means of Digital Image Correlation [99]

Maria Luisa Ruspi[1], Marco Palanca[1], Cesare Faldini[2,3], Luca Cristofolini[1]

1 Department of Industrial Engineering, School of Engineering and Architecture, Alma Mater Studiorum - University of Bologna, Bologna, Italy
2 Department of Biomedical and Neuromotor Sciences, Alma Mater Studiorum University of Bologna, Italy
3 2nd Orthopaedic and Traumatologic Clinic, Rizzoli Orthopaedic Institute

The authors wish to thank Muscles Ligaments and Tendon J for providing the permissions to re-use the manuscript titled *"Full-field in vitro investigation of hard and soft tissue strain in the spine by means of Digital Image Correlation"* in the present Ph.D thesis.

Published in: Muscles Ligaments and Tendon J, 2018, 16: 538-545

5.1 Introduction

The spine is one of the most complex structures of the musculoskeletal apparatus with the task of sustaining the body, permitting the movements and protecting the spinal cord. The mechanical structure consists of a sequence of hard tissues (vertebrae) and soft tissue (intervertebral discs), stabilized by other soft tissue (ligaments); they all control the movement in flexion-extension, lateral bending and axial rotation.[33] For instance, failure of posterior fixation and proximal junction kyphosis (PJK) are still unsolved problems.[19] Investigating the biomechanics of the spine is a fundamental task because it could help engineers and clinicians to design implants with a higher success ratio.[100] Spine segments were frequently analysed in experimental tests applying known motions or known loads.[56,101] During these tests, stiffness can be evaluated simulating the kinematics of the spine segment as a whole, in physiological conditions, pathological conditions and after treatments conditions.

Strain in the vertebral body can be measured using strain gauges, but these measures are limited to the point of application of the strain gauges.[38,35] A detailed quantification of the local strain distribution could be help to elucidate the failure mechanism and under- stand the reasons of many post-operative complications. The measurements techniques used so far to measure strains are inadequate in many respects to understand the origin of such problems. Measuring the distribution of strain in the spinal soft tissues (such as the intervertebral discs and ligaments) would be a key point. However, this is extremely difficult because of the inhomogeneous and anisotropic properties of such tissues. Strain gauges cannot be used to measure the deformations of the soft tissue, because they would increase the stiffness of the structure and would significantly bias the measurement.[102] Another technique which can be used to measure local strains is Digital Volume Correlation (DVC), which allows measuring strain inside the structure of the vertebral body.[103] Nevertheless, the use of DVC is affected by the time-consuming procedure of images acquisition, which could be a problem with viscoelastic specimens, such as the bone or the intervertebral discs.[104] Some of unsolved questions about the functionality of the spine concern what happens on the spine segment in terms of local deformation, presence of stress concentration, how the biomechanics of the spine is affected by spinal fixation devices, where the failure point is located (for instance slipped disc, proximal junctional kyphosis, pull-out of the screws, rupture of the bars), or how the spine ligaments work under the different loading conditions. All such clinical problems are not addressed with current *in vitro* methods.[19,100,105,106] Up to date, an experimental description of the strain distribution on the surface of a spine segment that includes the vertebrae, the discs and the ligaments at the same time is missing.

The spine is a combination of different organs (consisting of hard and soft tissues) acting in synergy with a complex biomechanical function. Therefore, it is very important to obtain quantitative and accurate information about the distribution of strain, simultaneously in the hard and soft tissues in order to better understand the behaviour and the failure mechanisms of such a complex structure. A preliminary study has demonstrated that the strain distribution on the surface of an entire spine segment can be measured with sufficient accuracy and precision.[40]

The aim of this work was to explore the feasibility and the potential of using DIC to measure the strain distribution simultaneously on the vertebral bodies, the intervertebral discs, and the spine ligaments of thoracic and lumbar spine segments in different *in vitro* loading configurations.

5.2 Materials and methods

5.2.1 Specimens

Three segments of four vertebrae (T7-T10, T11-T14, L2-L5) were extracted from porcine spines. The animals were sacrificed for alimentary purposes. The animals were approximately 9 months old and 100 kg at sacrifice. The specimens were cleaned using surgical tools: the muscles, the anterior longitudinal ligament, the periosteum and the ribs were carefully removed without damaging the vertebral bodies and the intervertebral discs. Conversely, the interspinous, supra- spinous and posterior longitudinal ligaments, and the capsules were left intact in order to preserve the natural kinematics during the tests15. The central disc of each segment (respectively, the disc between vertebrae T8 and T9 of segment T7-T10, between T12 and T13 of segment T11-T14, and between L3 and L4 of segment L2-L5) was aligned horizontally in the frontal and lateral views with the use of a six-degree-of-freedom clamp. The extremities of the specimens were potted in poly-methyl-methacrylate (PMMA). The two pots were parallel to one another (Fig. 5.1).

5.2.2 Mechanical testing

Different loading conditions were used to investigate the biomechanics of the multisegmental spine specimens in terms of deformation of the vertebral bodies, intervertebral discs and ligaments17. The load was applied using a servo-hydraulic universal testing ma- chine (8032, Instron, High Wycombe, UK) in displacement control. One extremity of the specimen was rigidly fixed to the testing machine while the other extremity was loaded through a spherical joint, which could move on a rail. This system avoided transmission of any other load component.
Two different loading configurations were simulated (Fig. 5.1) using an eccentric compression load (simulating flexion-extension and lateral-bending), similar to many past studies:

- anterior bending: the vertical force had an anterior offset equal to the 20% of the antero-posterior depth of the central intervertebral disc. In this case the rail was set in the anterior-posterior direction
- lateral bending: the vertical force had a lateral offset equal to the 20% of the lateral-lateral width of the central intervertebral disc. In this case the rail was set in the lateral-lateral direction.

The load condition did not aim to replicate any specific motor task, but to reproduce simplified scenario and highly reproducible loading conditions, in order to assess the feasibility of using DIC in this kind of application. Once verified the feasibility of DIC measurement, scenarios closer to real motor tasks can be reproduced to obtain useful quantitative information. Ten preconditioning cycles were applied between 0 and 1.0 mm of compression at 0.5 Hz. A compression of 3.0 mm was applied for each loading configuration in 0.1 mm steps, while DIC images were acquired at each step. The final compression of 3.0 mm corresponded to a force of the order of 600 N (approximately 60% of the animal's body weight) for anterior bending, and of 1100 N (approximately 110% of the animal's body weight) for lateral bending. The test was designed to avoid specimen damage, based on some preliminary tests: the strain in the vertebral body did not exceed 2000 microstrain[107], while strain in the intervertebral discs was below 100000 microstrain (these values were comparable to the values reported in literature associated to physiological load).

Published in: Muscles Ligaments and Tendon J, 2018, 16: 538-545

5.2.3 Digital Image Correlation

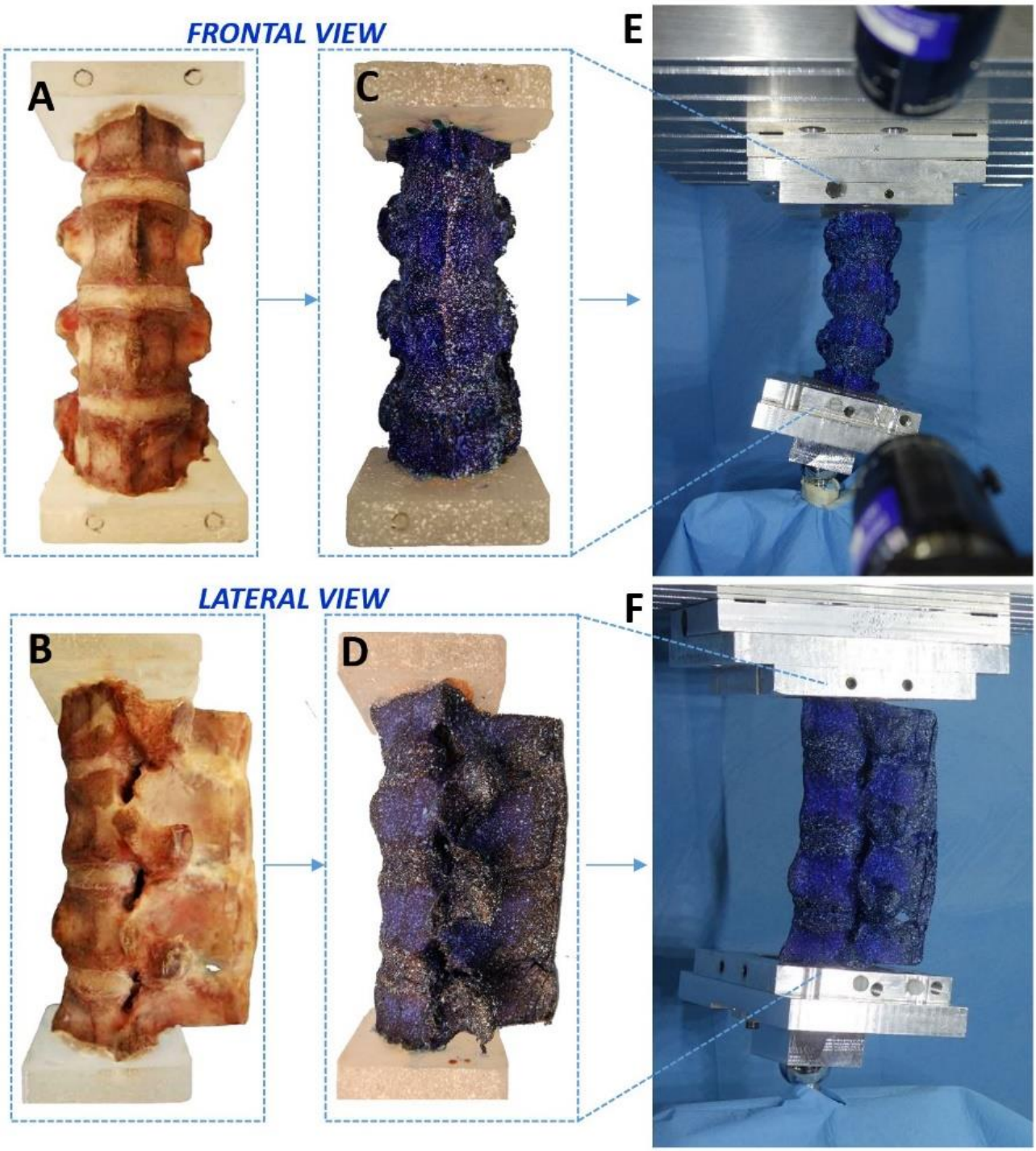

Figure 5.1 - The porcine spines were cleaned removing the sur- rounding tissues (A, B). A white-on- black speckle pattern was pre- pared, which covered the hard and soft tissues (C, D). Each specimen was subjected to lateral bending (E, in a frontal view) and to anterior bending (F, in a lateral view). The different loading configurations were reproduced using a universal testing machine and a dedicated system of low-friction linear and ball bearings to avoid transmission of undesired force components

In order to track the different areas of the specimen surface and compute the displacements and strains, digital image correlation systems require a high-contrast speckle pattern on the region of interest. A white-on-black pattern was prepared on the entire multisegmental spine specimens (both the vertebrae and the intervertebral discs)[103] (Fig. 5.1). The multisegmental spine specimens were first dyed with a dark background, with a solution of methylene-blue and water (4 g of methylene-

blue per 100 ml of water) for three times for the vertebral body and two times for intervertebral discs (to limit as much as possible the increase of stiffness in soft tissues). Methylene-blue preparation has been shown to only marginally alter the mechanical properties of soft tissue.[41] The white speckle pattern was then applied with the appropriate dot size, following an optimized procedure.[41, 96] To measure displacements and deformations, we used a commercial 3D-DIC system (Q400, Dantec Dynamics, Skovlunde, Denmark) with its proprietary software (Instra 4D, v.4.3.1, Dantec Dynamics). To obtain a stereoscopic vision, images were acquired by two cameras (5 Megapixels, 2440 x 2050 pixels, 8-bit) with high-quality 35 mm lenses (Apo-Xenoplan 1.8/35, Schneider-Kreuznach, Bad-Kreuznach, Germany). The field of view was set to 70 mm by 60 mm, which gave a pixel size of about 30 micrometers. Calibration was performed before the tests using a dedicated calibration target (Al4-BMB-9x9, Dantec Dynamics). To provide sufficient illumination, arrays of cold-light LEDs (10000 lumen in total) were specifically prepared for this test. The parameters for the acquisition of the images and for the correlation analysis were preliminarily studied and optimized to minimize errors[40]: facet size: 33 pixels, grid spacing: 19 pixels, contour smoothing: local regression with a kernel size of 5x5 pixels. These parameters provided a spatial resolution of the order of 3 mm. The DIC system permitted to investigate the displacement and the strain in a contact-less way providing a full-field view of the examined surface, including the intervertebral discs and the vertebrae (Fig. 5.1). In order to examine the biomechanical behaviour of the spine, two different acquisitions were performed for each loading configuration and each specimen (Fig. 5.1):

- frontal view: the cameras pointed to the anterior face of the spine segment;
- lateral view: the cameras pointed to the lateral side (either right or left) of the spine segment.

The tests started from the unloaded condition (reference step, no load applied). A total compression of 3.0 mm was applied in steps of 0.1 mm. Images were taken at each step with the DIC system.

5.3 Results

In all the tests, the DIC system permitted to success- fully evaluate the deformations of the entire multisegmental spine specimens from a frontal and sagittal view, with different loading configurations. More than 95% of the region of interest was successfully tracked by the DIC software, providing a truly full-field analysis of the displacements and deformations. Preliminary checks in an unloaded configuration confirmed that the errors with the selected settings did not exceed 140 microstrain.
The three specimens showed similar strain distributions. For all loading configurations, the intervertebral discs and the ligaments reached larger deformations than the vertebral bone of the vertebrae (Figs. 5.2-5.4). Since the specimens belonged to young animals, the DIC analysis showed larger deformations of the cartilage part of the vertebrae (growth plate), which are significantly softer than the vertebral bone.

5.3.1 Anterior bending

During the anterior bending, the intervertebral discs reached larger deformations than the vertebral bone. On the frontal part of the intervertebral discs, the maximum principal strain was in the order of +20000 microstrain (tension) and it was aligned circumferentially, while the minimum principal strain was in the order of -40000 microstrain (compression) and was aligned axially (Fig. 5.2). On the frontal part of the vertebrae, the strains were one order of magnitude lower: the maximum principal strain was in the order of +500 microstrain (tension), while the minimum principal strain was in the order of -5000 microstrain (compression) (Fig. 5.2).

Published in: Muscles Ligaments and Tendon J, 2018, 16: 538-545

In the lateral sides of the spine segment, the DIC analysis confirmed that there was a strain gradient on the intervertebral discs, with the largest tensile strains in the posterior region, and the largest compressive strain in the anterior region (Fig. 5.3). The maximum principal strain ranged between +15000 microstrain (tension) in the median disc of the specimen and +45000 microstrain (tension) in the upper and lower disc of the specimen, while the minimum principal strain was in the order of -50000 microstrain (compression) in the median and lower discs of the specimen. The lateral parts of the vertebrae showed lower strains than the disc due to the grater stiffness of the bone: the maximum principal strain was below +1000 microstrain while the minimum principal strain was in the order of -2500 microstrain (Fig. 5.3).
In anterior bending, the interspinous and supraspinous ligaments showed large tensile longitudinal deformations: the maximum principal strain was in the order of +45000 microstrain (tension). Additionally, the transversal shrinkage associated with the longitudinal stretching (due to Poisson effect) was visible in the ligaments: the minimum principal strain (compression) was between -20000 microstrain (in the interspinous ligament) and -40000 microstrain (in the supraspinous ligament) (Fig. 5.3).

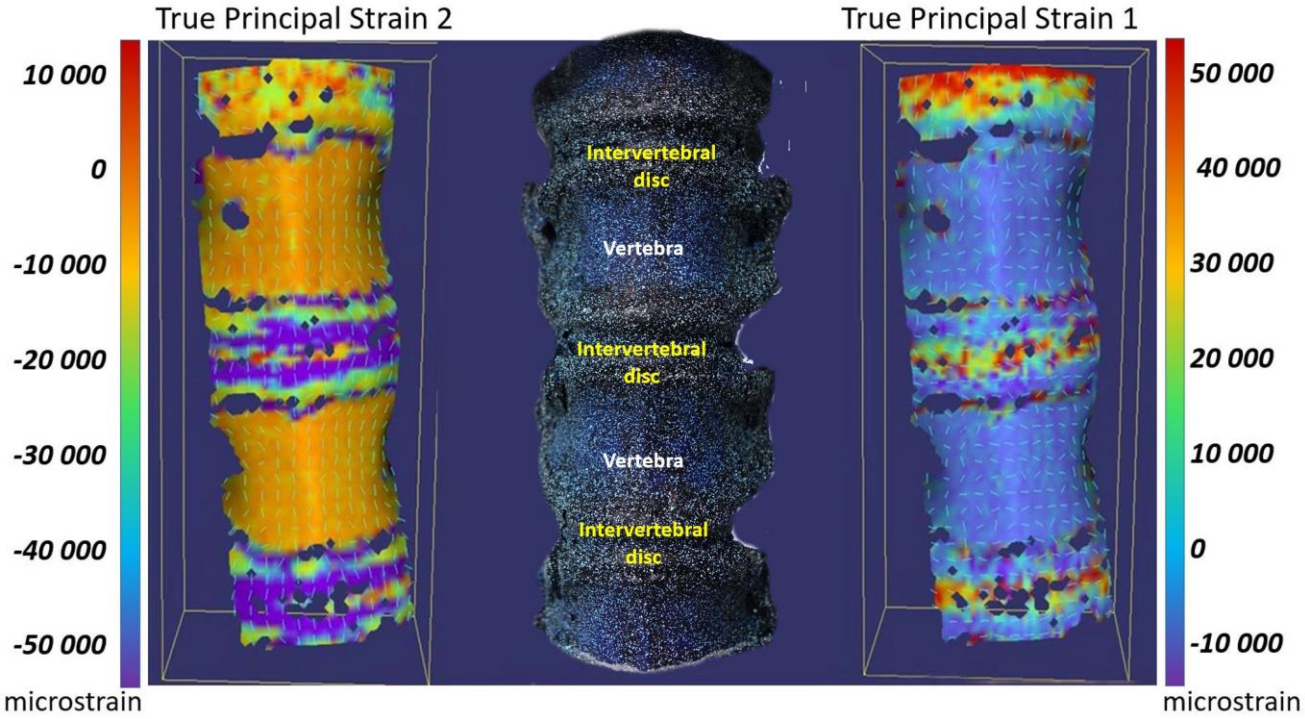

Figure 5.2 - Different deformation of vertebral body, growth cartilages and intervertebral discs during an anterior bending test from a frontal view. The image on the left shows the minimum principal strain (compression), the central image shows the specimen as viewed by the cameras, the image on the right shows the maximum principal strain (tension)

5.3.2 Lateral bending

Lateral bending was applied both towards the right and the left sides, to all specimens: the strain distribution measured on intervertebral discs and vertebrae in all the configurations was symmetrical. In the frontal region, the tensile and compressive strains measured by DIC were consistent with the direction of applied bending (Fig. 5.4). The maximum principal strain in the discs ranged between +20000 microstrain (tension) in the compressed side to +50000 microstrain (tension) in the stretched side. The minimum principal strains in the discs ranged from -50000 microstrain (compression) in the compressed side to +5000 microstrain (tension) in the stretched side. The orientation of the tensile

strain changed from circumferential on the compressed side of the disc (due to swelling) to axial on the stretched side (due to traction). The frontal portion of the vertebrae had lower strains than the discs: the maximum principal strains were lower than +500 microstrain (tension) while the minimum principal strains did not exceed -5000 microstrain (compression) (Fig. 5.2).
In the lateral view, the strain distribution measured on the intervertebral discs was approximately uniform (Fig. 5.3). The maximum principal strain in the discs reached +45000 microstrain (tension) in the compressed side while the minimum principal strain in the discs was -50000 microstrain (compression) in the compressed side. The lateral parts of the vertebrae had lower strains than the intervertebral discs: the maximum principal strains were lower than +1000 microstrain (tension) while the minimum principal strains did not exceed -2000 microstrain (compression).
As expected, in lateral bending, the interspinous and supraspinous ligaments showed smaller deformations than in anterior bending: the largest deformation was measured in the interspinous ligament: while the maximum tensile strain (tension) was negligible, the minimum principal strain (compression) was in the order of -25000 microstrain (Fig. 5.3).

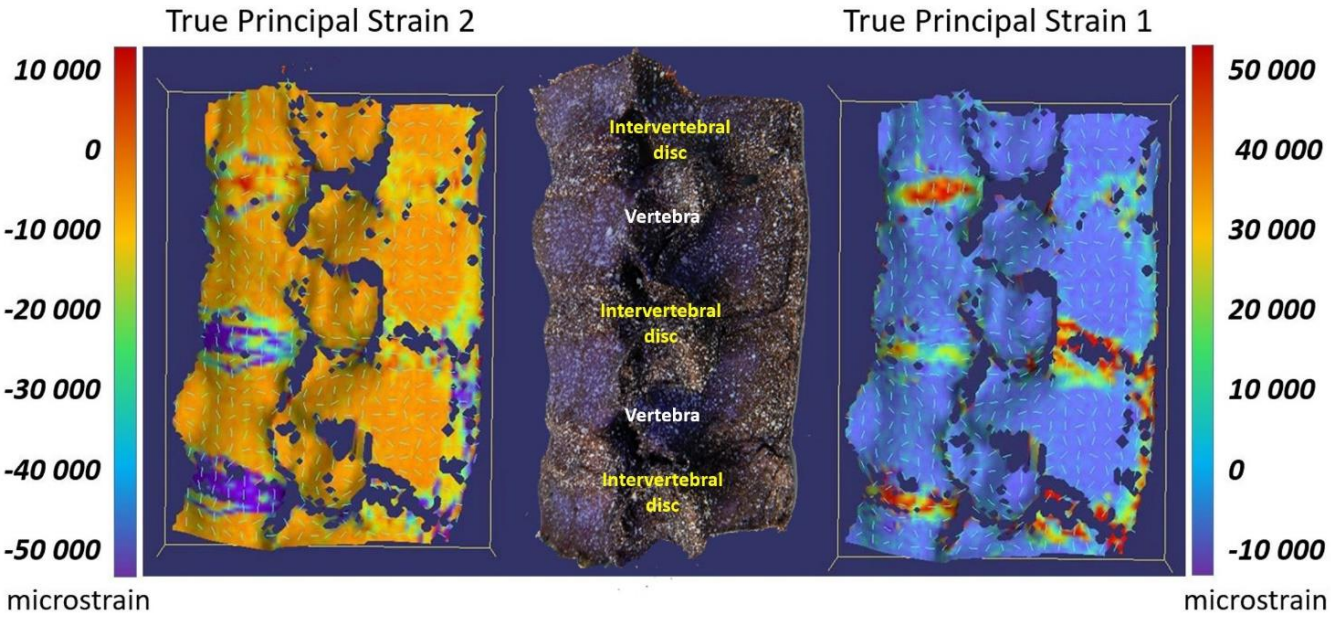

Figure 5.3 - Different deformation of vertebral body, intervertebral discs and ligaments (interspinous and supraspinous ligaments) during an anterior bending test from a lateral view. The image on the left shows the minimum principal strain (compression), the central image shows the specimen as viewed by the cameras, the image on the right shows the maximum principal strain (tension)

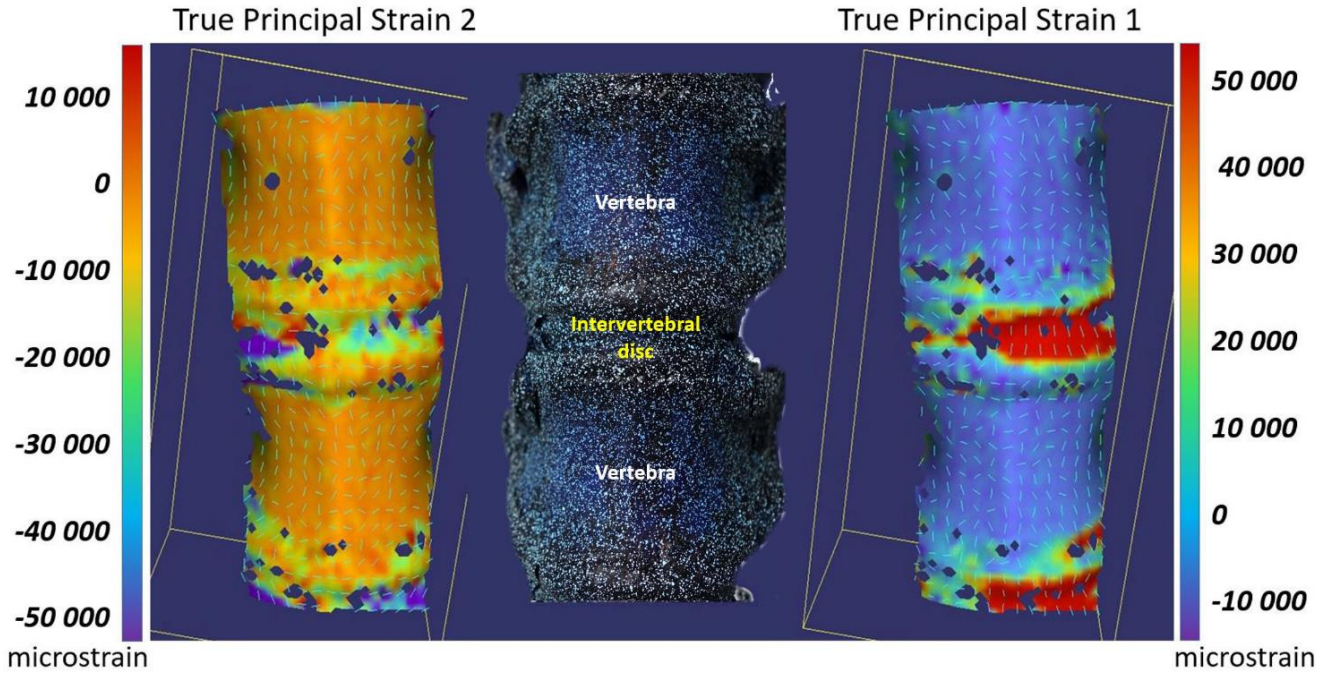

Figure 5.4 - Different magnitudes of strain were visible in the vertebral body, growth cartilages and intervertebral discs during a lateral bending test from a frontal view. The image on the left shows the minimum principal strain (compression), the central image shows the specimen as viewed by the cameras, the image on the right shows the maximum principal strain (tension)

5.4 Discussion

The main aim of this work was to analyse the biomechanics of the spine measuring the strain distribution on thoracic and lumbar multisegmental spine specimens, simultaneously on hard tissues (the vertebral bone) and soft tissues (the intervertebral discs and ligaments) using digital image correlation.

The spines were tested in two different loading configurations (anterior and lateral bending), frequently simulated in the biomechanics literature.[33,86] To examine both the hard and soft tissues, the specimens were observed from two different points of view. In all the tests, the DIC system evaluated successfully the deformations of the entire multisegmental spine specimens from a frontal and lateral view. The measurements showed the different magnitude and direction of the strain in the vertebral bones, in the intervertebral discs and in the interspinous and supraspinous ligaments. This confirms the importance of investigating the biomechanics of the spine with a full-field tool. It is worth remarking that the measurement technique adopted is contact-less and causes minimal perturbation to the biological specimen under observation. The strains measured in the vertebral body were lower than the strains in the intervertebral disc and in the supraspinous and interspinous ligaments. DIC identified that different portions of the intervertebral disc were subjected to compression or tension with different orientations of the principal strain: as expected, in the compressed side of the disc the compressive strains were axial, while circumferential tensile strains were observed. For instance, during the anterior bending, the frontal part of the intervertebral disc was compressed but at mid-height a small region with ten- sile hoop strain was visible. In fact, when the disc is compressed axially, it swells and the surface expands at mid-height. Since the specimen belonged to young animals, DIC showed also larger deformation in the growth plate than in the neighbouring vertebral bone. Also the deformations of interspinous and supraspinous ligaments were

successfully measured. As expected, in anterior bending the deformations of these two ligaments were greater than the deformations during lateral bending. At the same time, the transverse shrinkage associated with the longitudinal stretching could be observed.
Very few papers can be found in the literature that can be directly compared with our *in vitro* measurements. In the literature, usually multisegmental spine specimens were investigated in terms of range of motion[33, 100] and stiffness.[33,108] In the vertebrae, strains were evaluated in a point-wise way using strain gauges, which offer an accurate and precise value of the strain, but limited to those points where strain gauges are applied. The ranges of strain measured in the vertebral bone in the present study compare well with the range of strain experience by bone during physiological motor tasks.[109] The values measured in the porcine vertebral bone in the present study are similar to those measured with strain gauges in Cristofolini *et al.*[38] even if this study used human lumbar specimens. A problem associated with the use of strain gauges is due to the reinforcement effect caused by their application on the surface. Furthermore, strain gauges cannot be used on the intervertebral discs because the discs have a low elastic modulus and so direct comparison with strains in the intervertebral discs is difficult. Some studies analysed the vertebral body using DIC system but without taking into account the contiguous intervertebral discs.[40] For example, Gustafson *et al.*[110] tested the strains on segments of thoracic and lumbar porcine spine with strain gauges and DIC. While they reported serious problems with their application of strain gauges, direct comparisons are possible with their DIC measurements. The DIC-measured average peak minimum principal strain was -2731 microstrain while the average peak maximum principal strain was 514 microstrain. These values are similar to the values reported in the present study.
The vertebral bone was studied also with the DVC (Digital Volume Correlation). In Danesi *et al.*[111] the strain measured in the undamaged region of the vertebral bone of porcine spine did not exceed the value of -2000 microstrain and this result conformed to the values measured in the present study. Another study[112] performed tests on human spine, obtained data of strain similar to the ones reported in the present study.
Our measurements concerning the local strain distribution in the intervertebral discs can be compared with few previously published studies: in Spera *et al.*[113], they measured the strain distribution in the disc only, whereas their method does not seem applicable to segments comprising both hard and soft tissue. Recently, the feasibility of measuring the full-field strain distribution in the vertebrae and discs by means of DIC was successfully demonstrated.[112]
A limitation of this study is the use of porcine spines instead of human spines. This choice was adopted because this is a preliminary test made to investigate the applicability of the DIC to the vertebral body, the intervertebral disc and the spine ligaments. For ethical motivations, the feasibility study was done on animal specimens, while future studies on the spine biomechanics will be performed on human specimens. Porcine spines are different from human spines in some details (anatomy, different load conditions), but are a valid biomechanical model to demonstrate the feasibility of this new approach.[114] Another limitation relates to the fact that only simplified loading conditions were simulated in this study. However, the proposed approach based on DIC can be used to measure the distribution of strain with any physiological motor tasks (flexion, lateral bending and axial rotation, and any more complex combinations), thus allowing to address the biomechanics of the human spine.

5.5 Conclusion

This study aimed to test the feasibility of using digital image correlation to examine multisegmental spine specimens, with particular attention to soft tissues (intervertebral discs and ligaments). In fact, the strain distribution in the soft tissues cannot be analysed with the traditional techniques. Surface deformations were successfully measured in the vertebral bones, in the intervertebral discs and in the

spine ligaments, highlighting the different magnitude and direction of the strains for the different loading conditions and in the different portions of the spine. The use of DIC can increase the understanding of the biomechanics of the spine, opening the way to new researches in this area (understanding the role of ligaments, studying fixator devices, analysing failures that occur after surgery), and eventually improving spine treatments.

Chapter 6

The effect of loading rate on strain distribution

From the manuscript (under revision)

The effect of the loading rate on the full-field strain distribution on intervertebral discs [115]

Ruspi Maria Luisa[1], Cristofolini Luca[1]

[1] *Department of Industrial Engineering, School of Engineering and Architecture, Alma Mater Studiorum – Università di Bologna, Bologna, Italy*

6.1 Introdution

The anulus fibrosus (AF) is the external part of the intervertebral disc (IVD) and consists of elastic collagen fibers, which wrap the nucleus pulposus (NP) and is attached to the endplates of the cranial and caudal vertebrae.[6] The NP consists of a gelatinous structure rich of poly-anionic proteoglycans situated in the central part of the IVD. The great water content of the NP contributes to dampen the spinal loads and working as a shock absorber when transferring the loads to the surrounding tissues. The load is transferred from the NP to the AF because the nucleus can be likened to a sealed hydraulic system, in which a small loss of fluid leads to a large drop in pressure. In order to map the pressures in the NP and within the AF of the human spinal discs, pressure transducers were used by Ranu *et al.*[116] Pressures in the NP and in the AF were linearly related to each other and to the applied compressive loads. Mechanical strains of the vertebral body had a corresponding trend with the applied compressive loads, when the partial vertebral column was loaded up to the point of bony fracture. The kinematics of the IVD is complex: when the spine is flexed, the NP moves posteriorly, while when the spine is extended, the NP moves anteriorly.[117, 118]

Soft tissues are known to be viscoelastic, exhibiting generally higher stiffness and lower dissipation at high strain rates.[119] The NP exhibits also different characteristics in response to shear deformations depending on the rate of the load, and the NP can be described either as a fluid or as a solid.[120] With the application of the same load, a higher loading rate causes the stiffening of the NP and therefore a smaller displacement of the IVD. Conversely, a lower loading rate causes a lower stiffening of the NP and a greater displacements of the IVD.[121, 122] *In vivo* studies, measuring the intradiscal pressure with a pressure transducer, showed that an increase of the loading rate causes a higher hydrostatic pressure and lower solid matrix strains.[7, 123] This pressure generates tensile stress in the surrounding AF.[116]

Also the tissue of the AF exhibits strong viscoelasticity: there is a significant increase in the modulus at linear region as strain rate increased.[7, 124, 125] However, in the destructive tests, no significant differences in ultimate stress, ultimate strain and strain energy density were observed at different strain rates.[124] The rate dependency in mechanical properties of the AF could be primarily due to collagen fibers and not to the annulus matrix component.[124]

When a multi-vertebra spine segment or a functional spinal unit (FSU) is tested, the structural behaviour (stiffness, range of motion) can be expected to depend on the loading rate.[121, 126-129] High rates involve an increase of stiffness of the structures of the spine due to the viscoelastic response of the different tissues.[7] The ability of the IVD to dissipate energy, and therefore to absorb shock loads, increased with the decrease of the rate.[121] Regarding the range of motion and the neutral zone, no differences were found by Wilke *et al.* using different angular deformation rates (0.6°-5.1°/second).[37] Race *et al.*[121] examined the hysteresis of the load-displacement graphs indicating the energy dissipation of the IVD.

Since parameters related to stiffness are likely to be affected by loading rate, a study[130] examined the effect of those factors on motion parameters derived from continuous motion data. When the loading rate increased there were significant increases in hysteresis area, in hysteresis loop width, and in the upper and lower transition zone slopes.[130] At the same time transition zone width decreases significantly. These findings are quite counterintuitive as seem to contradict the consolidated findings at the tissue level, and past observation about the structural stiffness of the IVD as a whole.

While the structural behaviour of spine segments and the tissue-level viscoelastic properties have been extensively investigated, little is known at an intermediate scale. To investigate the strains on the AF surface and the disc bulging during simple and complex loads, Heuer *et al.* used a three-dimensional laser scanner device.[131] They observed regions with high compressive strain near the endplates. Furthermore, disc bulging stretched the disc at mid height, causing positive strains in that area both in the axial and in the circumferential direction.[131] However, the above study did not consider the possible effects of different loading rates on the superficial strain distribution.

So, what is missing is how the load is distributed between the different structures of the spine at different loading rates. In particular, there is a lack of knowledge of how the strain distribution on the surface of vertebra and of IVD changes as a result of a stiffening of NP with the increase of the loading rate.
The aim of this work was to investigate the local effects of the loading rate on the strain distribution in the IVD. The hypotheses of this work were:

- As the IVD stiffens when the loading rate increases, the strain distribution becomes more uniform between the IVD (more compliant and viscoelastic) and the vertebrae (stiffer and elastic).
- Pre-conditioning attenuates the strain-rate dependent behaviour of the IVD, thus making differences in strain distribution smaller at the different rates.

6.2 Materials and methods

6.2.1 Specimen preparations

Six segments of three vertebrae (L4-L6) were extracted from porcine spines (porcine spines are longer than human ones, up to 6-7 lumbar vertebrae). The animals were sacrificed for alimentary purpose. The specimens were cleaned of all muscles, while keeping intact all the ligaments, and paying attention not to damage the intervertebral discs. The two intervertebral discs were aligned horizontally in the frontal and lateral plane using a six-degrees-of-freedom clamp. The extremities of the segments were potted in poly-methyl-methacrylate (PMMA) cement.

6.2.2 Mechanical test

The load was applied using a servo-hydraulic universal testing machine (8032, Instron, high Wycombe, UK). The cranial side of the specimen was fixed to the upper part of the testing machine while the caudal side was placed on a spherical joint which could move on a rail in antero-posterior direction. To simulate a presso-flexion, a pure compression with an anterior offset of 25 mm was applied (Fig. 6.1).
Each test consisted of the application of a load at fast, medium and slow rate (with a ratio of 1:10:100 between the respective time to reach the full load):

- Fast rate: one load cycle with full load reached in 0.67 s (this was the maximum speed allowed by the frame rate of the DIC system)
- Medium rate: one load cycle with full load reached in 6.7 s
- Slow rate: one load cycle with full load reached in 67 s

The test at the medium rate was tuned so that the full load (generating a moment of 5 Nm) was reached in 6.7 seconds. In order to allow comparison between the test conditions, the same displacement required to reach the full load at the medium rate was imposed also at the fast and slow rates (Fig. 6.2).
Two sets of tests were performed on each specimen:

- One test (one fast, one medium and one slow cycle, with 60 seconds recovery between load cycles) without conditioning the specimen
- One test (same sequence) after conditioning the specimen with 60 cycles at 1 Hz. In order to verify if the conditioning was sufficient, a preliminary test of ten cycles were performed with a recovery time of 60 seconds (the same recovery time used in actual tests). A conditioning of 60 cycles was considered sufficient as after such conditioning differences among 10 consecutive cycles were smaller within 1% of the full load

The load and displacement were acquired using a multichannel data logger (Chassis PXIe-1078, Controller PXIe-8135, DAQ PXIe-6341, National Instruments) at 150 Hz. To keep the specimen hydrated between the first and the second test, the specimens were wrapped in a transparent film in which some water had been sprayed.

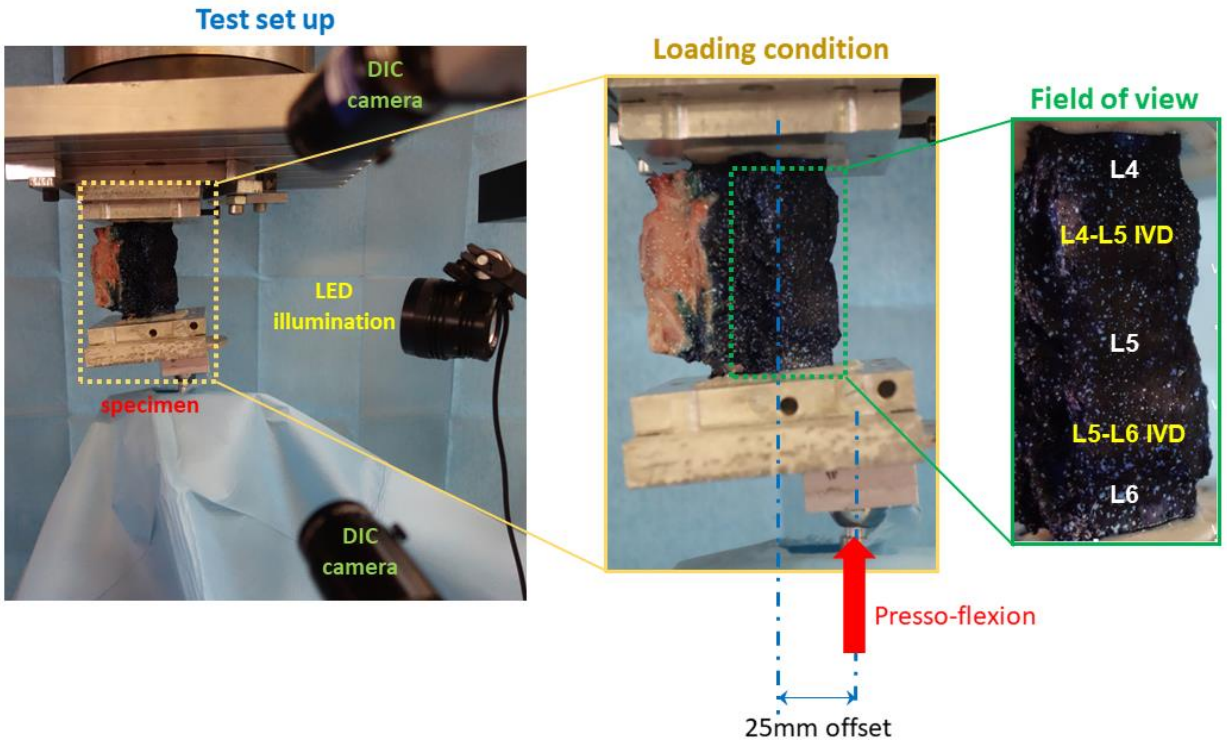

Figure 6.1 - Overview of the test configuration and the DIC system. Left: The testing machine with the loading setup and the two cameras of the DIC analysis (viewing the lateral part of the specimen). Center: specimen mounted (lateral view) in the two pots, with the loading system. Right: detail of the specimen with the white-on-black speckle pattern for the DIC analysis. The field of view recorded by the DIC cameras is indicated.

6.2.3 Full-field strain measurement

In order to measure a full-field strain map, Digital Image Correlation (DIC) was used. The surface of the specimens was dyed with a dark background using a 4% solution of methylene blue (Fig. 6.1). A white-on-black speckle pattern was prepared on the anterior surface of the specimen with the appropriate dot size, following an optimized procedure.[96, 112] A commercial 3D-DIC system was used (Q400, Dantec Dynamics, Denmark) with its software (Instra 4D, v. 4.3.1, Dantec Dynamics). Two cameras were used (5 MegaPixels, 2440x2050, 8-bit, black-and-white) in order to obtain a stereoscopic vision. Calibration was performed before the tests using a dedicated calibration target (Al4-BMB-9x9, Dantec Dynamics).
The region of interest of the specimens consisted of three vertebrae (L4-L6) and the two included intervertebral discs taken from a lateral view (Fig. 6.1).
The parameters for the acquisition of the images and for the correlation analysis were preliminarily studied and optimized to minimize errors based on a validated procedure[41]: facet size between 35 and 39 pixels, grid spacing of 21 pixels, contour smoothing of kernel size 5x5 (Table 6.1).
Full-field strain maps of true maximum and minimum principal strains (ε_1 and ε_2) were computed for all the specimens in correspondence of the two IVDs at the different loading rates and in the not-conditioned and conditioned scenarios.

Table 6.1.- Details of the parameters used for the correlation analysis with the DIC system (according to[132])

Parameters for the correlation analysis	
DIC Software Package Name and Manufacturer	Instra 4D, v. 4.3.1, Dantec Dynamics
Distance of the cameras	500 mm
Field of view	about 120 mm by 50 mm
Depth of field	70 mm
Lens aperture	f/22
Frame rate	15 frames per second
Grid spacing	21 pixels
Facet size	between 35 and 39 pixels
Contour smoothing	kernel size 5 x 5

6.2.4 Statistical analysis

In order to investigate what happens on the strain distribution in correspondence with the two IVDs (L4-L5 and L5-L6 IVDs), two rectangular regions of interest (ROIs) were delimited between the most posterior to the most anterior part of the IVDs (Fig. 6.3). On these ROIs, the medians over cranio-caudal (longitudinal) lines were computed separately for the two IVDs. The plot of the median values showed the posterior-to-anterior trend of the strain. Then, the median posterior-to-anterior trend was computed between the specimens. As the dimensions of the ROIs depended on the anatomy of each specimen, the data were re-sampled over the same number of points, so as to allow computing the median spatial trend among the specimens.
In order to assess if the differences of the spatial trends of the strains at the three loading rates and in the not-conditioned and conditioned scenarios were statistically significant, a two-sample Kolmogorov-Smirnov test was applied to the strain distributions around the IVDs. All statistical analyses were performed with Matlab (R2019b, MathWorks®, Natick, USA).

6.3 Results

6.3.1 Moment - displacement

For all the specimens, decreasing the loading rate was associated in a decrease of the peak load (while the same displacement was imposed, Fig. 6.2), and a decrease of the stiffness. The same trend was found both in the not-conditioned and conditioned scenarios. The variations of peak load can be described assigning a value of 100% to the medium rate (Fig. 6.4):

- In the not-conditioned scenario, the load increased by 11% for the fast loading rate, while the load decreased by 29% for the slow rate
- Similarly, in the conditioned scenario, the load increased by 14% for the fast loading rate, and it decreased by 30% for the slow rate

The difference between the not-conditioned and conditioned scenarios was less than 3% in all the tests.

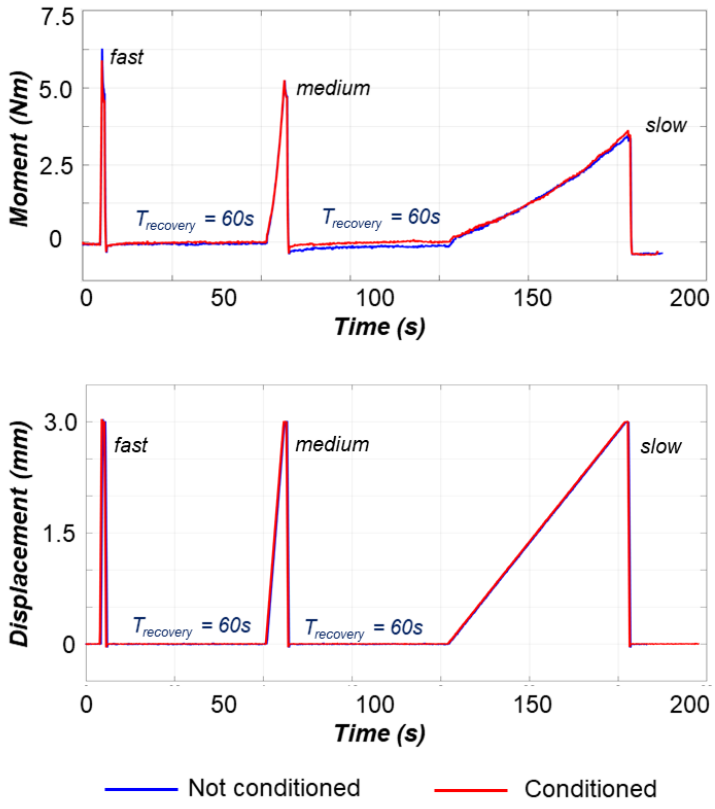

Figure 6.2 - The test consisted of a slow, medium and fast cycles (with 60 seconds recovery between cycles). The plot on the top shows the imposed displacement (the same at all rates, the same in the not-conditioned and conditioned scenarios). The plot at the bottom shows the load associated with such displacement for the three loading rates and for the not-conditioned and conditioned configurations. As the same displacement was imposed to allow comparison between the loading rates, this resulted in different peak load (the target of 5 Nm was reached at the medium loading rate, whereas the peak load at fast and slow rates were respectively higher and lower than 5 Nm). One typical specimen is plotted: the trend and the magnitudes were similar for all specimens.

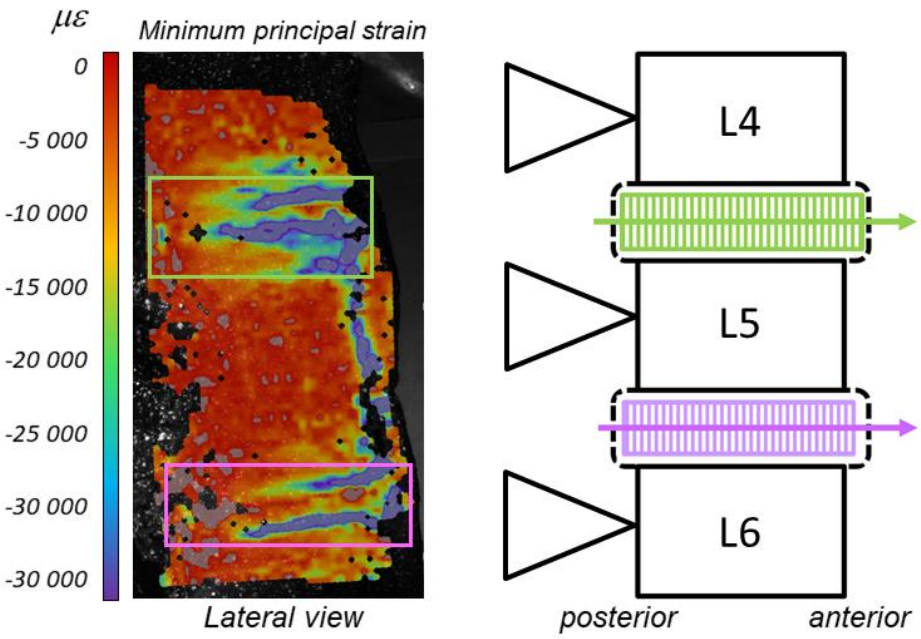

Figure 6.3 - Strain distribution (minimum principal strain) in one representative specimen from the lateral view: the rectangles show the ROIs placed on the two IVDs. The spatial trend from the posterior to the anterior side of each ROI was computed as the median values over cranio-caudal (longitudinal) lines.

6.3.2 Overview of the strain maps

For all specimens in all the tests, the strain maps showed a different order of magnitude of the strain for the vertebrae (ε_1 in the order of +300/+400 microstrain and ε_2 in the order of -2000/-3000 microstrain) and for the intervertebral discs (ε_1 in the order of +4000/+6000 microstrain and ε_2 in the order of -25000/-30000 microstrain) (Fig. 6.5). In all the cases investigated, flexion of the spine segment induced a bulging of the IVD associated with maximum principal strains (ε_1) in the circumferential direction on the lateral and anterior sides of the two IVDs, while the minimum principal strains (ε_2) were longitudinal. Conversely, the maximum principal strains (ε_1) were in the axial direction (and the associated minimum principal strains ε_2 were circumferential) on the posterior side of the two IVDs, showing an axial stretch in this region.

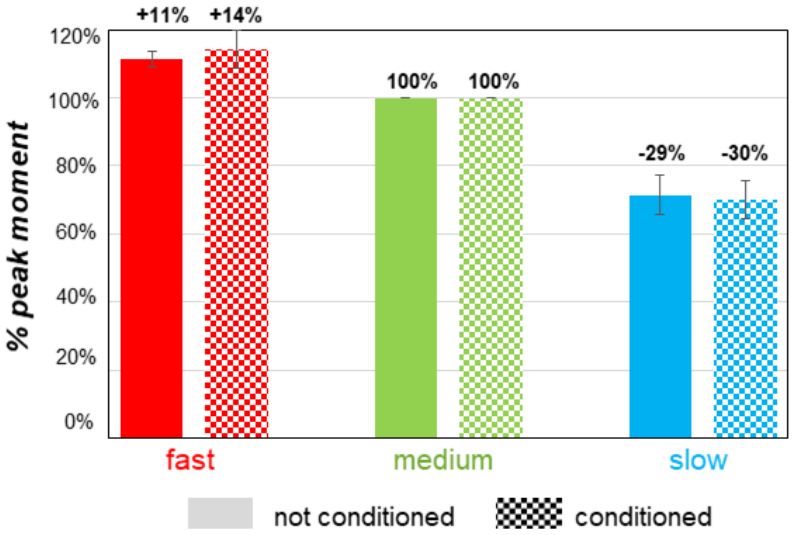

Figure 6.4 - Percentage differences of the peak loads between at the fast and slow loading rate with respect to the medium loading rate (which corresponds to 100%) in the not-conditioned and conditioned configurations.

6.3.3 Detailed analysis of the effect of the loading rate on the spatial trend

The medians of the trend distribution of strain among the specimens for the two IVDs were computed for the two principal strains (ε_1 and ε_2) for the three loading rates and for the not-conditioned and conditioned scenarios (Fig. 6.6 and 6.7).

The spatial trend of the principal strains showed an increase in absolute value moving from the posterior to the anterior side of the two IVDs. For the not-conditioned configuration and for all the loading rates, the strain on the posterior side was about 4 times smaller than the strain on the anterior side of L4-L5 and L5-L6 IVD (Fig. 6.6). For the conditioned configuration, the difference from the posterior to the anterior regions of the two IVDs was slightly higher (the ratio was about 5, Fig. 6.7). The difference between the spatial trends in the not-conditioned and conditioned scenarios was not statistically significant for both IVDs and for both principal strain components (Two sample Kolmogorov-Smirnov test, $p>0.1$ for all loading rates). This difference between the not-conditioned and conditioned tests was not evident in terms of strain value. Only slight differences appeared in the strain distribution: in the anterior region, near the endplates, with the slow rate, a smoother strain gradient was visible between the most deformed area (IVD) and the least deformed area (vertebra). With the fast rate there was a more abrupt variation between these two areas (Fig. 6.5).

For the L4-L5 IVD and for L5-L6 IVD, both for not-conditioned and conditioned tests, a slight variation was observed between the fast and slow loading rates for both principal strains (the difference between fast and slow for ε_1 and for ε_2 was less than respectively 1/10 and 1/20 of the

maximum measured value, Fig. 6.6 and 6.7). The difference between the spatial trends due to the loading rate was not statistically significant for both IVDs and for both principal strain components (Two sample Kolmogorov-Smirnov test, p=0.12-0.78 in the not-conditioned, and p=0.22-0.86 in the conditioned scenario).

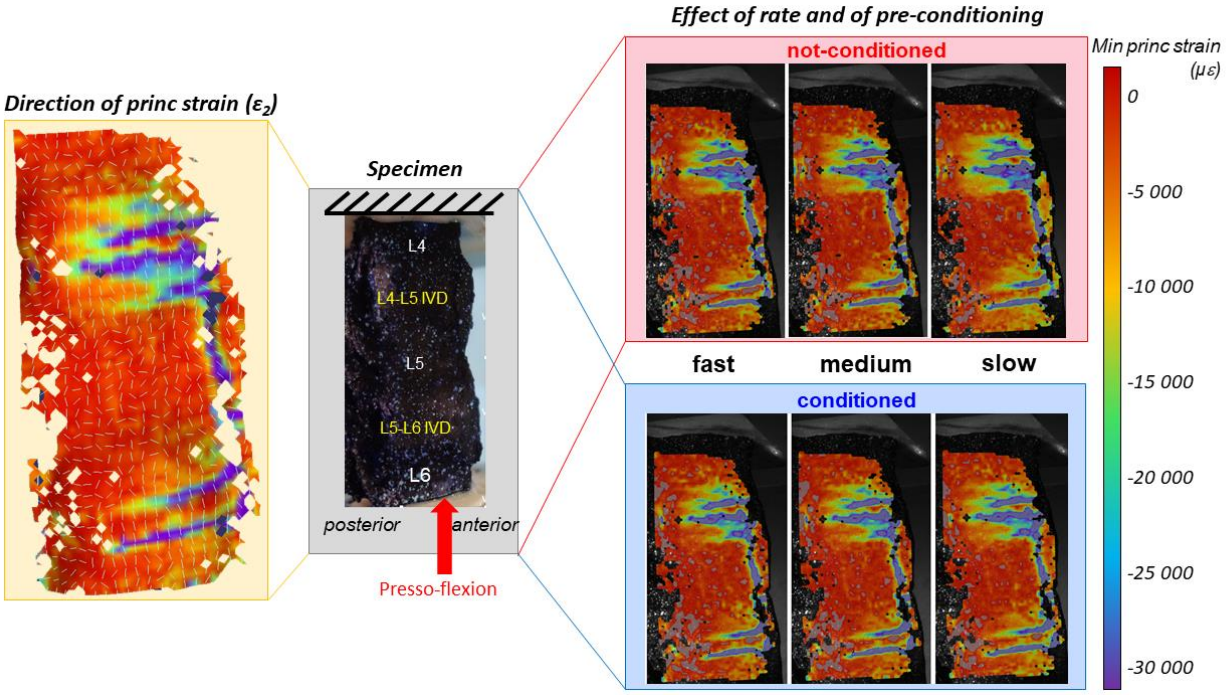

Figure 6.5 - The full-field strain distribution measured on the lateral side of one typical specimen by the DIC is shown. The image on the left side shows the true minimum principal strain (ε_2) with the directions of the strain. The images on the right side show the strain maps for the different loading rates (fast, medium and slow) and for the not-conditioned and conditioned scenarios. The minimum principal strain (ε_2) is represented as it was higher in absolute value than the maximum one (ε_1).

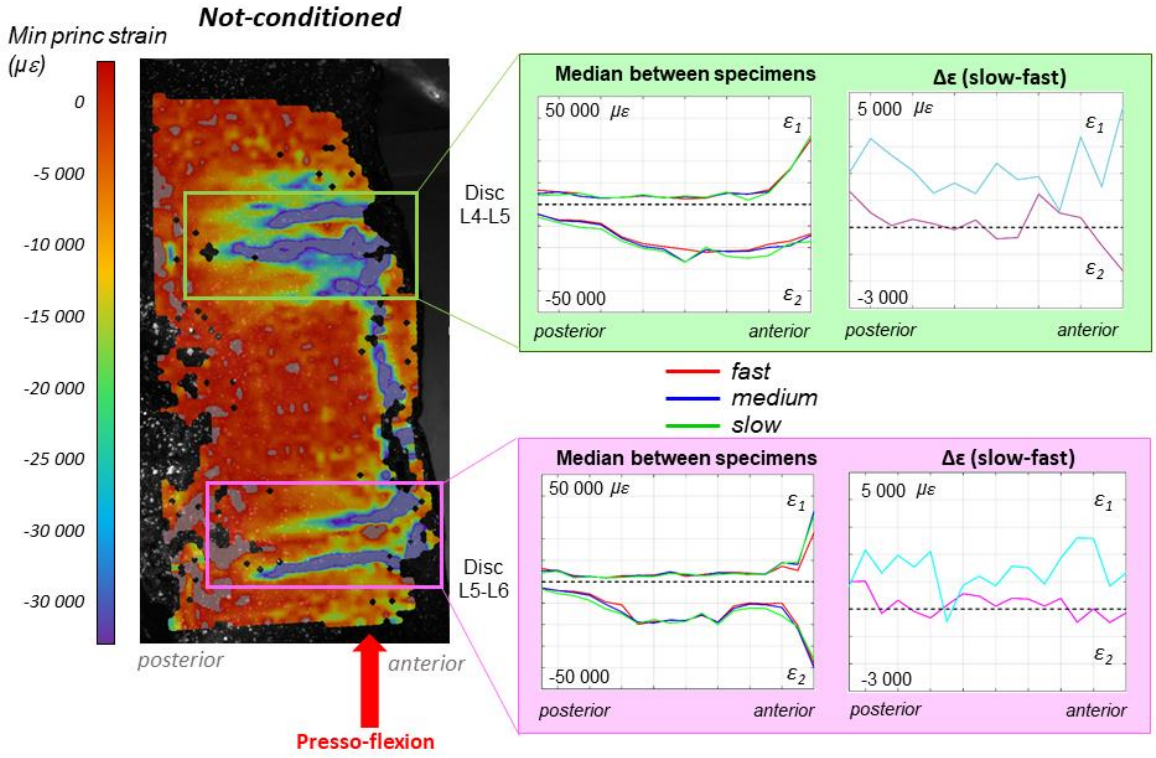

Figure 6.6 - Not-conditioned scenario: the full-field strain map on the lateral side of one typical specimen is shown on the left. The plots on the left show the spatial trend of the maximum and minimum strains (median of the six specimens), respectively the L4-L5 and L5-L6 IVDs, for the different loading rates (fast, medium and slow). On the right, the trend of the difference between the slow and fast loading rates is plotted for the maximum and minimum principal strains.

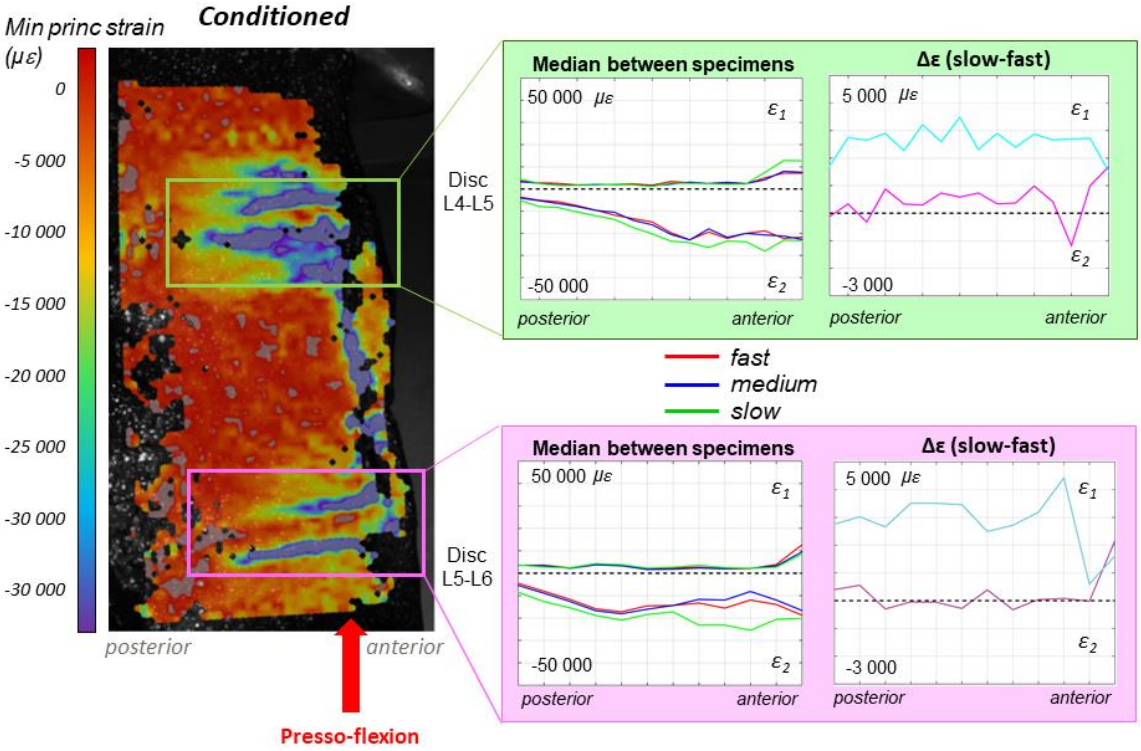

Figure 6.7 - Conditioned scenario: the full-field strain map on the lateral side of one typical specimen is shown on the left. The plots on the left show the spatial trend of the maximum and minimum strains (median of the six specimens), respectively the L4-L5 and L5-L6 IVDs, for the different loading rates (fast, medium and slow). On the right, the trend of the difference between the slow and fast loading rates is plotted for the maximum and minimum principal strains.

6.4 Discussion

Puzzling findings are reported in the literature concerning the viscoelasticity of the IVD: while the tissues composing the IVD show clear viscoelasticity[124], and FSU show the expected stiffening at high loading rates[37], an increased hysteresis was reported at high loading rates.[130] The aim of this study was to investigate how the strain distribution on the AF changes at different loading rates and if it is affected by conditioning.

A flexion test was performed on 6 porcine segments (L4-L6) applying the load at three different rates (fast, medium and slow) while the full-field strain distribution on was measured using Digital Image Correlation. To allow direct comparisons, the same displacement was imposed at the different rates, resulting in different values of the peak load in relation to the specimen's viscoelasticity. Furthermore, also the effect of conditioning on the strain distribution was investigated.

During flexion lower strains were reached in the posterior side of the IVDs than in the anterior one, at all loading rates. The increase from posterior to anterior was quite smooth (Fig. 6.6 and 6.7). This can be explained by NP migrating posteriorly during flexion[118] thus allowing the anterior side of AF to strain more, also in association with the anterior bulging of the disc.

The NP exhibits significant viscoelasticity, depending on the loading rate.[133] At high loading rate, the NP appears stiffer, causing an increase of the internal pressure and of the stiffness, leading to a hardening of the entire structure rate.[120, 121] With a low loading rate, the NP is more fluid, decreasing the stiffness of the structure and absorbing more easily the load.[133] A similar trend is found in the tissues composing the AF.[7, 116] In the present study, the way in which the surface of AF and the endplates were deformed did not change significantly with different loading rates (Fig. 6.5). In the transition zones between the disc and the vertebra, only slight differences due to the loading rate appeared, but with no statistical significance: with high loading rates this zone was less uniform showing a more abrupt transition between disc and vertebra respect to what was observed during slow loading rates. This could mean that the viscoelastic behavior of the tissues composing the NP and the AF did not directly affect the overall kinematics of the disc, and only slightly affected the transition zone between disc and vertebra where a large discontinuity of stiffness is localized.

During flexion, the directions of the principal tensile strain (ε_1) in the anterior side of the disc were circumferential (and ε_2 was longitudinal, Fig. 6.5) with the specimen showing a swelling of the disc. Conversely, towards the posterior region of the disc the two principal strain components were small and similar in magnitude, and therefore the principal directions were more unpredictable.The direction of the strain on the different structures of the spine (vertebrae, endplates, IVDs) remained unchanged at the different loading rates, showing that the way the loads were transferred through the different structures of the column was not affected by the loading rates.

For what concerns the role of conditioning, this did not significantly affect the strain distribution on the surface of AF. Both for the not-conditioned and conditioned scenarios, distribution of strains around the IVD was similar. The maximum difference between the not-conditioned and conditioned scenarios was negligible around the disc and slightly higher (up to 10%) in the anterior side, where more measurement artefacts are also present.

One of the most frequent spine pathologies is disc herniation, consisting in the rupture of the AF and leakage of part of the NP. It is still not completely clear if and to what extent this phenomenon is related to the loading rate.[7] The fact that no significant differences in strain distribution were observed with the different loading rates would suggest that the risk of disc herniation is not related to the loading rate, within the range explored in the present study. The present findings therefore agree with the results obtained by Gregory *et al.*[134] The study asserted that, at strain rates achievable through voluntary motion that could result in herniations of the AF, the tensile response of the AF tissue is not affected by strain rate.

A limitation of the present work was the use of porcine specimens instead of human specimens. Animal specimens are easier to obtain than human ones. Porcine are similar to human in size and biomechanical response.[29, 135]

Conversely, the range of motion (ROM) of porcine spines are different from the ROM of human spines.[136] Therefore, the findings of the present study can be extended to the human spine as a trend, even if possibly not as absolute magnitudes.
A further limitation was related to the range of loading rate. The rates explored from relatively fast movement (0.67 second) to very slow ones (67 seconds), which covers the range of daily activities. What was not considered in this analysis is the high loading rate simulating trauma (which can be up to 1/100 of a second).

6.5 Conclusion

In conclusion this study has shown that the loading rate has negligible effects on the strain on the surface of the annulus fibrosus. Similarly, also conditioning did not alter the strain distribution, nor the effect that the loading rate has on the strain distribution. For these reasons, disc herniation would seem not to be due to a specific rate of the applied loads. Furthermore, these findings could be useful also for the design of other *in vitro* biomechanical tests and of more realistic numerical models of the spine, knowing what effect different loading rates and conditioning entail on the biomechanics of the intervertebral discs.

Chapter 7

The strain distribution of a specific ligament: the Anterior Longitudinal Ligament

From the manuscript

The strain distribution in the lumbar anterior longitudinal ligament is affected by the loading condition and bony features:

an *in vitro* full-field analysis [137]

Palanca Marco[1], Ruspi Maria Luisa[1], Cristofolini Luca[1], Liebsch Christian[2], Villa Tomaso[2 3], Brayda-Bruno Marco[4], Galbusera Fabio[3], Wilke Hans-Joachim[2], La Barbera Luigi[3]

[1]Department of Industrial Engineering, School of Engineering and Architecture, Alma Mater Studiorum – Università di Bologna, Bologna, Italy
[2]Institute of Orthopaedic Research and Biomechanics, Trauma Research Center Ulm (ZTF), University Hospital Ulm, Ulm, Germany
[3]Laboratory of Biological Structure Mechanics, Department of Chemistry, Materials and Chemical Engineering "G. Natta", Politecnico di Milano, Milan, Italy
[4]IRCCS Istituto Ortopedico Galeazzi, Milan, Italy
[5]Department of Spine Surgery III, IRCCS Istituto Ortopedico Galeazzi, Milan, Italy

Published in: PLOS ONE, 2020: 1-21

7.1 Introduction

The anterior longitudinal ligament (ALL) is a fundamental component of the spine. It covers the anterior aspect of the spine running along the entire length of the spine.[6] To elucidate the contribution of the different anatomical elements to the biomechanics of the spine, it is important to identify the specific behaviour of the ALL. Microdissection and anatomical studies showed that the ALL comprises distinct layers. More superficial fibers attach to central regions of the vertebrae, running longitudinally and spanning up to 4-5 functional spinal units (FSUs - consisting of two vertebrae and one intervertebral disc). Much shorter intermediate fibers cover more intervertebral discs (IVDs) and insert onto the anterior aspect of the adjacent vertebrae, spanning 2-3 FSUs. The deepest layer covers longitudinally and obliquely (i.e.: alar fibers) a single IVD.[138] The ALL deeper fibers are solidly attached on the periosteum of the vertebrae and they continue in the external lamellae of the anterior part of the IVD. The ALL has an important role in stabilizing and limiting movements in the sagittal plane, and in confining the anterior wall of the intervertebral discs (IVD).[139] Its mechanical role has direct implications on low-back pain, since it limits primary and coupled motions in extension. As the ALL can prevent the bulging of the IVD, it contributes to maintain the height between two adjacent vertebrae in flexion. Consequently, the ALL prevents closure of the foraminal spaces and compression of the nerve roots. Such effects are even more important in case of disc degeneration. Furthermore, the ALL, like most spine ligaments, is rich with mechanoreceptors and plays a fundamental role in the neuromotor control.

The biomechanical function and strain distribution in the vertebrae and IVD have been investigated *in vitro* in detail.[35, 60, 140] Often, only FSUs were tested[60] whereas multi-vertebra spine specimens should be preferred in *in vitro* tests[32] for the investigation of those ligaments spanning more than one FSU, indeed this represents a more realistic and complete loading condition. From these tests, the range of motion[56, 141] and/or the neutral zone and stiffness[56] under the different physiological loading conditions were evaluated for the different spinal levels. This type of measurements provides useful information about the global description of the spine biomechanics, but it is unable to elucidate in detail what happens locally on the spine segment.

The investigations on the spinal ligaments are somehow limited. Specifically, the ALL, which is one of the strongest ligamentous structure in the spine, has only partially been investigated so far. Generally, the ALL was tested separately at the tissue level: evaluating the mechanical properties of dissected tissue specimens[61, 142], and at the system level: evaluating its structural behaviour when it was included in spine tests.[32, 143] However, a biomechanical characterization of the ALL tissue when it was incorporated in the spine, with the typical and complex loading conditions, is missing. No studies were found in which the strain distribution was measured on the ALL, in its complete mechanical and anatomical complex, as part of a multi-vertebra spinal segments, and under different loading conditions representative of physiological loading.

In this work, the evaluation of multi-vertebra spine segments (i.e.: 7/8 vertebrae and 6/7 intervertebral discs) through flexibility tests was integrated with a full-field measurement of the strain distribution of the anterior surface.[96, 144] The overall aim of this study was to investigate in depth the biomechanical function of the ALL in front of the lumbar vertebrae (L3-L5) and of the intervertebral discs.

Specifically, we aimed measuring the strain distribution in the ALL for different directions of motions under pure moments, and so understanding how the strain distribution changes through the progression of the loading cycle analysing discrete steps.

We hypothesized the ALL undergoes non-uniform strain distribution when the spine segment is subjected to pure moments, potentially related to the unique specimens' anatomy/morphology (e.g.: presence of osteophytes); moreover, opposite loading directions (e.g.: flexion/extension, or right/left lateral bending, or clockwise/counterclockwise axial torsion) translate to non-mirrored strain distributions.

7.2. Materials and Methods

7.2.1 Study design

This study was approved by the Institutional Review Board (Ethikkommission) of Ulm University, (Document of approval Nr. 307/17). In order to investigate the strain distribution on the anterior longitudinal ligament in the lumbar region, cadaveric multi-vertebra spinal segments were subjected to non-destructive pure moments in different directions, with a state-of-the-art spine tester. The tests were performed twice on each specimen under identical conditions. Preliminarily, the range of motion was measured, with an optical motion tracking system, to allow comparisons of the tests results. Subsequently, the strain distributions on the anterior surface of the L3-L5 region, were measured by means of digital image correlation (DIC) with a recently validated protocol, for identifying stretched/compressed regions. The strain distributions were analysed firstly qualitatively, and then quantitatively.

7.2.2 Specimens

Five fresh-frozen human thoracolumbar spine segments were obtained through an ethically-approved international donation program (Science Care Inc., Phoenix, AZ). The donors were all Caucasian, three males and two females (Table 1). Inclusion criteria were: no history of spine fracture or major spine deformity; no tumour; physically active, i.e.: ambulatory activities and daily living activities, up to date of death. The median age of the subjects at the time of death was 62 years and their median weight was 133 kg. To check the state of degeneration and determine the bone mineral density (BMD), each specimen was scanned using a calibrated clinical computed tomography (CT) scanner (Philips Brilliance 64, Philips Healthcare, Cleveland, USA). The BMD was expressed averaging the measurements collected on the trabecular bone of L1, L2 and L3 vertebrae.
The volumetric CT reconstructions of the specimens are available in the Supplementary Material, otherwise a conventional x-rays image (Faxitron 43805N, Hewlett Packard, Palo Alto, USA) is provided. No critical damages were observed; however, most specimens showed some osteophytes as can be expected with elderly donors. The osteophytes and reduction of IVD height was quantified with objective metrics, according to[145].
The soft tissues (muscles, fat) on the anterior side of the spines were carefully removed to expose the anterior longitudinal ligament and the lateral side of the vertebral bone and of the intervertebral discs; the posterior elements were left in place.[146]
The upper half of the most cranial vertebra and the lower half of the most caudal vertebra were embedded in poly-methyl-methacrylate (PMMA, Technovit 3040, Heraeus Kulzer, Werheim, Germany) blocks. After the preparation, the specimens were frozen in plastic bags at -20°C until the day of the tests. Thawing at 6°C for 10 h prior to preparation and testing of the specimens were performed within 20 h to avoid alteration of their mechanical properties.

7.2.3 Mechanical loading

All specimens were tested at room temperature (ca. 23°C) and the hydration was preserved spraying saline solution during the tests. In order to mount the specimens in a universal spine tester, flanges were fixed to the PMMA blocks[146, 147] so that the L3-L5 segment was vertical. Initially the cranial side was connected to the top of the spine simulator with the gimbal with three integrated stepper motors (FT 1500/40, Schunk GmbH & Co. KG, Lauffen/Neckar, Germany), then the caudal side with the natural slope for each specimen was fixed on the bottom side of the testing machine (Fig. 7.1).

The coordinate system of [146] was used in this work. Each specimen was tested without any preload in flexion/extension (My), right/left lateral bending (Mx) and clockwise/counterclockwise axial torsion (Mz) applying pure moments (M) up to +/-7.5 Nm. Flexion/extension and lateral bending were applied at a rate of 1°/s, while the axial torsion was applied at a rate of 0.5°/s. As the thoraco-lumbar spine is about twice as stiff in torsion, the rate in torsion was half of that in bending, so as to reach the fully loaded condition in approximately the same time. Each test consisted of three consecutive cycles for each direction of loading: the first two cycles for pre-conditioning, the last one for the actual analysis.[37] All motions started and finished in the unloaded neutral position. In order to avoid application of any additional undesired loading component, the specimens were unconstrained in the other uncontrolled five degrees of freedom. A six-components load cell (FT 1500/40, Schunk GmbH & Co. KG, Lauffen/Neckar, Germany) measured the moments and the forces applied.

Specimen number	Segment	Gender	Age at death (years)	Height (cm)	Weight (kg)	BMD (mg/cm^3)	Disc height loss	Osteophytes formations	Overall degree of degeneration - Other remarks
#1	T11-S1	M	60	N.A.	N.A.	153	No remarks (grade 0)	No osteophytes (grade 0)	Healthy
#2	T11-S1	M	66	183	141	82	Mild (25%, grade 1)	Moderate (grade 2)	Mild degenerative signs (grade 1)
#3	T11-S1	M	62	178	164	94	Moderate (42%, grade 2)	Moderate (grade 2)	Moderate degenerative signs (grade 2) - thickening of L4 anterior cortical wall
#4	T11-S1	F	60	163	114	123	Moderate (40%, grade 2); T12-L1 and L4-L5 discs herniated towards L1 and L5	Moderate (grade 2)	Moderate degenerative signs (grade 2) - mild scoliosis (Cobb angle T12-L5 of 10°); concave L5 superior endplate
#5	T12-S1	F	63	157	125	157	Moderate (33%, grade 2)	Severe (grade 3)	Moderate degenerate signs (grade 2)
Median	-	-	**62**	**170**	**133**	**123**	-	-	-

Table 7.1 - Details of the specimens: the first columns report the donor's information. The last three columns report the radiographic assessment for L4 and L5, evaluated through CT scans (the CT scans for each individual specimen is reported in the Supplementary Material. The IVD height loss and osteophytes formations were assessed according to[145]

7.2.4 Measurement of structural properties

In order to confirm that the overall kinematics of the specimens was consistent with the literature, the mechanical tests were first performed with a motion tracking system. Each single vertebra was equipped with three spherical reflective markers, which were attached frontally and laterally to the vertebral body. The motion of the single vertebrae was simultaneously captured with six cameras of the optical system (Mod. MX13, Vicon Motion Systems Ltd., Oxford, UK), synchronized with the mechanical loading apparatus. After evaluating the relative intervertebral motions using the software Nexus 1.8.5 (Vicon Motion Systems Ltd.), the kinematic data were matched with the moment data to analyse the resulting load-deformation curves. The global range of motion (ROM) as well as the global neutral zone (NZ) of each motion segment between T12 and the sacrum were quantified using dedicated scripts (in MatLab R2014b, MathWorks, Natick, USA).

7.2.5 Measurement of the local distribution of the strain

In order to measure the full-field strain distribution on the anterior spinal ligaments, the same mechanical tests were performed while a 3D DIC system was used. A white-on-black speckle pattern was prepared before the test on the anterior surface of the specimens following an optimized procedure.[112] The dark background was prepared staining the ALL, the intervertebral discs and the vertebrae with a solution of methylene-blue (4 g of methylene-blue per 100 ml of water) until a uniform dark background was obtained. The white dots were created with a white water-based paint (Q250201 Bianco Opaco, Chrèon, Italy) diluted at 40% with water and sprayed with an airbrush-airgun (AZ3-THE-2, nozzle 1.8 mm, Antes-Iwata, Italy) with 100kPa air pressure, from a distance of 300 mm. Such settings were refined in order to obtain the optimal size of the speckle dots following a validated protocol.[40, 41]

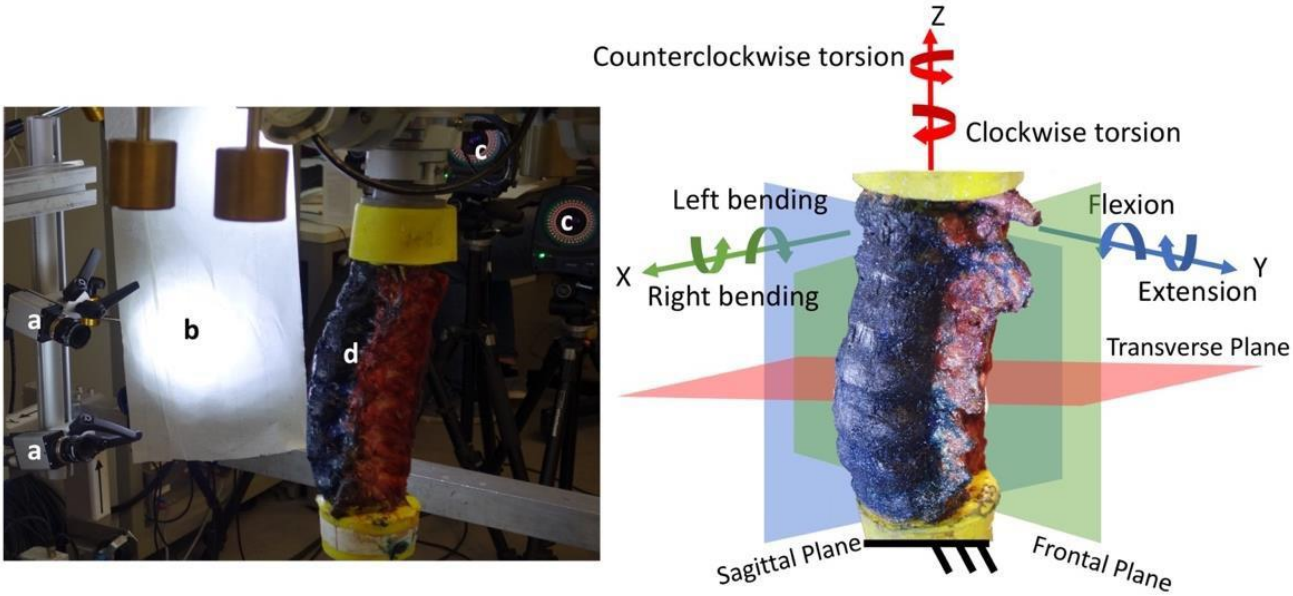

Fig. 7.1 - Left: overview of the testing setup showing (a) the DIC cameras, (b) the DIC light system, (c) the optoelectronic cameras and (d) the m. Right: detail of the spine segment. The white-on-black pattern is visible. Also shown is the three-dimensional coordinate system used by the different measurement tools: the transverse plane of the spine segment corresponds to the xy-plane of the coordinate system, the sagittal plane to the xz-plane and the frontal plane to the yz-plane. The X-axis is forward, the Y-axis left and the Z-axis cranial

The DIC system (Q400, Dantec Dynamics, Denmark) was configured with two 5 Mpixels cameras (2440x2050, 8-bit, black-and-white) equipped with high-quality metrology-standard 17 mm lens (Xenoplan, Schneider-Kreuznach, Germany; 65 mm equivalent) to acquire images of the specimens providing a stereoscopic vision. A directional custom system of LEDs (10'000 lumen in total) was placed to light up the specimen with oblique light minimizing the glares on the specimen typical of direct illumination. The cameras were placed at a distance of 540 mm from the specimen. The cameras were aligned vertically in order to take advantage of the sensor shape in framing the region of interest (ROI) of the spine segment (three vertebrae and two intervertebral discs - from L3 to L5) without scarifying the measurement spatial resolution, Fig. 7.1). In this configuration, the field of view was of about 120 mm by 160 mm, it was depending on the individual specimen, resulting in a pixel size of about 0.08 mm, and a depth of field of 70 mm with the aperture adopted (f/22). Images of the ROI were acquired at 5 frames per second.

To enable the stereoscopic reconstruction within the measurement volume and correct the distortion of the lenses, a calibration was performed before each acquisition using a proprietary calibration target (Al4-BMB-9x9, Dantec Dynamics). The analysis of displacements and strains through correlation of the images was achieved using the proprietary software Istra 4D (v4.3.1, Dantec Dynamics, Denmark). The maximum (ε_1) and minimum (ε_2) engineering principal strains, as well as

Published in: PLOS ONE, 2020: 1-21

their direction, were computed using a facet size between 39 and 59 pixels, a grid spacing between the facets of 4 pixels and contour smoothing with a kernel size of 5x5 facets.

7.2.6 Measurement uncertainties, Metrics and statistical analysis

7.2.6.1 Uncertainties

The accuracy of the motion tracking system was evaluated using special custom-made calibration object. An extensive validation and optimization of the DIC measurement system and protocols were previously performed.[112] Here, an estimation of the unavoidable measurement uncertainties was performed just before each mechanical test. A couple of images of each specimen in the unloaded condition (zero-strain) was acquired. The images were analysed using the chosen settings. The systematic and random errors were evaluated as the mean and standard deviation of ε_1 and ε_2 over the entire ROI, which theoretically should be zero.

7.2.6.2 Metrics and statistics

Global (T12-S1) range of motion (ROM) was defined as the maximum deflection of the respective motion segment at full load (7.5 Nm). The global neutral zone (NZ) was evaluated as the difference of the angle at 0 Nm of the hysteresis cycle. The NZ specifies the motion of the specimen in the unloaded region, representing the laxity.[146]
The full-field ε_1 and ε_2 maps were computed by the DIC system during the entire load cycle. For a qualitative analysis, the strain maps, in the region of interest from L3 to L5 were reported for each loading scenario during the progression of the load.
For a quantitative analysis, two sub-regions of interest (sub-ROIs): in front of the L4 vertebra and in front of the L4-L5 IVD, were defined. For each sub-ROIs, the strain field at the maximum load was analysed through a MatLab script computing the principal strains medians. To assess the significance of the difference between the strains in front of the vertebra and in front of the IVD, the medians over such areas were compared with the two-sample Mann-Whitney test for each loading scenario. To describe how the principal strains were distributed in the circumferential direction of the ALL in front of the L4 vertebra and in front of the L4-L5 IVD, the median over cranio-caudal (vertical) lines were computed, separately, over the vertebra and over the IVD, both for ε_1 and ε_2, for each specimen. Similarly, to describe how the principal strains were distributed in the cranio-caudal direction of the ALL in front of the vertebra and in front of the IVD, the median over circumferential (horizontal) lines were computed, separately, over the vertebra and over the IVDs. Then, the data from the five specimens were pooled and the median trend plotted together with the standard deviation. As the sub-ROIs were dimensionally different in the different specimens and the number of measurement points is connected with the physical dimension of the spine segments, the data were re-sampled over the same number of points. In order to assess the significance of alterations of such distribution of strain in relation to the different loading scenarios, a two-sample Kolmogorov-Smirnov test was applied both to the circumferential and cranio-caudal strain distributions of the L4 vertebra and the caudal IVD, discriminating the opposite directions of loading.

7.3 Results

All the tests were successfully performed with no visible damage of the specimens. A preliminary check of the bending moment-rotation plots from the spine tester confirmed that the difference between the two series of loading cycles (i.e.: those to measure the structural properties with the

motion tracking system, and those to measure the strain distribution with the DIC) were smaller than 5° with a rotation of 33° at full load. The only problems encountered was the poor correlation for flexion-extension for specimen #1 and the loss of the dataset of specimen #4 for extension.

7.3.1 Measurement uncertainties

An in-house validation showed that the motion tracking system has an accuracy of better than 0.1 mm and better than 0.1°. The zero-strain tests, before each test, indicated that DIC-measured strains had a systematic error of better than 20 microstrain and a random error of better than 60 microstrain.

7.3.2 Structural properties

The median ROM at 7.5 Nm was 12.0° in flexion-extension (range: 9.7°-14.6°), 13.6° (range: 12.4°-24.9°) in lateral bending and 7.8° in axial torsion (range: 4.6°-9.3°). The NZ was 3.7° in flexion-extension (range: 1.9°-5.9°), 6.2° in lateral bending (range: 4.4°-20.1°) and 0.8° in axial torsion (range: 0.2°-1.8°).

7.3.3 Local distribution of strains

The full-field strain maps showed a non-homogeneous distribution in the ALL (Fig. 7.2-7.7). The peak values of the maximum and minimum principal strains had the same order of magnitude, in all loading scenarios. Strains did not increase linearly during the progression of load (0.0, 2.5, 5.0, 7.5 Nm, Fig. 7.2, 7.4, 7.6): in some regions the strain magnitude reached a high value already with small moments, and then remained rather constant for higher moments. The different loading scenarios generated different strain patterns. These strain maps allowed to identify which portions of the ALL were actually working (in tension or compression), and which portions were unstrained (Fig. 7.3, 7.5, 7.7). Some stripes characterized by larger strains were visible in all specimens with a preferential cranio-caudal orientation (Fig. 7.2, 7.4, 7.6). In most specimens, also some spots with larger strains were visible, especially close to the endplates. While common trends were visible in all specimens, inter-specimen differences were found in association with specific bony-defects and individual defects highlighted by the CT images (Fig. 7.8).

7.3.3.1 General trends for flexion/extension

During the application of flexion/extension, strains increased more pronouncedly, in absolute value, in the ALL in the areas in front of the IVDs, and especially close to the endplates (Fig. 7.2). The same regions reached the maximum strain values when the full load was applied. At the maximum flexion, the median ε_1 and ε_2 over the portion of the ALL in front of the L4 vertebra were respectively 3910 microstrain and -15170 microstrain (median between 5 specimens); in front of the IVDs $\varepsilon_1$and ε_2 were respectively 19160 and -23020 microstrain. At the maximum extension, the median ε_1 and ε_2 in the ALL in front of L4 were respectively 13890 microstrain and -1890 microstrain (median between 5 specimens); in front of the IVDs ε_1 and ε_2 were respectively 18730 and -10710 microstrain. The only significant difference was found for flexion between ε_1 in front of the IVDs and in front of the L4 vertebra (two-sample Mann-Whitney, Table 7.2). The median values for the individual specimens are reported in the Supplementary Material. During flexion, ε_1 were circumferential, indicating an axial compression. During extension ε_1 were directed longitudinally, indicating traction of the ALL. The direction of principal strains in the ALL did not change during the progression of the load.

The plot showing the distribution of ε_1 and ε_2 in the cranio-caudal and circumferential directions of the ALL highlighted larger strain in front of the discs with respect to the vertebrae, both in flexion and extension (Fig. 7.3). While in extension, the strains were quite uniformly distributed both in the circumferential and in cranio-caudal direction of the vertebra and disc, in flexion some regions were more strained: the intervertebral disc, at mid-height, and at its right and left extremities. The distributions of strains were significantly different between flexion and extension both in the circumferential and in cranio-caudal direction of the ALL, for ε_1 only in front of the vertebra, and for ε_2 both in front of the vertebra and the IVD (two-sample Kolmogorov-Smirnov, Table 7.3).

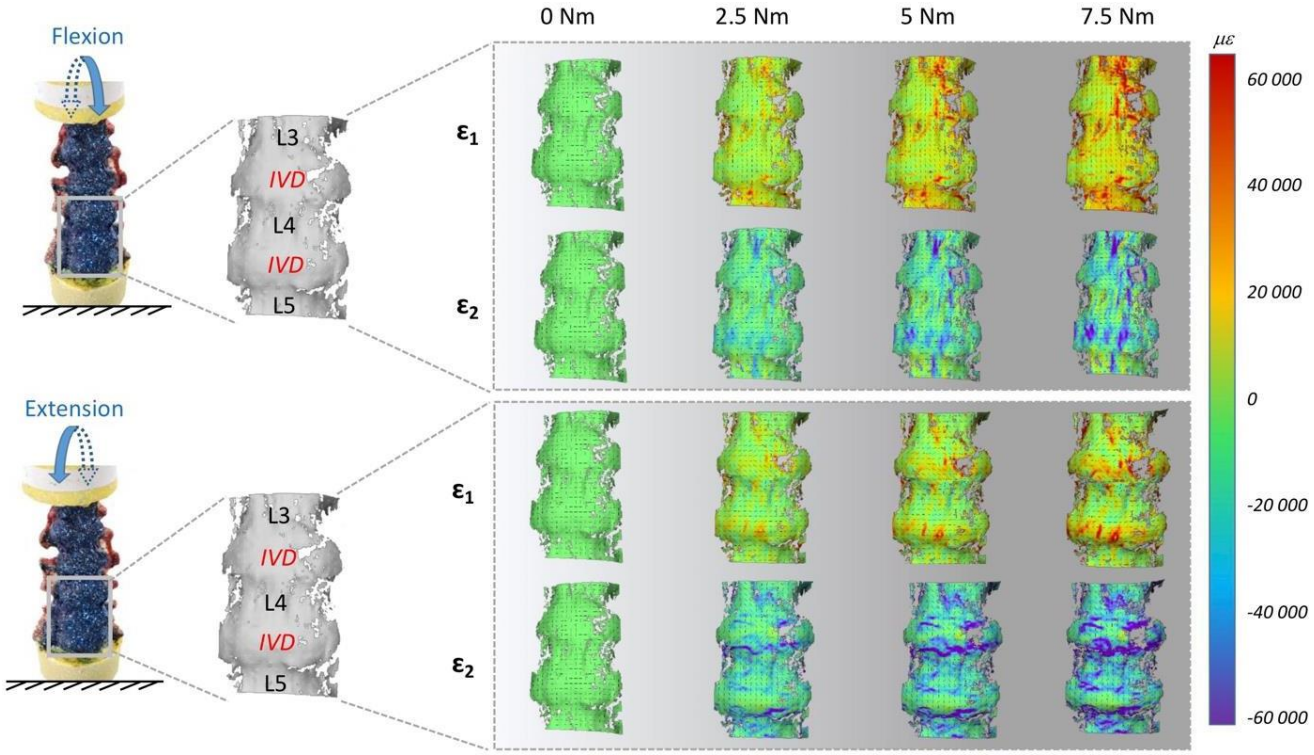

Fig. 7.2 - Flexion and extension: Maximum (ε_1) and minimum (ε_2) principal strain fields during the progression of the loading cycle (0.0, 2.5, 5.0, 7.5 Nm) in both opposite directions. The images on the left show the actual specimen under load and the correlated (the vertebrae and IVDs are labelled). The false-colours maps show the non-uniform distribution of strain. The black dashes indicate the principal strain directions. A typical specimen (#2) is shown here. Similar patterns were observed in all 5 specimens (the strain maps for all the individual specimens are reported in the Supplementary Material

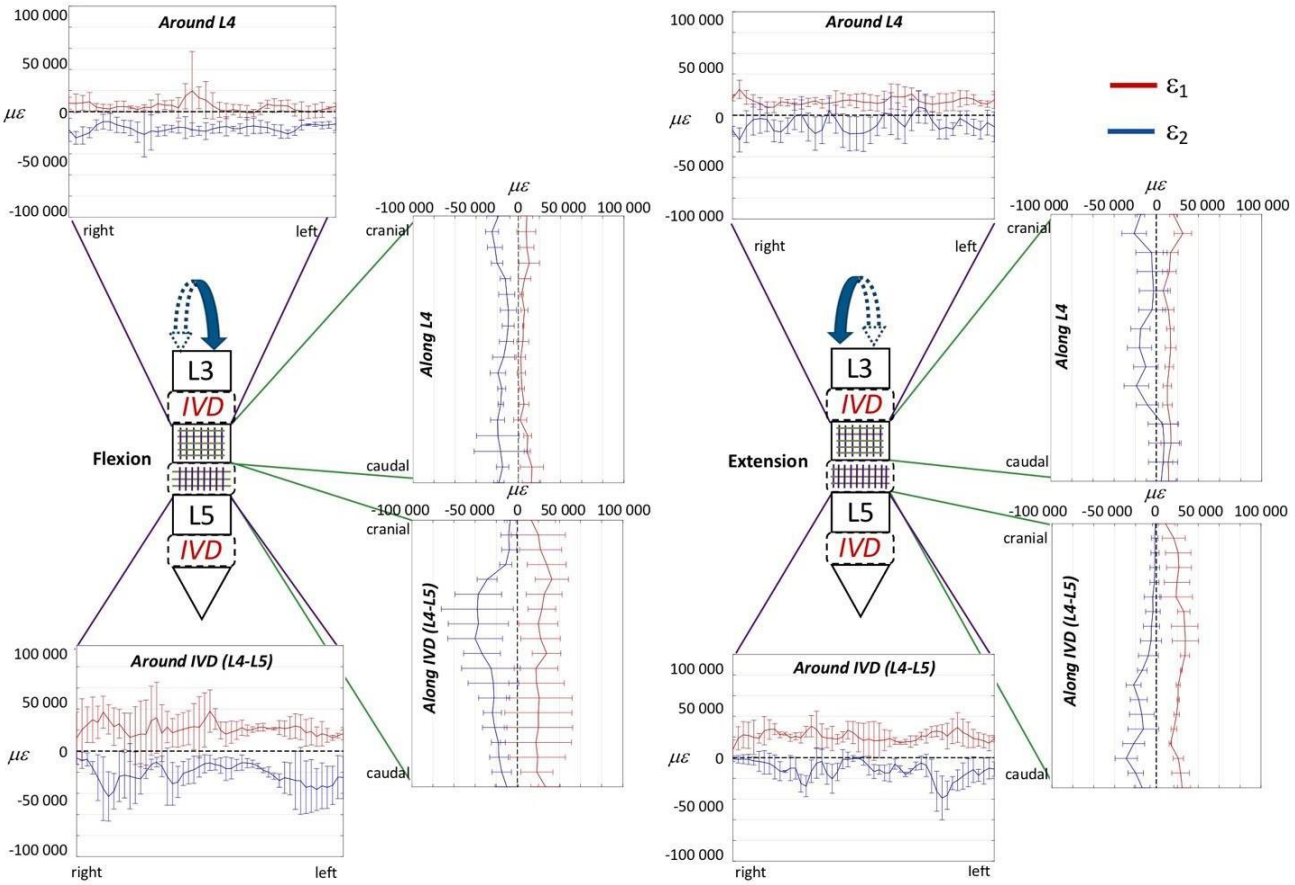

Fig. 7.3 - Flexion and extension at the maximum loading (7.5 Nm): To describe the strain distribution around the ALL, the median over cranio-caudal lines were computed in the sub-ROI in front of the L4 vertebra and in the sub-ROI in front of the L4-L5 IVD. Similarly, to describe the strain distribution along the ALL, the median over circumferential lines were computed in the sub-ROI in front of the L4 vertebra and in the sub-ROI in front of the L4-L5 IVD. The plots show the distribution of ε_1 (red) and ε_2 (blue) around L4 and the IVD (purple lines) and along L4 and the IVD (green lines). The median and standard deviation within the sample are reported

7.3.3.2 General trends for lateral bending

During the application of lateral bending (Fig. 7.4), strains markedly increased in regions both in front of the IVDs and in front of the vertebra. Those regions initially more strained, also reached the maximum strain values at full load. The median ε_1 and ε_2 in front of the vertebra, at the maximum left bending, were respectively 4250 microstrain and -6600 microstrain; in front of the IVDs were 8510 microstrain and -10090 microstrain. The median ε_1 and ε_2 in front of the vertebra, at the maximum right bending, were respectively 6363 microstrain and -9570 microstrain; in front of the IVDs were respectively 15590 microstrain and -11030 microstrain. None of these differences between the vertebra and the IVD was statistically significant (two-sample Mann-Whitney, Table 7.2). The median values for the individual specimens are reported in the Supplementary Material. The ε_1 had circumferential direction in the compressed side (left side for the left lateral bending, and vice versa) and longitudinal direction in the tensile side (right side for the left lateral bending, and vice versa). The trends of strain circumferentially the spine segment for the right and left lateral bending were mirrored with respect to the vertical axis (Fig. 7.5). However, there were differences in magnitude, with larger strains for the right lateral bending, compared to left. No large differences between the two lateral bending scenarios were found in the cranio-caudal strain distribution of the spine segment. The distribution of strains over the vertebra L4 were significantly different between right and left bending, with the exception of ε_1 circumferentially the vertebra; the distribution over the IVD were

significantly different, with the exception of ε_2 circumferentially the IVD (two-sample Kolmogorov-Smirnov, Table 7.3).

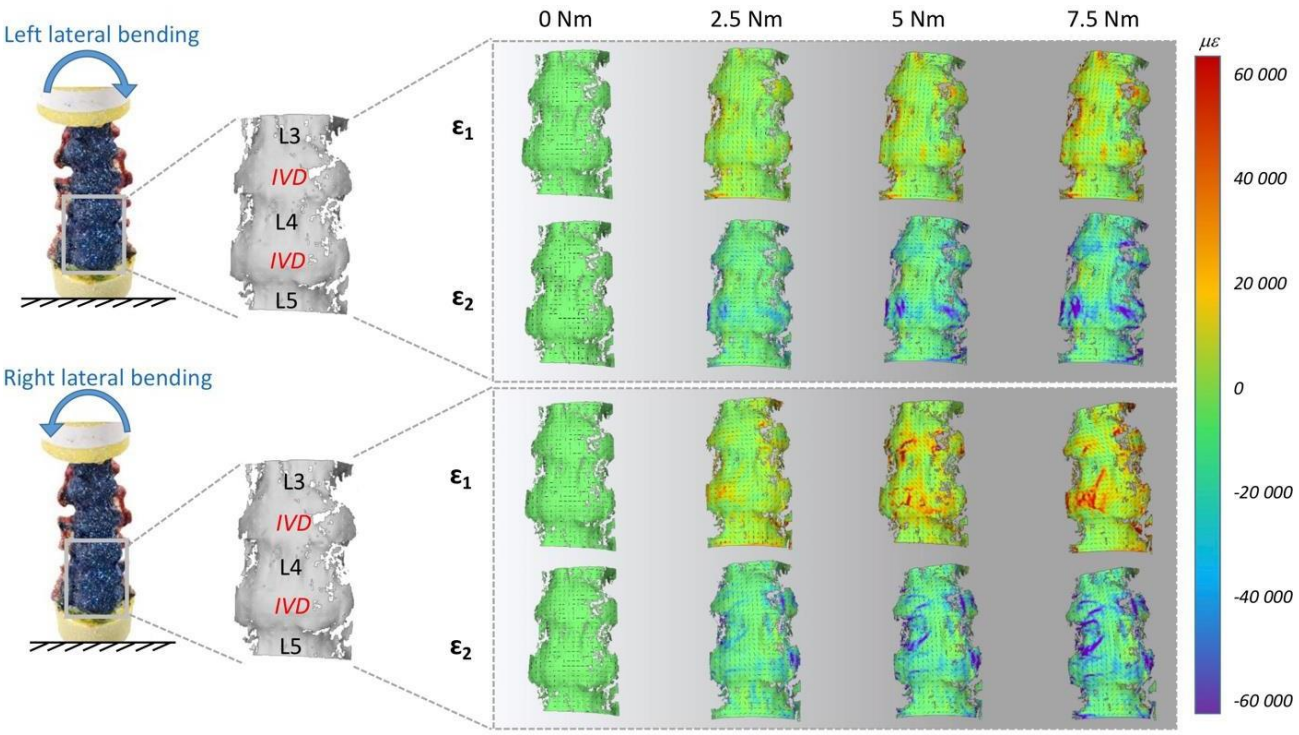

Fig. 7.4 - Lateral bending: Maximum (ε_1) and minimum (ε_2) principal strain fields during the progression of the loading cycle (0.0, 2.5, 5.0, 7.5 Nm) in both opposite directions. The images on the left show the actual specimen under load and the correlated (the vertebrae and IVDs are labelled). The false-colours maps show the non-uniform distribution of strain. The black dashes indicate the principal strain directions. A typical specimen (#2) is shown here. Similar patterns were observed in all 5 specimens (the strain maps for all the individual specimens are reported in the Supplementary Material

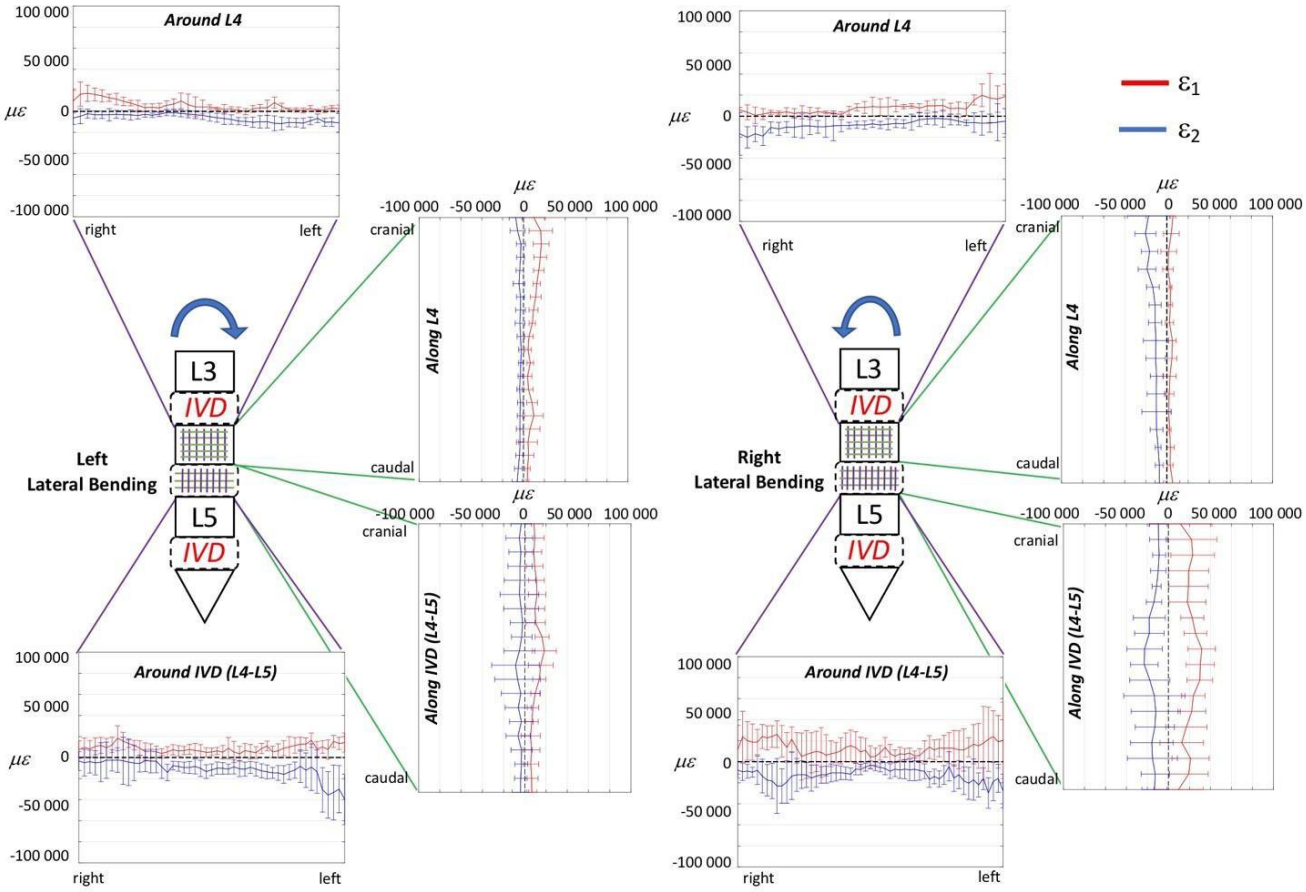

Fig. 7.5 - Lateral bending at the maximum loading (7.5 Nm): To describe the strain distribution around the ALL, the median over cranio-caudal lines were computed in the sub-ROI in front of the L4 vertebra and in the sub-ROI in front of the L4-L5 IVD. Similarly, to describe the strain distribution along the ALL, the median over circumferential lines were computed in the sub-ROI in front of the L4 vertebra and in the sub-ROI in front of the L4-L5 IVD. The plots show the distribution of ε_1 (red) and ε_2 (blue) around L4 and the IVD (purple lines) and along L4 and the IVD (green lines). The median and standard deviation within the sample are reported

7.3.3.3 General trends for axial torsion

During the application of torsion (Fig. 7.6), the strains had a visible twisting trend and increased more pronouncedly in front of the IVD. The median ε_1 and ε_2, at the maximum clockwise torsion, in front of the vertebra were respectively 7720 microstrain and -5180 microstrain; in front of the IVDs were respectively 23170 microstrain and -23420 microstrain. The median ε_1 and ε_2, at the maximum counterclockwise torsion, in front of the vertebrae were respectively 7350 microstrain and -3860 microstrain; in front of the IVDs were 38880 microstrain and -31340 microstrain. All these differences between the vertebra and the IVD were statistically significant (two-sample Mann-Whitney, Table 7.2). The median values for the individual specimens are reported in the Supplementary Material. Although the magnitude of the moment in both direction of torsion was the same, the magnitude of the ε_1 for clockwise and counterclockwise were different; conversely the ε_2 were similar between clockwise and counterclockwise torsions. The ε_1 were roughly oriented at +45° for clockwise torsion and -45° for counterclockwise torsion both on the vertebrae and intervertebral discs. The plot of the strain in the circumferential direction of the ALL showed a pattern mirrored with respect to the vertical axis for clockwise and counterclockwise torsions (Fig. 7.7). No differences were present in terms on magnitude between the two axial torsion scenarios. The distribution of strains in the cranio-caudal direction of the ALL in front of the vertebra was significantly different between clockwise and counterclockwise torsion only for ε_2; conversely, the distributions in the discs were significantly different in all cases (two-sample Kolmogorov-Smirnov, Table 7.3).

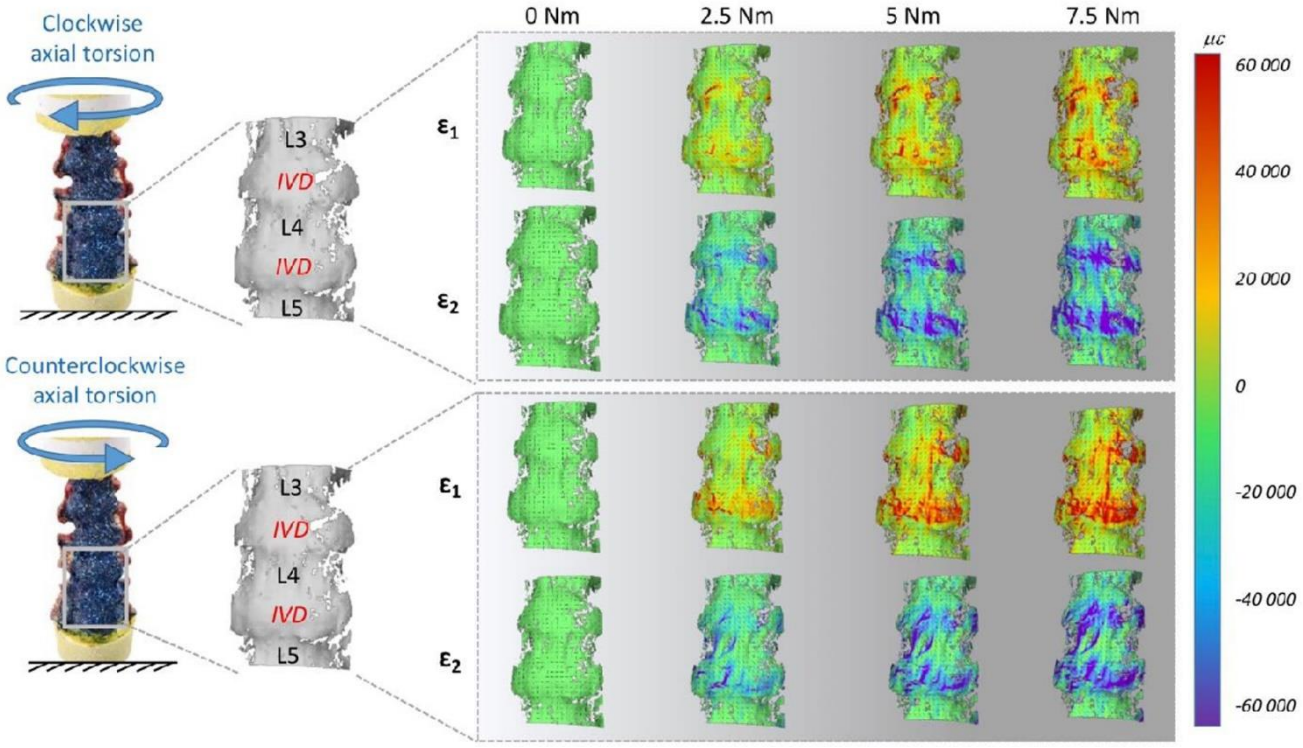

Fig. 7.6 - Axial Torsion: Maximum (ε_1) and minimum (ε_2) principal strain fields during the progression of the loading cycle (0.0, 2.5, 5.0, 7.5 Nm) in both opposite directions. The images on the left show the actual specimen under load and the correlated (the vertebrae and IVDs are labelled). The false-colours maps show the non-uniform distribution of strain. The black dashes indicate the principal strain directions. A typical specimen (#2) is shown here. Similar patterns were observed in all 5 specimens (the strain maps for all the individual specimens are reported in the Supplementary Material)

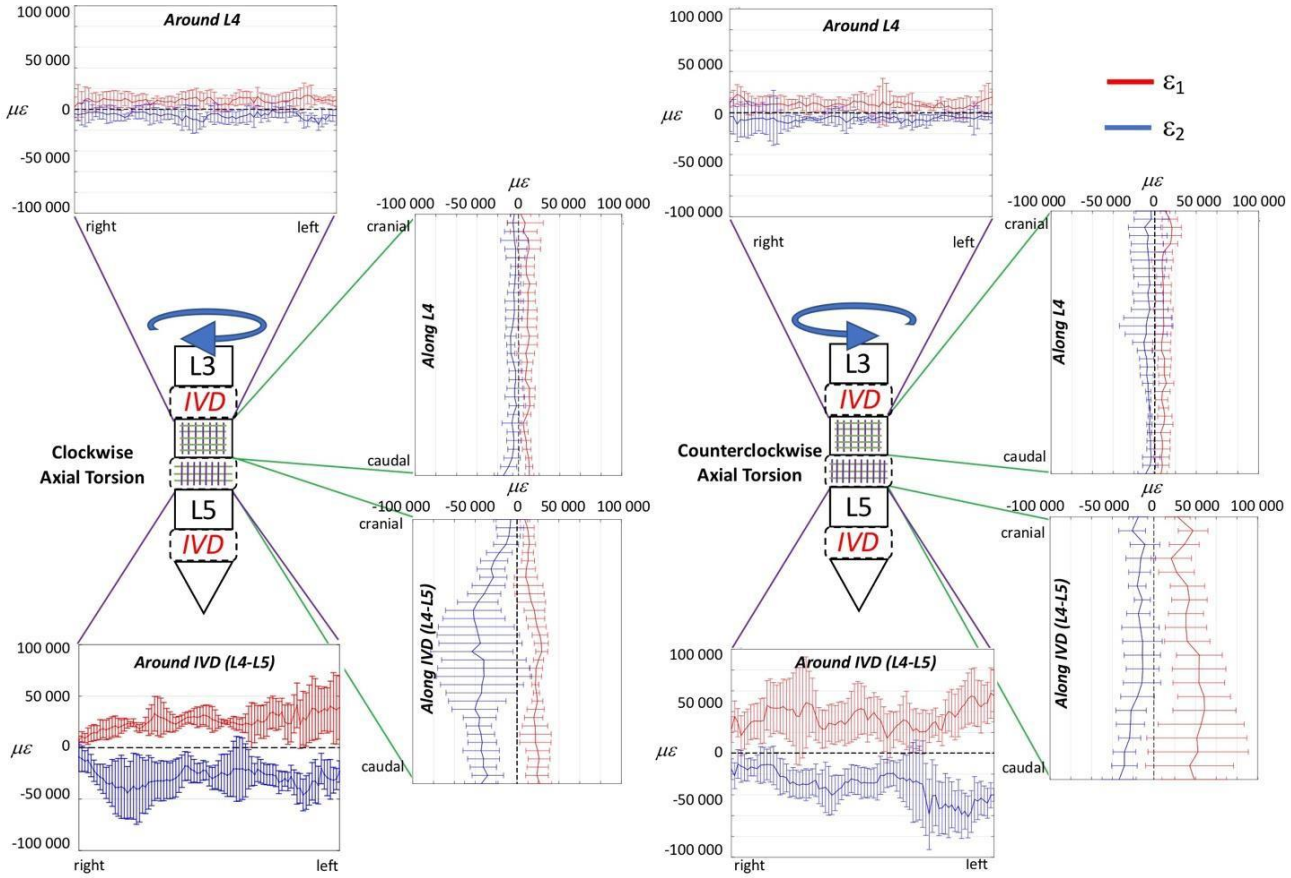

Fig. 7.7 - Axial Torsion at the maximum loading (7.5 Nm): To describe the strain distribution around the ALL, the median over cranio-caudal lines were computed in the sub-ROI in front of the L4 vertebra and in the sub-ROI in front of the L4-L5 IVD. Similarly, to describe the strain distribution along the ALL, the median over circumferential lines were computed in the sub-ROI in front of the L4 vertebra and in the sub-ROI in front of the L4-L5 IVD. The plots show the distribution of ε_1 (red) and ε_2 (blue) around L4 and the IVD (purple lines) and along L4 and the IVD (green lines). The median and standard deviation within the sample are reported

7.3.3.4 Specimen-specific analysis

In this section, the specific findings for the individual specimens are reported in terms of strain distribution (Fig. 7.8), also in relation to the peculiar bony-defects (e.g. osteophytes, scoliosis, etc.) of each specimen (Table 7.1):

- Specimen #1: this specimen was considered healthy based on x-ray imaging (the CT scan was not available). The strain patterns showed a right/left symmetry for both flexion and extension, and a specular distribution of strains for right vs. left lateral bending, and for clockwise vs. counterclockwise torsion
- Specimen #2: moderate osteophytes were visible at the both endplates of L4 and on the cranial endplate of L5. The L4-L5 segment had a score for the osteophyte formation of 11 points, equivalent to Grade 2 according to[143]. The DIC analysis highlighted some local intensification of the strain distribution in the ALL in front of the L4-L5 IVD, in correspondence of these osteophytes for all loading scenarios with exception of the left bending. Furthermore, a local thickening of the anterior wall of the vertebral body of L4 was visible in the CT scan. This corresponded to a region with lower strains in front of L4
- Specimen #3: the CT images exhibited moderate degenerative signs, with prominent osteophytes on the cranial endplates of L4 and of L5 (one on the right, one on the left of each

vertebra), which could act as strain concentrators cranially, while shielding the strains in the ALL surrounding them. The L4-L5 segment had a score for the osteophyte formation of 11 points, equivalent to a Grade 2. The DIC analysis showed an intensification of the strains in front of L3-L4 and L4-L5 IVDs, in the most cranial portion of the disc, and areas with much lower strains caudal to these spots

- Specimen #4: this specimen was mildly scoliotic with a Cobb angle T12-L5 of 10° and concavity on the right side. The DIC analysis showed a non-specular strain pattern between right and left lateral bending, and between clockwise and counterclockwise torsion. Furthermore, it had several osteophytes at all endplates. The L4-L5 segment had a score for the osteophyte formation of 15 points, equivalent to a Grade 2. The DIC analysis revealed strain concentrations near such osteophytes. The largest osteophyte projected upwards from the central-left margin of the superior endplate of L5 partially covering the caudal portion of the L4-L5 IVD. In this area a strain attenuation was visible in the area where the osteophyte covered the IVD, especially for flexion
- Specimen #5: the CT images showed that this specimen had prominent osteophytes on the right and left sides of the cranial endplates of L5. The L4-L5 segment had a score for the osteophyte formation of 17 points, equivalent to a Grade 3. The strain distributions showed an intensification in the right and left areas around L4-L5 IVD in flexion. More details about the individual specimens, the distribution of strains along and around the vertebrae and IVD can be found in the Supplementary Material.

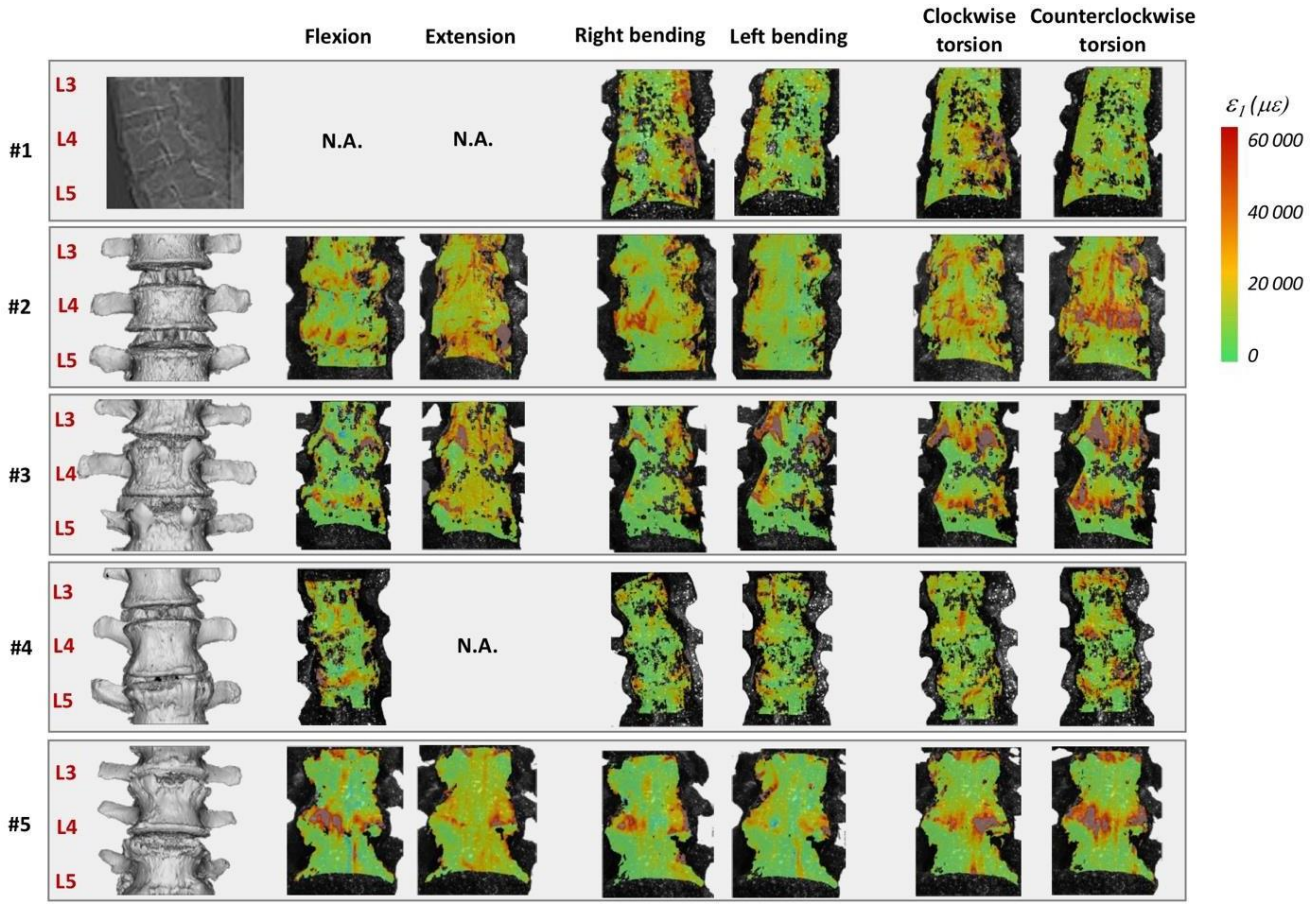

Fig. 7.8 - Specimen-specific analysis of the strain distribution: the CT images of each specimen are reported on the left (for Specimen #1 the CT was not available). On the right, the distribution of the maximum principal strain (ε_1) are plotted for each loading condition, at full load (7.5 Nm). The minimum principal strain (ε_2) and the analysis of the distribution of strain along and around the vertebra and the IVD are reported in the Supplementary Material

7.4 Discussion

The aim of this work was to explore the biomechanical behaviour of the most superficial layer of the anterior longitudinal ligament focusing on the anterior aspect of the lumbar vertebrae and intervertebral disc, applying a new paradigm. Structural flexibility tests and local strain analysis were performed on the anterior surface of spine segments loaded in flexion/extension, lateral bending and torsion. The hypotheses of the work were that: (i) the strain field on the surface of the ALL is not homogeneous between different regions (i.e.: in front of the vertebrae and of the intervertebral discs); (ii) the strain distribution is not homogenous within each such region, possibly due to specific bony-defects; (iii) inside the same region the strain field depends on the different loading scenarios; and (iv) opposite directions of loading translate to non-mirrored strain distributions.

In order to test these hypotheses, segments of multi-vertebra human spine segments, to reproduce a better loading transmission on the ALL, were used. Each specimen was tested in flexion/extension, lateral bending and axial torsion up to 7.5 Nm with a state-of-the-art spine tester.[147] The global ranges of motion and neutral zones were identified for each specimen and each loading scenario through flexibility tests using optical motion tracking system. These data were integrated with a full-field measurement of the strain distribution in front of 3 lumbar vertebrae and intervertebral discs using a validated digital image correlation approach.[96]

The global range of motion under load and the evaluation of the neutral zone, for the different loading scenarios, confirmed the typical trend and values for human lumbar spine, as reported in the Busscher *et al.* work.[33] They showed that segments from L1 to L4 at 4 Nm had a range of motion of 5° in flexion/extension, 6° in lateral bending and 2° in axial torsion. These results were in accordance with our study, indeed for L1-L4 segments at 4 Nm the following range of motion were obtained: 5.6° flexion/extension, 7.8° lateral bending and 2.9° axial torsion. The full-field strain maps (Fig. 7.2, 7.4, 7.6 and Supplementary Materials) highlighted the non-homogeneity of strain in the different areas of the ALL: different trends were observed both in the cranio-caudal and circumferential direction of the ALL for the different loading conditions (Fig. 7.3, 7.5, 7.7 and Supplementary Materials). The strain fields suggested that some fibers were pronouncedly more strained than the rest of the ALL during loading, both in front of the vertebra and of the IVDs. Furthermore, there was a clear effect of the stress concentrators: in most specimens, also some spots with larger strains were visible, especially close to the endplates. No strain concentration was detected close to the markers screws insertions, confirming that the ALL was not damaged during the flexibility test. A detailed inspection of the CT scans of the specimens highlighted that such strain concentrations corresponded to the position of local osteophytes and bony-defects (See Fig. 7.8 and the Supplementary Material for details). For instance, protruding osteophytes were associated with strain concentrations towards the tip of the osteophyte, but shielded the ALL in the areas where the osteophyte covered the IVD. Interestingly, despite osteophytes were found to reduce the flexibility of a severely degenerated spine[148], our results may contribute in elucidating the underlying biomechanical principles. A possible interpretation, suggested by the peculiar morphology of the osteophytes protruding from the endplates, may be that the relative distance of the outer ALL layers from to the instantaneous center of rotation of the FSU (i.e. lever arm)[149] is increased, thus, resulting in a higher local strain. A further characterization of the local tissue composition and properties would be needed in order to clarify this aspect.

The most strained portion of the ALL superficial layers was in front of the IVDs with a strain magnitude that was between 1.15 and 8.12 times larger than in front of the vertebrae (Fig. 7.2, 7.4, 7.6); these differences were statistically significant only for some loading scenarios (Table 7.2). This condition could be due to a series of reasons: the ALL in IVDs regions is thinner compared to the regions in front of the vertebrae[142], the ALL deep layers are less constrained in front of the IVD than in front of the vertebra[6], in front of the IVD the ALL is subjected to the large deformation of the IVD itself.[131] It is worth noting that, while the vertebral bone is at least two orders of magnitude stiffer

than the adjacent IVD[2, 53], the differences in strain of the superficial layer of the ALL in front of the vertebra and disc were relatively smaller: this is probably explained by the fact that the ALL act as a long ribbon, spanning across multiple FSU, with some motion relative to the underlying bone. Among the different direction of bending (flexion, extension, and lateral bending), flexion resulted in the highest strains and therefore seemed the most demanding loading scenario for the ligament (Fig. 7.2). In fact, due to the action of the underlying pressurized and bulging discs, the ALL is largely strained circumferentially. During flexion, the ALL can provide only a limited direct contribution to the spinal stability. However, the presence of large strains in the ALL seems to be due to anterior disc bulging during flexion, and indicates a role of the ALL in protecting the discs against herniation on the anterior face. Such a finding is consistent with[150], who observed that strain increased in the anterior portion of the IVD after ALL removal. Nevertheless, the ALL may have a significant bi-axial pre-strain *in vivo* depending on the region where it is attached (IVD or vertebra).[139] As the only way to measure a pre-strain is through destructive testing, this phenomenon cannot be captured by our current non-destructive analysis.

Also in extension the ALL in front of the IVD and of L4 underwent an appreciable longitudinal strain, confirming the important mechanical role of ALL in constraining extension, in conjunction with the action of the facet joints.[2]

Lateral bending seemed to be the loading scenario that strained less the ALL in terms of absolute values of strains. This is due because the ALL covers the regions in proximity of the neutral axis for lateral bending. Nevertheless, the strain distribution during right and left lateral bending was rather mirrored with respect to the vertical axis in front of the disc but not in front of the vertebra (Fig. 7.4-7.5, and Table 3). While the strains in the circumferential direction of the ALL for the left lateral bending showed the trend that one would expect based on the distribution of tension/compression in bending, this trend was not confirmed for right lateral bending. It is possible to hypothesize that this systematic difference was due to the scoliosis of the donors. Unfortunately, no information was available about their dominant side (left-handed or right-handed) that could influence this systematic difference.

The torsional scenario was associated with large strains in the ALL, with smaller differences between the regions in front of the vertebrae and of the IVD (Fig. 7.6). The lack of symmetry between right and left torsion (Fig. 7.7 and Table 7.3) could again be explained by some asymmetry due to laterality of the donors. Furthermore, scoliotic specimens showed different strain maps between bending in the two directions, and between the two opposite directions of torsion. Therefore, not only we were able to identify general trends, but also to detect localized effect of large and small anatomical anomalies.

To the best authors' knowledge, this is the first work where the full-field strain distributions were computed on the ALL in lumbar spine segments. Previous works explored the mechanical behaviour of ALL through strain analysis. [151]measured the mechanical properties of the ALL in situ under pure tension, after removal of the IVD. The evaluation of the tensile strain was performed on macro-regions of the ALL: insertions and free-length, in the cranio-caudal direction of the ALL; outer and central regions, circumferentially the ALL. They showed larger strain in the substance and outer regions of the ligaments, similar to the present study. [131, 150]evaluated the strain on the entire surface of the intervertebral discs through a laser scanner device while the FSU segments was loaded in the same spine tester and the same conditions as the present work. The strain magnitude and distribution reported in those papers are comparable with the median strains obtained in the present work, confirming the suitability of the measurement technique and corroborating the present results.

Other works studied the mechanical properties of the ALL removing it from the spine and testing it in pure tensile tests. These conditions were far from the scenarios implemented in the present study; nevertheless some qualitative comparisons are possible. [61, 142]revealed the weakness of the ALL at the level of the IVDs. Unfortunately, the non-destructive testing procedure did not allow to analyse the different layers of the ALL and how each layer influenced the strain distribution. According to our observations, we can surely appreciate that under consistent loading conditions, specific regions of different specimens lead to comparable strain patterns.

A limitation of the present work is the sample size: five specimens have a limited statistical power. It worth noticing that the results here reported are in agreement with the kinematics data reported for a larger specimens' cohort.[152] As this study is extremely demanding in terms of costs, testing and strain analysis, it was not possible to extend to a larger sample. However, the differences between the different anatomical regions, and between loading scenarios were sufficiently large to show statistical significance in most cases.

Some specimens showed some typical defects of elderly donors, such as osteophytes and consequent disc degeneration. Our detailed DIC strain investigation on the region of interest allowed identifying the associated perturbations on the strain distributions. However, some of the results may be biased by a relatively high BMI of the donors, and a relatively low BMD. While the present findings are directly applicable to spines of subjects with similar BMI, an extension to cases with normal BMI is possible because the donors were physically active until death, and therefore their ALL can be expected to have normal mechanical properties. Conversely, slightly different behaviour would possibly be observed in healthier spines with different BMD: the bone/ligaments insertions would play a fundamental role, in particular their stiffness could modify the local behaviour of the ALL.

The experimental setup had intrinsic limitations such as the reduced loading rate, which is far from physiological.[121] This was necessary to ensure that the soft tissues were not subjected to trauma, and a series of cycles can be repeated.[37] Furthermore, the focus of this study was not on the absolute magnitude of the strains which would be affected by the loading rate, but on a comparison between different regions and different loading scenarios under quasi-static loading conditions. Although, muscles forces and weight contribution were not considered in the current study, pure unconstrained moments remains the preferred option for *in vitro* reproducing relevant loading conditions.[146] Furthermore, this loading condition allows better control and reproducibility compared to follower loads (an experimental technique for applying compressive loads along the whole spine segment) or a compressive load.[36, 153]

The accuracy and precision of the DIC was optimized for each acquisition; however, testing fresh specimens entailed leakages of biological fluid that can lead to some local loss of correlation.[112] In the worst case, correlation was lost on 20% of the region of interest. Nevertheless, the entire acquisition and post-processing protocol allowed to clearly show what happened in the different specimens and different loading conditions. Finally, only what happened on the visible surface of the ligaments was evaluated. Currently, it is the only possible compromise to study the ALL in physiological range of motion.

7.5 Conclusions

This is the first time that the distribution of strain in the anterior longitudinal ligament was measured in multi-vertebra intact spine segments. The obtained results showed the non-uniform strain distribution, under the different loading scenarios. The vertebrae and intervertebral discs, with their peculiar defects (e.g.: osteophytes, etc.) played a fundamental role in defining the behaviour of the ALL. The current analysis including a spine tester and an unpreceded measurement of the strain distribution is so detailed that not only we could investigate the average effects of the different loading scenarios, but also the local effect that subject-specific defects may have on strain distribution. These results suggested again the importance of a full-field strain analysis to understand the biomechanics of the human spine and the interaction between different tissue types. This work could be the starting point for future studies where the effect of surgical procedures will be compared with intact spines.

Table 7.2 - The reported p-values show the statistical significance of the difference between the median on the vertebrae and intervertebral discs for the same loading condition (two-sample Mann-Whitney test). The median of strains on the ALL in front of the L4 vertebra and the L4-L5 intervertebral disc were examined

	Maximum principal strain (ε_1)	**Minimum principal strain (ε_2)**
	Vertebra Vs IVD	**Vertebra Vs IVD**
Flexion	p = 0.03 (*)	p = 0.34
Extension	p = 0.10	p = 0.70
Left Bending	p = 0.10	p = 0.42
Right Bending	p = 0.06	p = 0.31
Clockwise torsion	p = 0.03 (*)	p = 0.01 (*)
Counterclockwise torsion	p = 0.03 (*)	p = 0.02 (*)

Note: (*) highlights significant differences (p<0.05).

Table 7.3 - The reported p-values show the statistical significance of the difference between the trends for opposite directions of loading (two-sample Kolmogorov-Smirnov). The distribution of strains (Figs. 7.5, 7.6 and 7.7) along the L4 vertebra and along the L4-L5 intervertebral disc (computed as median strains over circumferential lines), and the distribution of strains around the L4 vertebra and around the L4-L5 intervertebral disc (computed as median strains over cranio-caudal lines) were examined for the different loading scenarios

	Maximum principal strain (ε_1)	**Minimum principal strain (ε_2)**
	Flexion Vs Extension	
Along L4	p = 8.9 x 10-6 (*)	p = 2.8 x 10-3 (*)
Along IVD	p = 7.4 x 10-1	p = 1.8 x 10-2 (*)
Around L4	p = 1.3 x 10-13 (*)	p = 8.2 x 10-7 (*)
Around IVD	p = 5.2 x 10-1	p = 3.5 x 10-5 (*)
	Right Vs Left	
Along L4	p = 1.5 x 10-4 (*)	p = 2.4 x 10-8 (*)
Along IVD	p = 5.3 x 10-6 (*)	p = 1.6 x 10-9 (*)
Around L4	p = 1.5 x 10-1	p = 2.8 x 10-2 (*)
Around IVD	p = 1.4 x 10-3 (*)	p = 8.2 x 10-2
	Clockwise Vs Counterclockwise	
Along L4	p = 8.2 x 10-1	p = 6.8 x 10-3 (*)
Along IVD	p = 4.2 x 10-9 (*)	p = 2.4 x 10-5 (*)
Around L4	p = 1.5 x 10-1	p = 3.7 x 10-1
Around IVD	p = 1.9 x 10-8 (*)	p = 3.9 x 10-2 (*)

Note: (*) highlights significant differences (p<0.05).

Supplementary Materials

For each specimen (#1 to #5, in separate sheets) the following are reported:

- Left: An image of the specimen with an indication of the vertebrae and disc under consideration, and of the sub-ROIs where strains were computed along and around the ALL in front of the L4 vertebra and in front of the L4-L5 IVD
- For each loading scenario, the maps of the maximum (ε_1) and minimum (ε_2) engineering principal strains are shown in the top images. Below each loading scenario, the distributions of the maximum (ε_1) and minimum (ε_2) strains are plotted around and along the ALL, both in front of the L4 vertebra and of the L4-L5 IVD
- On the right, a volumetric reconstruction of the vertebrae from the CT scan is reported: the arrows highlight the osteophytes, graded as 1 (<3 mm), 2 (between 3 and 6 mm) or 3 (>6 mm) according to Wilke *et al.* 2006
- The table at the bottom right reports the median strains (maximum (ε_1) and minimum (ε_2) engineering principal strains) both in front of the L4 vertebra and in front of the L4-L5 IVD, for each loading scenario.

Published in: PLOS ONE, 2020: 1-21

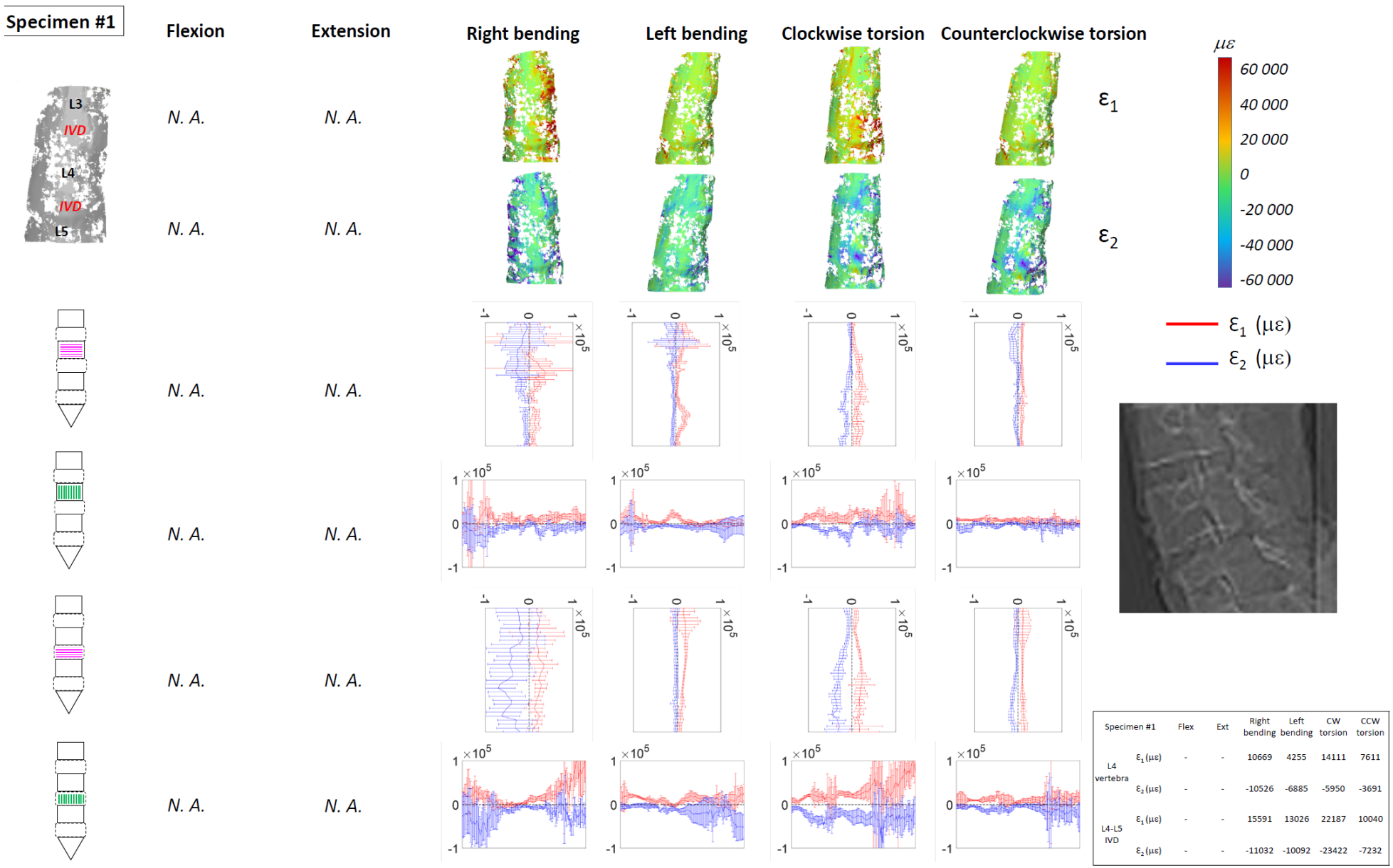

Specimen #1		Flex	Ext	Right bending	Left bending	CW torsion	CCW torsion
L4 vertebra	ε_1 (με)	-	-	10669	4255	14111	7611
	ε_2 (με)	-	-	-10526	-6885	-5950	-3691
L4-L5 IVD	ε_1 (με)	-	-	15591	13026	22187	10040
	ε_2 (με)	-	-	-11032	-10092	-23422	-7232

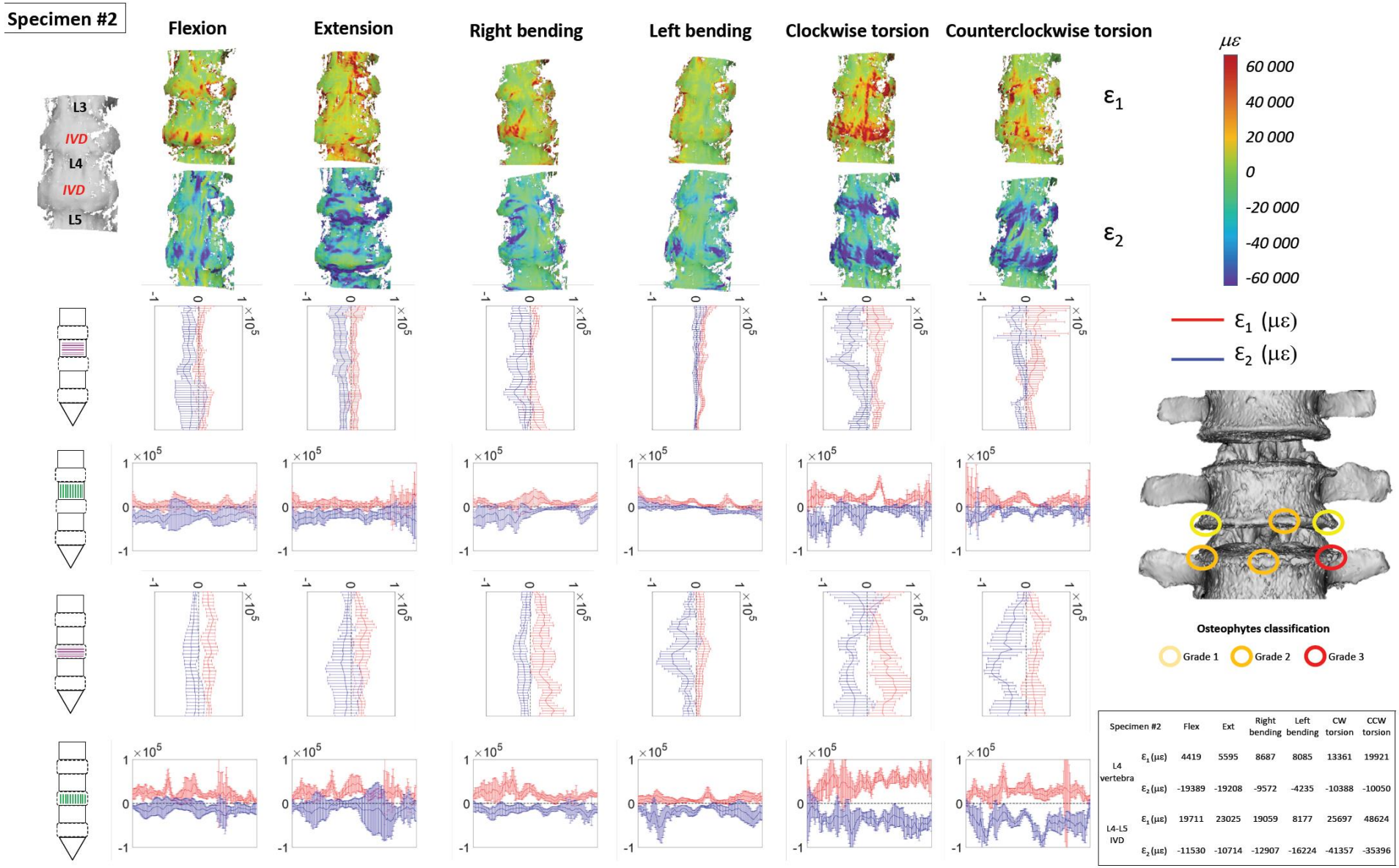

Specimen #2		Flex	Ext	Right bending	Left bending	CW torsion	CCW torsion
L4 vertebra	ε_1 (με)	4419	5595	8687	8085	13361	19921
	ε_2 (με)	-19389	-19208	-9572	-4235	-10388	-10050
L4-L5 IVD	ε_1 (με)	19711	23025	19059	8177	25697	48624
	ε_2 (με)	-11530	-10714	-12907	-16224	-41357	-35396

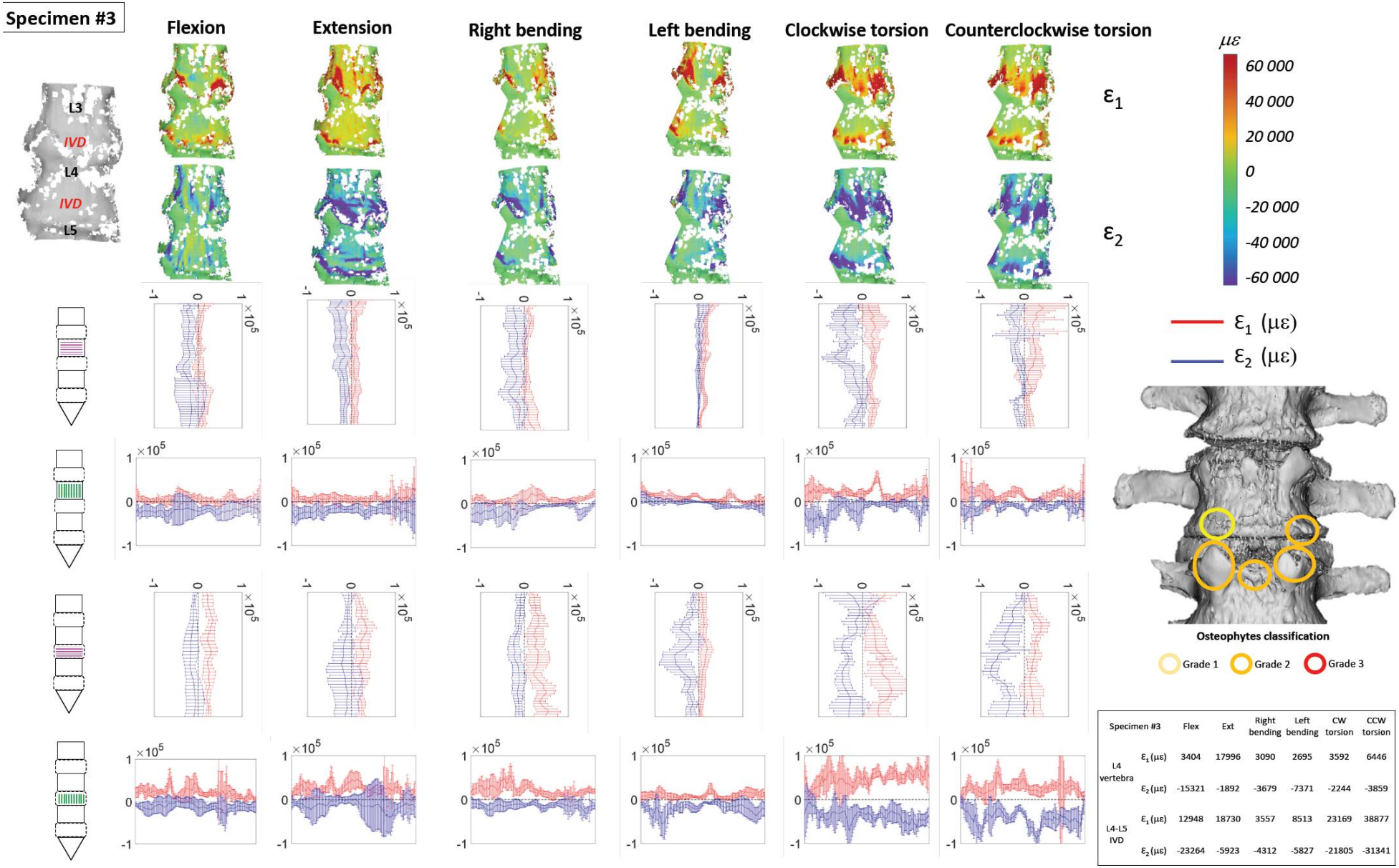

Specimen #3		Flex	Ext	Right bending	Left bending	CW torsion	CCW torsion
L4 vertebra	ε_1 (με)	3404	17996	3090	2695	3592	6446
	ε_2 (με)	-15321	-1892	-3679	-7371	-2244	-3859
L4-L5 IVD	ε_1 (με)	12948	18730	3557	8513	23169	38877
	ε_2 (με)	-23264	-5923	-4312	-5827	-21805	-31341

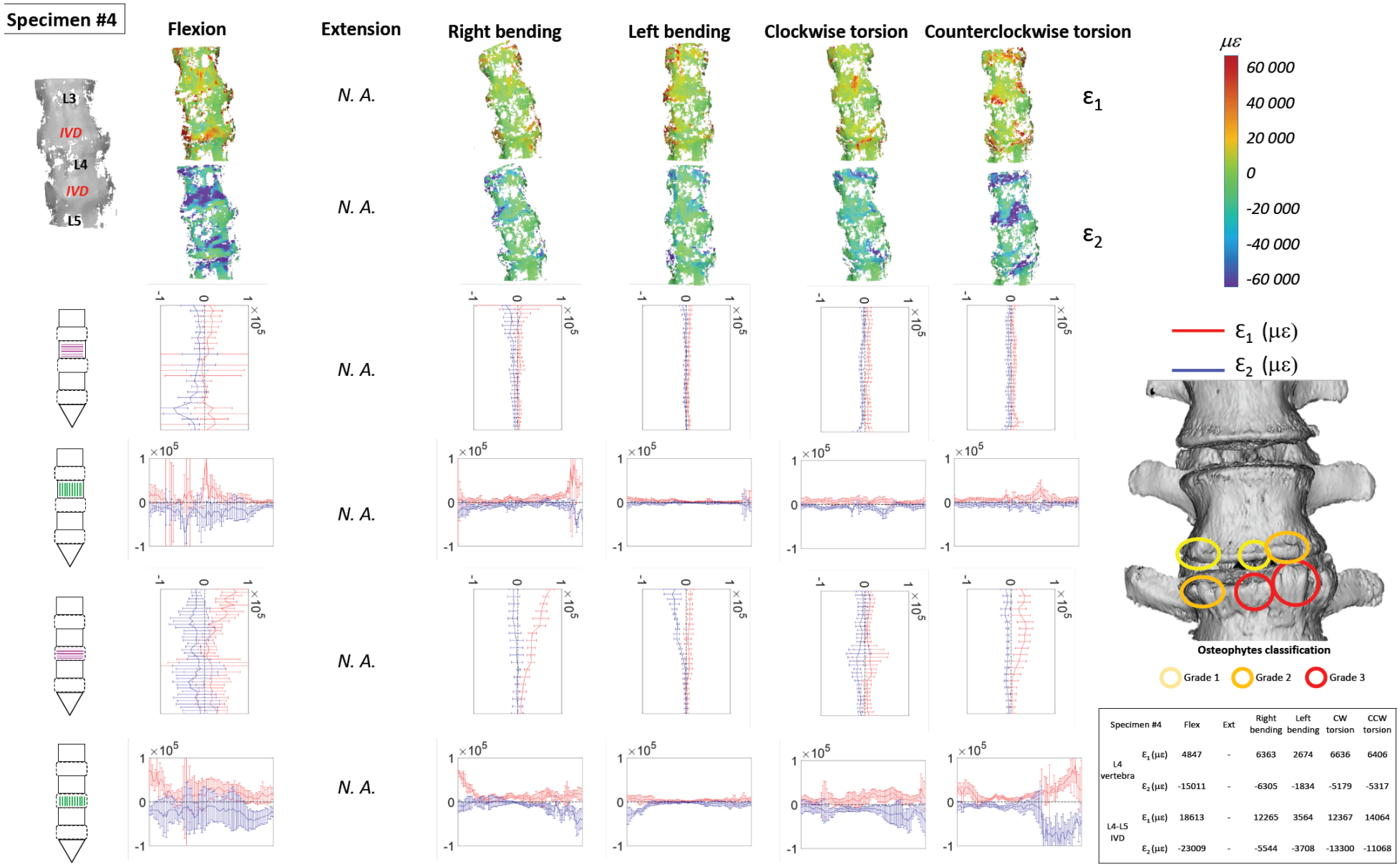

Specimen #4		Flex	Ext	Right bending	Left bending	CW torsion	CCW torsion
L4 vertebra	ε_1 (με)	4847	-	6363	2674	6636	6406
	ε_2 (με)	-15011	-	-6305	-1834	-5179	-5317
L4-L5 IVD	ε_1 (με)	18613	-	12265	3564	12367	14064
	ε_2 (με)	-23009	-	-5544	-3708	-13300	-11068

Published in: PLOS ONE, 2020: 1-21

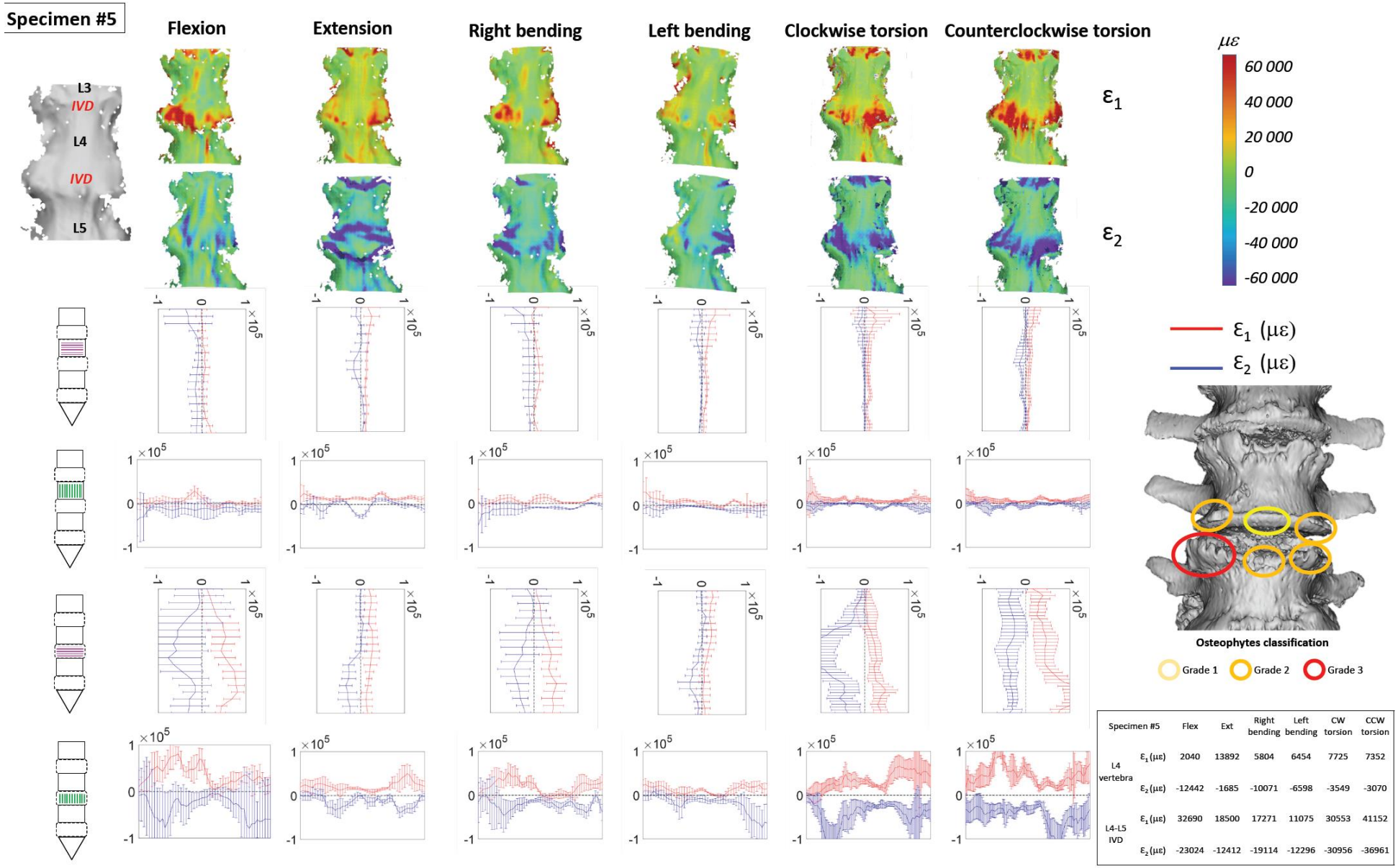

Specimen #5		Flex	Ext	Right bending	Left bending	CW torsion	CCW torsion
L4 vertebra	ε_1 (με)	2040	13892	5804	6454	7725	7352
	ε_2 (με)	-12442	-1685	-10071	-6598	-3549	-3070
L4-L5 IVD	ε_1 (με)	32690	18500	17271	11075	30553	41152
	ε_2 (με)	-23024	-12412	-19114	-12296	-30956	-36961

Chapter 8

Analysis on the non-linear response of the Anterior Longitudinal Ligament

From the manuscript

Digital Image Correlation (DIC) assessment of the non-linear response of the Anterior Longitudinal Ligament of the spine during flexion and extension [154]

Maria Luisa Ruspi[1], Marco Palanca[1], Luca Cristofolini[1], Christian Liebsch[2], Tomaso Villa[3], Marco Brayda-Bruno[5], Fabio Galbusera[4], Hans-Joachim Wilke[2], Luigi La Barbera[3,6,7]

1 Department of Industrial Engineering, School of Engineering and Architecture, Alma Mater Studiorum – Università di Bologna, Bologna, Italy
2 Institute of Orthopaedic Research and Biomechanics, Trauma Research Center Ulm (ZTF), University Hospital Ulm, Ulm, Germany
3 Laboratory of Biological Structure Mechanics, Department of Chemistry, Materials and Chemical Engineering "G. Natta", Politecnico di Milano, Milan, Italy
4 IRCCS Istituto Ortopedico Galeazzi, Milan, Italy
5 Department of Spine Surgery III, IRCCS Istituto Ortopedico Galeazzi, Milan
6 Department of Mechanics, Polytechnique Montréal, Montréal, Canada
7 Sainte-Justine University Hospital Center, Montréal, Canada

Published in: Materials (Digital/Volume Correlation of Biological Tissues and Biomaterials), 2020, 13, 384: 1-14

8.1 Introduction

The Anterior Longitudinal Ligament (ALL) represents a band covering the anterior aspect of the spine from cervical to lumbo-sacral levels. It contains a high proportion of stiff closely packed collagen fibers, in contrast with other spinal ligaments with more elastin.[62] The most superficial longitudinal fibers span over multiple functional spinal units (FSUs), while the deepest integrate on the periosteum of adjacent vertebrae and cannot be histologically distinguished from the annulus fibrosus of the intervertebral disc (IVD).[8, 138] The collagen fibers, initially broadly organized with a wavy pattern in the unloaded state, are progressively recruited, aligned and stretched along the loading direction, thus yielding a characteristic highly non-linear mechanical response.[62]
Experimental studies at the tissue level on isolated ALL and on vertebra-ALL-vertebra specimens reported a highly non-uniform and non-linear biomechanical response. In addition the failure stress decreases with age and disc degeneration.[151, 155] The stiffness and the failure tensile force increased with bone mineral content.[156, 157] Viscoelasticity of isolated ALL has also been reported.[62, 64, 142, 156] Several authors also demonstrated the presence of longitudinal and transversal pre-strains on the ALL *in vivo*.[62, 139, 142]
In vitro studies on single FSUs demonstrated that the ALL is almost linearly loaded in flexion-extension and contributes to stabilize the FSU, while protecting the spinal cord from excessive strain.[143, 158] Step-wise reduction studies on single thoracic and lumbar FSUs, highlighted the fundamental stabilizing effect of the ALL in extension both following a posterior-to-anterior[150] and an anterior-to-posterior resection protocol.[71] Moreover, the ALL contributes to stabilizing the IVD and constraining the anulus fibrosus from excessive bulging, primarily during flexion.[150]
Although previous studies provide some insights on the biomechanical role of the ALL, they present some intrinsic limitations. Analyses at tissue level require the disruption and/or the dissection of the ligamentous structures, therefore neglecting the potential interplay with the surrounding structures (vertebrae and IVDs) on the local mechanical response. When a single FSU is tested, only a short portion of the ALL is included: this preserves the deep fibers (connecting two adjacent vertebrae) but not the superficial ones (spanning over several vertebrae). Therefore, only the contribution of the short fibers is properly assessed, while the effect of the long ones is partly compromised. In fact, *in vitro* tests on long multi-segmental spinal segments pointed out the importance of preserving the integrity of the ligamentous structures extending over multiple FSUs to correctly catch the complex behaviour of the spine.[32]
Although a topographical description of the strain values along the length and the width of the ALL has already been reported on multiple lumbar FSUs, the evaluation was based on only few discrete points.[139] Another analysis based on a laser scanner allowed indirectly evaluating the local strains of the IVD under complex loading [149], but it completely neglected the ALL. More recently, Digital Image Correlation (DIC) overcame these limitations allowing the evaluation of the full-field strain distribution on the entire surface of the ALL under different loading conditions.[96]
The present *in vitro* study addressed the behavior of the superficial layers of the ALL using full-field DIC analysis on intact multi-segmental spinal specimens. The focus was on the lumbar spine, in detail in the L4-L5 region, where the greatest number of soft tissue lesions are reported (such as disc herniation).[159] This is a basic science study aiming to provide data about the non-linear contribution of the ALL during the different phases of spinal flexion and extension. This information could provide identification criteria to build better multibody spine models able to capture the changing stiffness of the ALL during motion, or to include more realistic material properties in finite element models. The specific aims were to:

1. Characterize the strain distribution of the ALL in situ during flexion-extension
2. Compare the strain in specific regions of interest (ROIs), in front of L4 vertebral body (VB) and L4-L5 IVD

3. Analyse the non-linear relationship between the measured strain and the imposed rotation and the resultant moment.

8.2. Material and methods

8.2.1 Specimens

In order to analyse the behaviour of the ALL, three fresh-frozen human thoracolumbar spine segments (consisting of 6 FSUs from T12 to sacrum) were obtained through an ethically approved international donation program (Science Care Inc., Phoenix, AZ). The donors were all Caucasian, two males and one female (Table 8.1). Clinical computed tomography (CT) scans (Philips Brilliance 64, Philips Healthcare, Cleveland, USA) were used to verify the state of degeneration and determine the bone mineral density (BMD).[145] No fractures, tumours were observed; however, all specimens showed some osteophytes as can be expected with aged donors.[148]
The spines were carefully cleaned on the anterior side removing fat tissue and muscles in order to expose the ALL, while all the posterior osteo-ligamentous structures were left intact. The two extremities of the specimens were potted in poly-methyl-methacrylate cement (PMMA, Technovit 3040, Heraeus Kulzer, Werheim, Germany). During tests, the hydration of the specimens was assured spraying saline solution.

Tab. 8.1 - Details of the specimens with the donor's information. The last column reports the grading of the osteophytes (scored according to[145])

Specimen	Segment	Sex	Age at death (years)	Height (cm)	Weight (kg)	BMI (kg/m2)	BMD (mg/cm3)	Assessment of the osteophytes in the L4-L5 area
A	T11-S1	M	66	183	141	42.1	82	2 osteophytes (both grade 2) centrally-located on the endplate of both L4 and L5
B	T11-S1	M	62	178	164	51.7	94	1 osteophyte (grade 2) centrally-located on the endplate of L5
C	T12-S1	F	63	157	125	50.7	157	2 osteophytes (grade 1 and grade 2) centrally-located on the endplate of respectively L4 and L5

8.2.2 Mechanical test

The load was applied using a state-of-the-art spine tester[37, 147]: the caudal side was fixed, while the cranial side was connected to the gimbal with three integrated stepper motors (FT 1500/40, Schunk GmbH & Co. KG, Lauffen/Neckar, Germany) (Fig. 8.1). A six-components load cell measured the moments and forces applied. All specimens were tested in flexion-extension (up to ±7.5 Nm at a rate of 1°/s) at room temperature (ca. 23°C). All motions started and finished in the unloaded neutral position.[37] Each test consisted of three consecutive cycles of loading: the first two cycles for pre-conditioning and the last one for the actual analysis.[37]

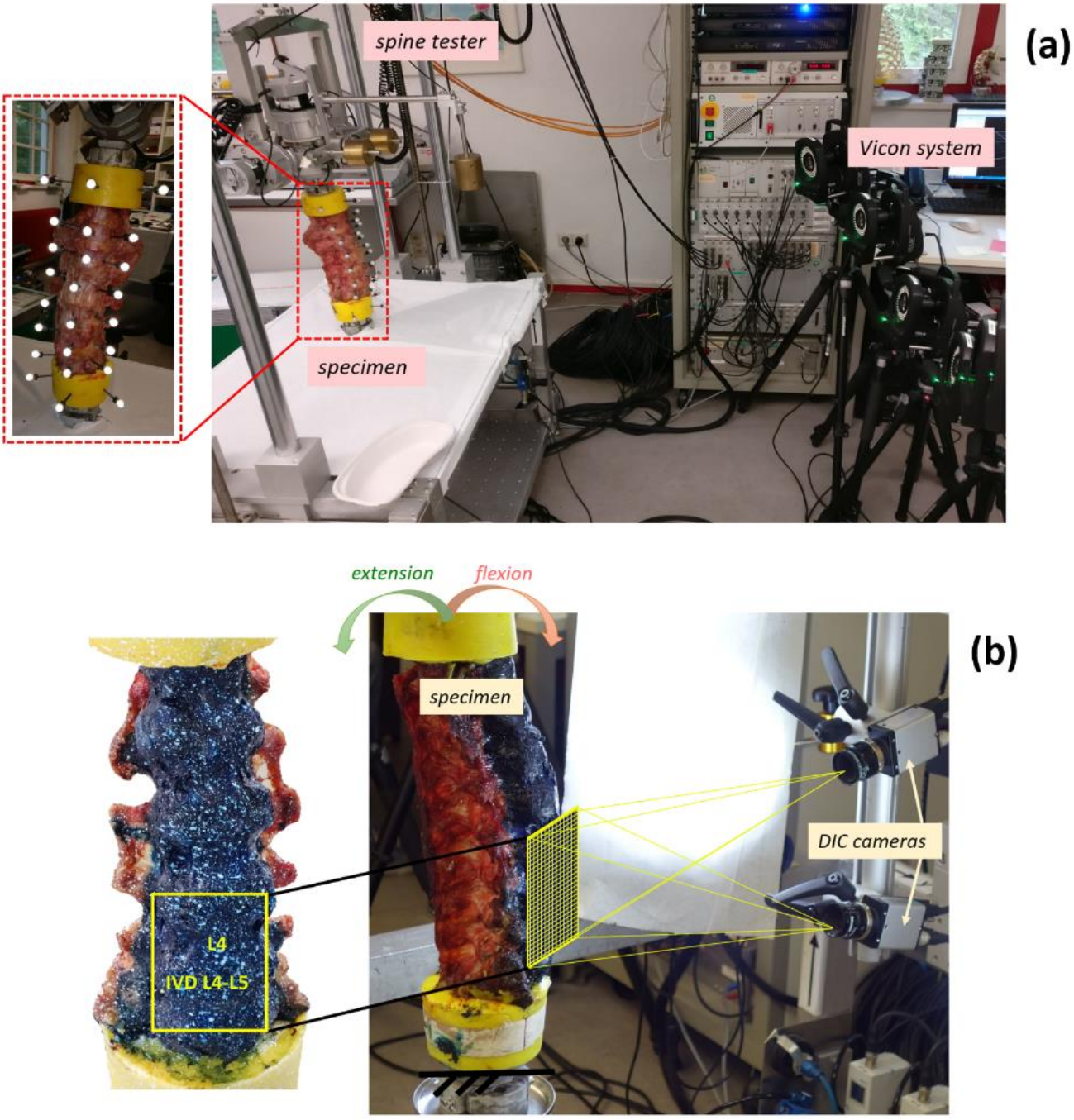

Fig. 8.1 - Overview of the test configuration and data acquisition systems. The top part (a) shows the test session where motion was measured: the spine segment with the markers (three on each vertebra) is visible on the left. The spine tester and four of the six cameras of Vicon system are visible on the right. The bottom part (b) shows the session where strains were measured: the specimen with the white-on-black speckle pattern for the DIC analysis is visible on the left. The field of view recorded by the DIC cameras is indicated. On the right, the specimen mounted in the spine tester in front of the DIC system is shown

8.2.3 Measurement of intervertebral motions

The different levels of the spine exhibit different values of flexibility, range of motion (RoM) and stiffness. The analysis focused on lumbar spine (in detail on L4-L5 vertebrae) because this region of the spine is more subject to pain especially due to soft tissue lesions (such as disc herniation).[159] So, in order to measure the RoM in terms of angle between L4 and L5, an optical motion tracking system was used. Six cameras (MX13, Vicon Motion Systems Ltd., Oxford, UK) quantified the 3D coordinates of three reflective markers positioned on L4 and L5 vertebrae. Starting from these data, the L4-L5 intervertebral angle was calculated in the sagittal plane during the three loading cycles (Fig. 8.2).

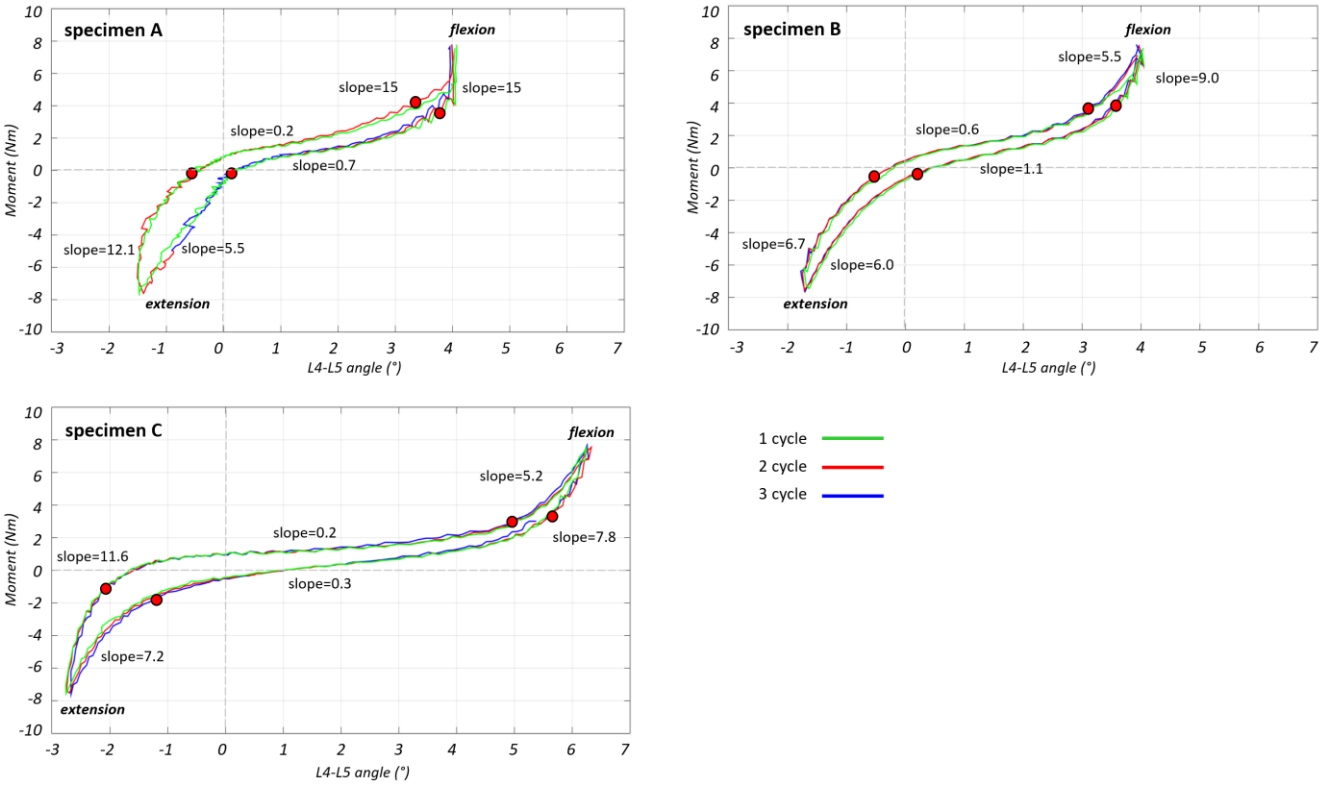

Fig. 8.2 - The moment-angle curves for the three loading cycles are reported for each specimen. Positive values of moment correspond to flexion, while negative values of moment correspond to extension. The circles indicate the end of the NZ and the beginning of the EZ (identified where the slope of the curve reached 2 Nm/deg). The values of minimum and maximum slope for the NZ and EZ are reported both for the curve flexion-to-extension and extension-to-flexion

8.2.4 Digital Image Correlation

The test (three additional loading cycles) was repeated after removing the markers, using DIC to obtain a full-field strain distribution on the ALL. A white-on-black speckle pattern was prepared on the anterior surface of the specimens. The multi-segmental spine segments were first stained with a 4% solution of methylene blue and water.[20, 96] The white speckle pattern was applied using an airbrush gun following an optimized procedure.[41] This method has been demonstrated to not significantly affect the biomechanical behaviour.[41]

A commercial 3D-DIC system was used (Q400, Dantec Dynamics, Denmark) with its software (Instra 4D, v. 4.3.1, Dantec Dynamics), equipped with two cameras (5 MegaPixels, 2440x2050, 8-bit, black-and-white) with 17 mm lenses. The specimens were illuminated with a system of LEDs (10000 lumens in total). The field of view was set to 120 mm by 160 mm which gave a pixel size of about 0.08 mm and a depth of field of 70 mm with the adopted aperture (f/22). Images were acquired at 5

Published in: Materials (Digital/Volume Correlation of Biological Tissues and Biomaterials), 2020, 13, 384: 1-14

frames per second. Calibration was performed before the tests using a proprietary calibration target (Al4-BMB-9x9, Dantec Dynamics).
The main source of error in DIC-measured strain derives from the image noise, which translates to random strain errors. Therefore, the parameters for the correlation analysis were preliminarily optimized during a zero-strain test for each specimen to minimize the errors (Table 8.2).

Table 8.2 - Details of the parameters used for the correlation analysis with the DIC system (according to[132])

Parameters for the correlation analysis	
DIC Software Package Name and Manufacturer	Instra 4D, v. 4.3.1, Dantec Dynamics
Distance of the cameras	540 mm
Field of view	about 120 mm by 160 mm
Depth of field	70 mm
Lens aperture	f/22
Frame rate	5 frames per second
Grid spacing	4 pixels
Facet size	between 39 and 59 pixels
Pixel size	about 0.08 mm
Contour smoothing	kernel size 5 x 5

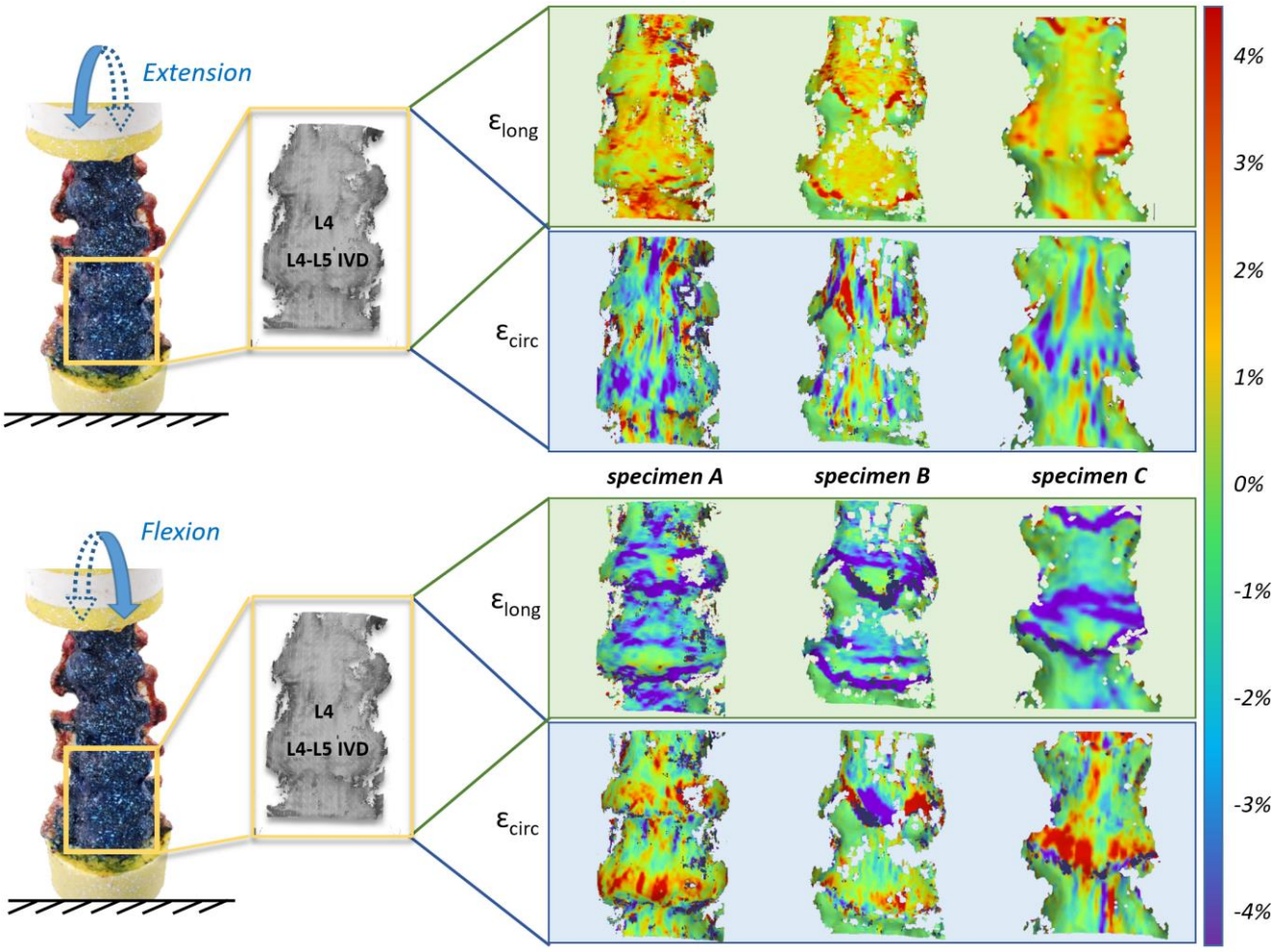

Fig. 8.3 - Full-field strain maps obtained from the DIC analysis for all the specimens at the peak load (±7.5 Nm). The longitudinal (ε_{long}) and circumferential (ε_{circ}) percent strain are reported for extension (top) and flexion (bottom). The colour maps show the non-uniform distribution of strain

8.2.5 Analysis of strain

The distribution of strain was evaluated on the ALL in front of the L4 vertebra and in front of the L4-L5 IVD. In order to focus on the ALL and investigate its mechanical contribution, regions of interest (ROIs) were identified in correspondence with the most strained areas of the ALL. The spots with the peak longitudinal strain (ε_{long}) were first identified, both in front of the vertebra and in front of the IVD. The two ROIs were then selected on each specimen so as to include the area around such spots where strains were higher than 50% of the corresponding peak previously identified. This way, roughly rectangular areas of about 200-250 mm2 were identified. For each ROI, the values of longitudinal strain were analysed throughout the entire load cycles as the mean over the ROIs.

8.2.6 Analysis of the non-linearity

In order to analyse the non-linear behaviour of the spine segment, first of all the neutral zone (NZ) and elastic zone (EZ) were identified on the third cycle of the moment-angle curve (Fig. 8.4, 8.5, 8.6). The slope of the curve was calculated throughout the load cycle with a moving linear regression on 10 points (which corresponded to 2% - 4% of the total points of the curve, and to an interval of 2-3 seconds).
The limit of the NZ was defined where the slope became greater than 2 Nm/deg. The EZ limit was defined from the end of NZ and to the peak of the moment-angle curve. The NZ and the EZ zone were identified for both directions of motion (from flexion-to-extension and from extension-to-flexion).

Published in: Materials (Digital/Volume Correlation of Biological Tissues and Biomaterials), 2020, 13, 384: 1-14

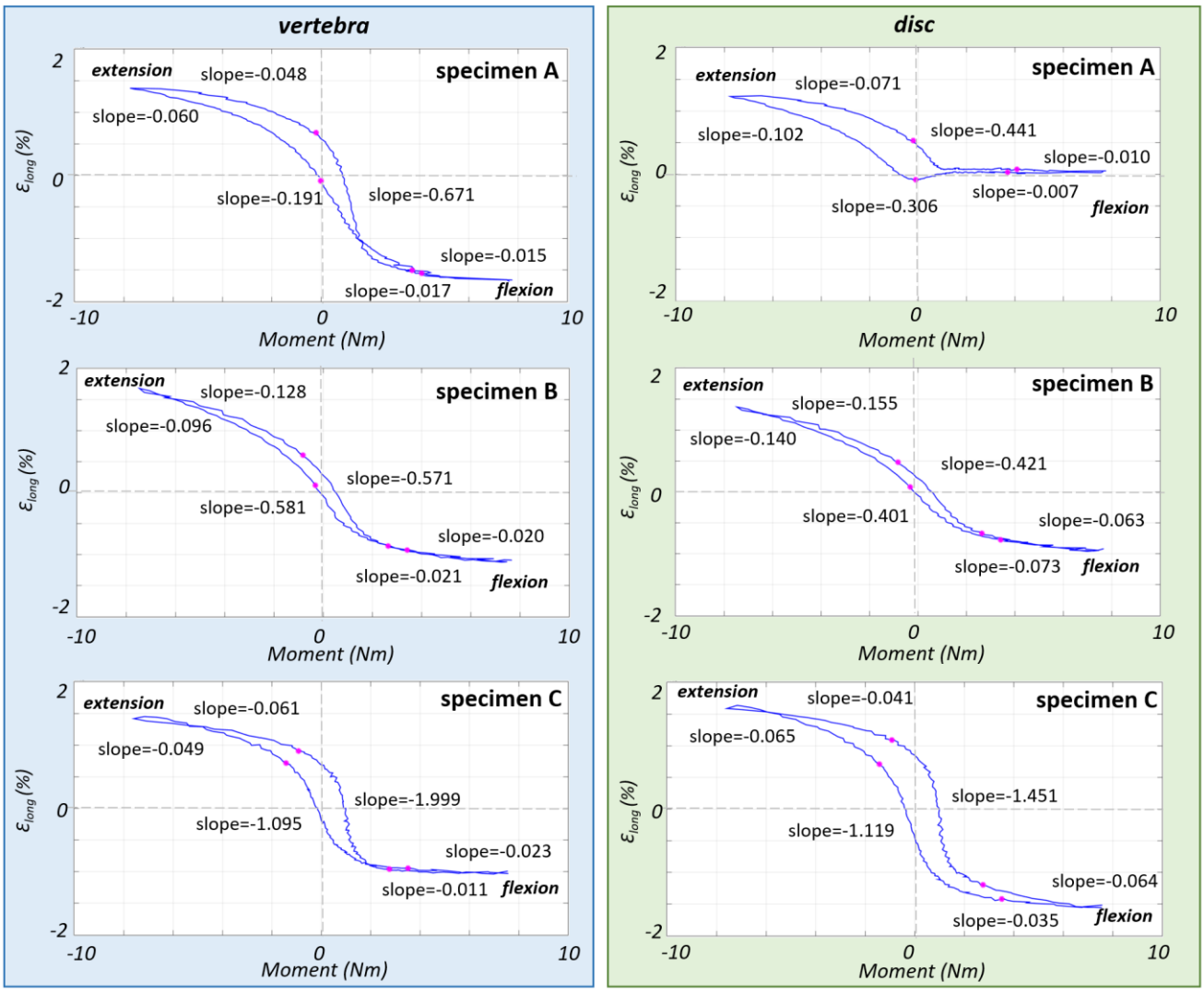

Fig. 8.4 - The strain-moment curves of the third loading cycle are reported for each specimen, showing how the strain in the ALL varied in front of the vertebra (left charts) and in front of the disc (right charts). The end of the NZ and the beginning of the EZ (identified on moment-angle curves, Fig. 8.2), are reported here with circles. The values of minimum and maximum slope (% strain / Nm) for the NZ and EZ are reported both for the curve flexion-to-extension and extension-to-flexion

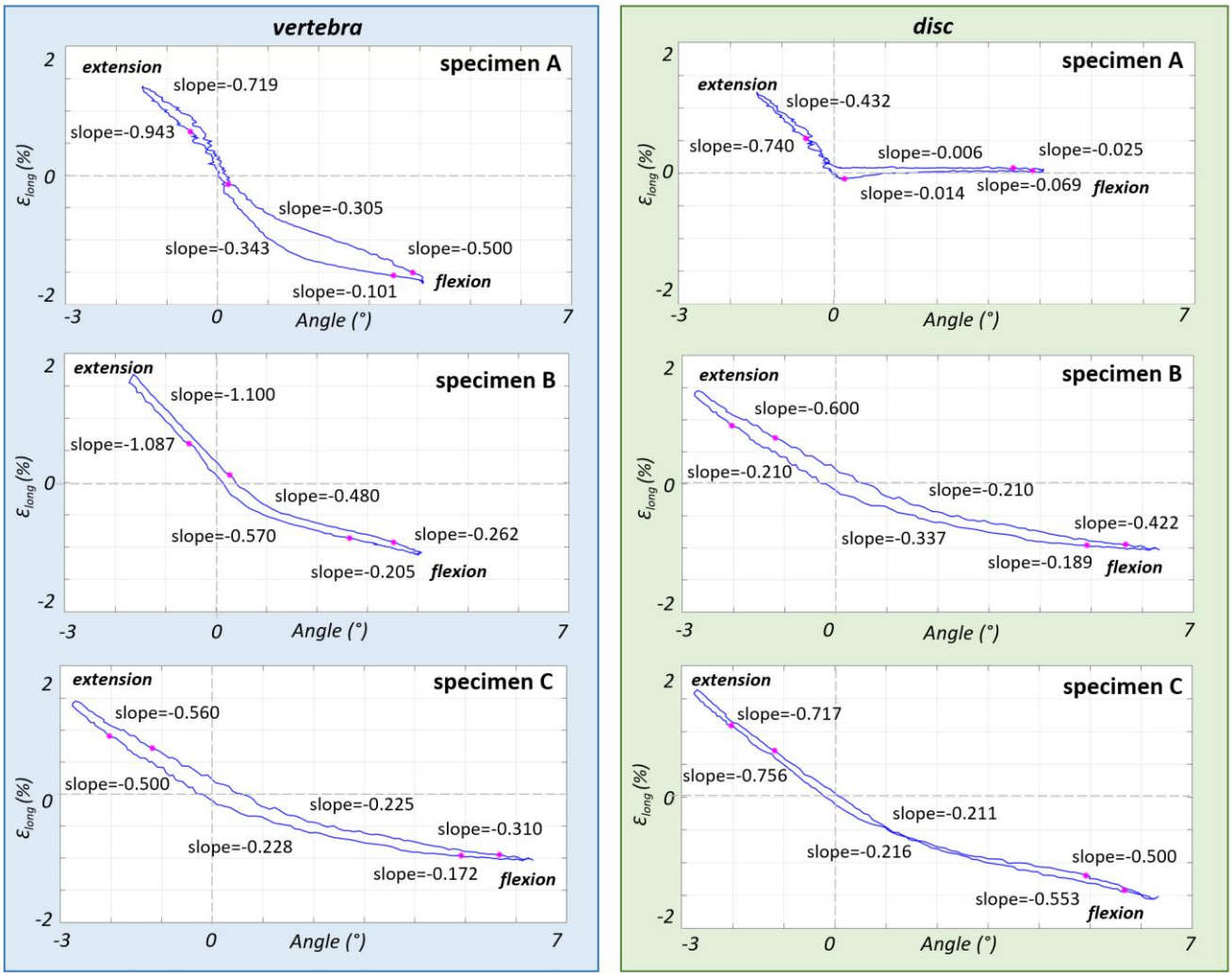

Fig. 8.5 - The strain-angle curves of the third loading cycle are reported for each specimen, showing how the strain in the ALL varied in front of the vertebra (left charts) and in front of the disc (right charts). The end of the NZ and the beginning of the EZ (identified on moment-angle curves, Fig. 8.2), are reported here with circles. The values of minimum and maximum slope (% strain / ° degree) for the NZ and EZ are reported both for the curve flexion-to-extension and extension-to-flexion

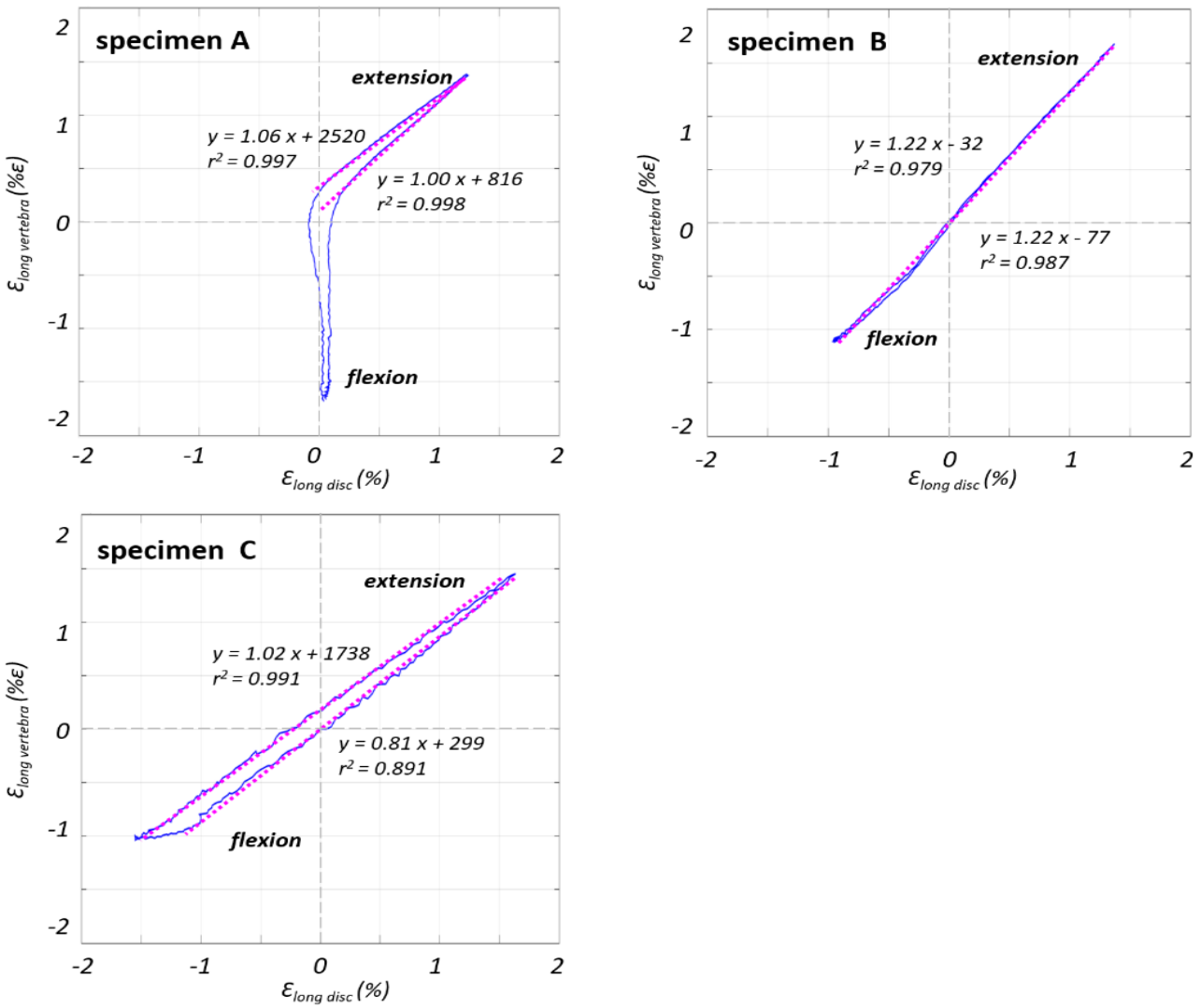

Fig. 8.6 - The strain in the ALL in front of the vertebra is plotted against the strain in front of the disc for the third loading cycle, showing a highly linear trend. The regression line is reported with its equation and the r square, separately for the curve flexion-to-extension and extension-to-flexion

Tab. 8.3 - The values of moment, angle between L4 and L5 and strain (in front of the vertebra and in front of the disc) in correspondence to the end of LZ and the beginning of EZ are reported in the range of angles corresponding to spine flexion and extension, both for the direction flexion-to-extension (f-e) and for the direction extension-to-flexion (e-f)

Specimen	Moment (Nm)				Angle (°)				Strain in front of vertebra (%)				Strain in front of disc (%)			
	flexion		extension		flexion		extension		flexion		extension		flexion		extension	
	f-e	e-f	f-e	e-f	f-e	e-f	f-e	e-f	f-e	e-f	f-e	e-f	f-e	e-f	f-e	e-f
A	3.70	4.09	-0.10	-0.20	3.86	3.48	0.21	-0.53	-1.55%	-1.50%	-0.14%	0.73%	0.04%	0.08%	-0.08%	0.54%
B	3.42	2.65	-0.31	-0.82	3.52	2.65	0.27	-0.53	-0.92%	-0.86%	-0.12%	0.66%	-0.77%	-0.67%	0.08%	0.48%
C	3.52	2.77	-1.42	-0.92	5.68	4.92	-1.18	-2.03	-0.95%	-0.96%	0.97%	0,79%	-1.42%	-1.19%	1.09%	0.71%

8.2.6 Assessment of measurement uncertainties

The measurement uncertainties were evaluated with preliminary analysis:

- Range of motion (from the Vicon system): the error on the measurement of the angle between L4-L5 was less than 0.1°[160]
- Strain uncertainty (DIC system): two images of each unloaded specimen were captured with the DIC system and analysed with the optimal software parameters to evaluate the strain measurement uncertainties in a known configuration (zero-strain).[40] Being in a zero-strain configuration, any strain different from zero was accounted as measurement error. DIC-measured strains had a systematic error less than 0.002% and a random error less than 0.006%
- Intra-operator variability: in order to analyse the reliability of ROIs identification, the same operator was asked to identify the ROIs three times on different days in correspondence. The difference among the three repetitions was less than 0.2% of the mean value inside the ROI.

These values were considered satisfactory if compared to the typical rotations (of the order of 10° from full flexion to full extension), and to the typical strain peaks measured in the ALL (4-6%).

8.3 Results

8.3.1 Range of motion and strain maps

For all the specimens, there was an asymmetry in the RoM between flexion and extension when the same moment of ±7.5 Nm was applied (Fig. 8.2):

- During flexion, the L4-L5 angle reached 4.0° for specimens A and B, and 6.3° for specimen C
- During extension the angle reached 1.5° for specimen A, 1.7° for specimen B and 2.7° for specimen C.

The full-field strain maps were successfully computed using DIC for all the specimens throughout the tests. During extension, the longitudinal strain was positive (traction) while during flexion it was negative (compression) (Fig. 8.3). An opposite behavior was found for the circumferential strain: in extension the values were negative, showing a circumferential narrowing of the ligament, while in flexion the values were positive showing a transversal stretching due to IVD bulging.
The strain distributions on the ALL in correspondence with L4 vertebra and L4-L5 IVD were significantly different: in general on the vertebra the largest deformation was in the order of ±1.5%; on the IVD the largest deformation was in the order of ±4%. However, for all the specimens, comparable strain was measured on average in the ROIs in front of L4 and in front of the IVD (the longitudinal strain averaged 1.5% for extension and -1.5%: -1% for flexion, while the circumferential strain averaged 3% for flexion and 2% for extension).
While a similar trend was observed in most cases, a different behaviour was seen for specimen A with respect to the strain in front of the IVD during flexion (in this ROI the strains were one order of magnitude lower than for the other specimens). Also in in the full-field maps, specimen A showed positive strains in correspondence with the central part of the IVD.

Published in: Materials (Digital/Volume Correlation of Biological Tissues and Biomaterials), 2020, 13, 384: 1-14

8.3.2 Non-linear trend of the strain in the different parts of the ALL

The slope of the final part of EZ was similar in flexion and in extension (Fig. 8.2). The slope of the EZ was one order of magnitude larger than the slope in NZ for all three specimens.
The limits of the EZ and NZ were reported on strain-moment and angle-strain curves so as to match the points previously identified in the moment-angle curves (Fig. 8.4-8.5). The strain-moment curves (Fig. 8.4) showed a non-linearity similar to the moment-angle curves (Fig. 8.2). In fact, the strains in the EZ grew (in terms of slope of the strain-moment plots) 1-2 orders of magnitude slower than in the NZ. Furthermore, the non-linear trend of the strain-moment curves was not symmetrical: in flexion the change of slope of the curve was much more abrupt than in extension. In addition, the difference between the slope of the NZ and EZ was much more pronounced in front of the vertebra (roughly a factor 4) than in front of the disc (factor 2). Conversely the strain-angle curves showed a more linear trend, with much smaller changes of slope (Fig. 8.5). In fact, the ratio between the slope of the NZ and the slope of the EZ was between 0.3 and 3.
In table 8.2, the values of moment, angle and strain on vertebra and IVD are reported separately for the flexion-to-extension and extension-to-flexion curves in correspondence of the points which identified the transition from NZ to EZ. These two regions were not symmetric respect to the moment: during flexion the EZ started at a moment between 2.6-4.0 Nm while during extension the EZ started at a moment value around 0 Nm. For what concerns the angles, in flexion the EZ started at 2.6°-5.6° while in extension it started at 0.2°-2.0°.
To verify whether there was a correlation between a variation in the longitudinal strain on the ALL in front of the vertebra and in front of the L4-L5 IVD, these variables were plotted in the same graph (Fig. 8.6). This trend was close to a straight line, with a slope close to 1.0 (in the range of 0.8-1.2).
All specimens had the same behavior, again with the exception of specimen A during flexion which showed no change in the strain values on the IVD while the strain on the IVD reached -2%. Conversely during extension, specimen A showed the same behaviour of the other specimens.

8.4. Discussion

The aim of this study was to investigate the behavior of the ALL using full-field DIC analysis on intact multi-segmental spinal specimens, so as to gather data about the non-linear contribution of the ALL during the different phases of spinal flexion and extension. This information is currently missing in the literature, and could contribute to build better multibody models, and better finite element models of the spine, able to capture the changing stiffness of the ALL during motion.
A flexion-extension test was performed measuring the range of motion, the neutral zone, and the elastic zone of the spine, and the strain distribution over the superficial fibers of the ALL. The use of long segments of spine (6 FSUs) allowed to preserve the continuity of the ALL whose superficial fibers span over several vertebrae and IVDs.[62, 64, 142] A full-field strain distribution on the ALL in front of L4 vertebra and in front of L4-L5 IVD was measured using an established DIC tool. In the present study, in order to analyze the non-linear behaviour of the ALL, specific regions of interest (ROIs) were identified on its surface in front of the vertebra and in front of the IVD, and for each region the longitudinal strains were analyzed.
In general, ligaments fibers transmit only tensile forces. The ALL stretches longitudinally in extension, but works in traction too (in circumferential direction) when the spine is in flexion. During this movement the IVD is compressed and bulges transmitting tension to the ALL.[8] In fact, the role of the ALL is to limit the movement of the spine during extension.[131, 158] Similarly, the Posterior Longitudinal Ligament (PLL) limits the movement of the spine in flexion.[8, 71] In addition, longitudinal ligaments (ALL and PLL) are much stiffer than the other ligaments (such as ligamentum flavum): longitudinal ligaments are closer to the neutral bending axes and so in order to provide the same moment, the stiffness must be greater.[61, 62, 161]

In this work, during extension, the analysis of strain maps (both in correspondence with vertebra and IVD) highlighted a stretch of the superficial layers of the ALL in the longitudinal direction. This is in accordance with literature, reporting that the fibers of the ALL are aligned longitudinally with the axes of the spine.[62] Conversely, during flexion, the strain maps showed negative longitudinal strains, which highlighted a shortening of the ALL in the same direction. At the same time, during flexion there was a stretching in the circumferential direction.

In order to deeply investigate the local spinal RoM, the moment-angle curves were calculated using the testing machine and Vicon system. These curves were asymmetrical and the spine reached higher intervertebral rotations during flexion than during extension (6° degrees respect to 2.7° degrees for the specimen with the highest RoM). These findings are compatible with previous studies on the spinal range of motion.[1, 37, 56] Furthermore, the moment-angle curves showed a very accentuated non-linear behaviour as already described in the literature.[56] The slope of these curves changed more abruptly in flexion, while on the contrary the slope changed more damped in extension. The EZ zone was larger for extension than for flexion, in fact the beginning of EZ during flexion corresponded to values of moment and angle greater than during extension. As soon as the column moves towards extension, the ALL is stretched and limits this movement immediately but with a gradual slope (in fact the slope of the curve is smaller in extension respect to flexion). This may be due to the mechanical role of the facet joints and the capsular ligaments, which contribute with the ALL to stabilize extension.[162] Conversely, during flexion the lumbar spine allowed more degrees of movement in flexion before stiffening. This may be discussed considering that higher rotations may be needed to win the high tensile longitudinal pre-stretch typical of the ALL ([62, 139, 142] before reaching negative values during bulging of the annulus.[150]

Like for moment-angle curves, also the strain on ROIs in front of the vertebra and in front of the IVD showed a non-linear and asymmetric trend for flexion and extension. This behaviour is in agreement with the non-linear behaviour measured in isolated spinal ligaments in the past.[61, 151] The ALL consists of fibers which are pre-stretched both in longitudinal and transverse direction over the column and resist immediately in extension.[62, 158] Conversely, there are other ligaments which are slack and limit the movement only when certain angles are reached.[62, 158] At the beginning of the movement, in the NZ, the first fibers that are recruited are the elastin fibers which however do not contribute in giving great resistance. For this reason, large variations of strain were measured in the NZ with small variation of moment. Subsequently, collagen fibers (which are stiffer) were also recruited contributing in this way in limiting the movement.

Specimen A showed a different behaviour compared to the other specimens for what concerns the trend of strain only during flexion. The strain maps showed that the IVD did not bulge during flexion and so in this way the ALL was not stretched in circumferential direction avoiding the decrease of its length longitudinally; this differs from the behaviour usually observed in healthy spines.[131] This was associated to the presence of osteophytes[145] on the endplates of adjacent vertebrae[137], which may alter the load transfer on the ALL. Although also specimens B and C demonstrated some degenerative signs, the presence of lower grade osteophytes was noticed only on one endplate. The correlation between the longitudinal strain values on the ROIs in front of the vertebra and the IVD demonstrated a linear relationship with a slope of about 1.0. This meant that, in the most deformed areas of the superficial layers, the ligament was deformed in the same way both on vertebra and on IVD. This could be a further proof of the effect of the longitudinal arrangement of the ALL, which influenced its deformation both in front of the vertebra and in front of the IVD. It is true that the deeper layers are attached to the vertebra and to the external layers of the IVD; conversely the most superficial layers of the ALL are not constrained in such a way, and are affected by the effect of the adjacent joints and the longitudinal extension of the fibers of this ligament, as documented in the past.[62, 64, 138]

A limitation of the present work was the small number of specimens tested (N=3), which was constrained by the extensive measurement campaign required by this DIC analysis. For this reason, the present findings must be taken with caution. For instance, specimens from other groups of donors (e.g. younger, or with severe deformity) could yield different results. However, the behavior of the

ALL was similar for all specimen. Furthermore, only direction of loading (flexion and extension) was considered in this study. A pure moment was applied so as to deliver a highly-controlled loading. The rationale is that the ALL constraints mainly the movements on the sagittal plane limiting the extension, while it gives a marginal contribution during lateral bending or axial torsion. A further limitation relates to the relatively slow motion imposed (1°/ second). This condition was chosen for consistency with previous similar studies.[131]
This could be a starting point for other studies in which the behavior of other ligaments could be investigated under different loading conditions or after surgical interventions on the spine.[152]

8.5. Conclusions

DIC was shown to be a valid tool to measure the strain in a full-field way while preserving the complex structure of the spine, including its ligaments. To investigate the behavior of the ALL, it is important not to separate it from the other structures but to consider the spine as a whole. A high non-linearity and asymmetry between flexion and extension was observed in the strains measured in the ALL, which to a large extent explains the non-linear behaviour of a spine segment. In addition, the non-linear response of the ALL between the neutral zone and the elastic region, and its different behaviour in flexion and extension should be considered for instance for multibody modeling of the spine kinematics of finite element models investigations.

Chapter 9

Conclusions

In this PhD project, a full-field strain analysis of some structures of the spine (ligaments and intervertebral discs) was performed. Strain measurements were obtained on the surface of spine specimens in a full-field and contactless way using the Digital Image Correlation.
The first part of my research started with a deep review of the methods used to study the biomechanical behavior of the spine (*in vivo*, *in vitro* and FE model), focusing in detail on *in vitro* studies and considering the various types of tests. I also analysed in depth what was reported in the literature mainly regarding the biomechanics of ligaments and the possible consequences of different types of osteotomies. This was useful to understand what types of information were missing in the knowledge of the biomechanics of the spine. Moreover this could be also a starting point to choose which type of test is better to use in order to answer the scope of the research.
During the first tests, DIC was used to measure a full-field strain distribution simultaneously on hard and soft tissues (in particular on vertebrae, intervertebral discs and ligaments). In this way the biomechanics of different types of tissues could be investigated (in terms of deformation) considering the spine as a whole, without separating one tissue from the others, remaining closer in this way to the real conditions in which the spine works. Moreover this approach permitted to study the interaction between different types of tissues and how the deformation of one structure could influence the others.
After these preliminary tests, the biomechanics of the intervertebral disc was studied applying a flexion on porcine spines. A full-field strain map of the surface of the discs was obtained and analysed in detail to understand which part of the disc was more deformed and how its kinematics could change in relation to the different loading rates and to the application or not of conditioning. The disc tended to stiffen as the loading rate increased but the loading rate did not affect the way the disc was deformed. This could mean that the viscoelastic behavior of the tissues composing the nucleus pulposus and the annulus fibrosus did not directly affect the overall kinematics of the disc, and only slightly affected the transition zone between disc and vertebra where a large discontinuity of stiffness is localized. From this study, disc herniation would seem not to be due to a specific rate of the applied loads. Furthermore, this information could be useful also for the design of other *in vitro* biomechanical tests and of more realistic numerical models of the spine, knowing what effect different loading rates and conditioning entail has on the biomechanics of the intervertebral discs. The findings of the present study can be extended to the human spine as a trend, even if possibly not as absolute magnitudes.
The other structures of the spine which were studied in depth are the spinal ligaments. The supraspinous and interspinous ligament were studied analysing how they were deformed under different loading conditions. These ligaments limited the movement of the spine during flexion reducing in this way the overload on the intervertebral disc; conversely these ligaments did not give significant mechanical resistance during extension and lateral bending.
Another ligament which was investigated in depth on human spine was the anterior longitudinal ligament which extends along the front part of the spine improving its stability mainly on sagittal

plane. This ligament limited mainly the extension of the spine reducing the range of motion of the column; during flexion the ligament limited also the bulging of the disc. The anterior longitudinal ligament did not offer great mechanical strength during lateral bending and axial torsion even if larger deformation values have been recorded during torsion and the deformation was oriented following the direction of the fibers. Furthermore, the anterior longitudinal ligament, unlike other ligaments (such as the ligament of the knee or of the ankle) does not intervene limiting the movement only when large range of motion are reached by the joint, but intervenes immediately by offering mechanical resistance to the column mainly during flexion and extension. Analysing the trend distribution of strain, a non-linear behavior was observed: at the beginning of the movement the fibers of the ligament aligned longitudinally and so there was no great mechanical resistance, while once the collagen fibers were aligned, the ligament was very resistant and offered great resistance limiting the movement of the spine. In addition to a biomechanical analysis of spinal ligaments, the non-linear response of the ALL between the neutral zone and the elastic region, and its different behavior in flexion and extension should be considered for instance for multibody modelling of the spine kinematics of finite element models investigations.

Overall, these results suggested the importance of a full-field strain analysis to understand the biomechanics of the human spine and the interaction between different types of tissue. In these studies, the biomechanics, the non-linear behaviour and the viscoelastic effects of intervertebral discs and ligaments were investigated without altering their functionality. The results reported in this thesis could be useful also to build better multibody spine models and to include more realistic properties in finite element models. This work could also be a starting point for future studies where the effect of surgical procedures could be compared to intact spines. The results that can be obtained using DIC could improve the knowledge of the role of ligaments and of intervertebral discs in order to elucidate pathology and lesions, and also help improving surgical techniques.

References

1. White AA, Panjabi MM. The basic kinematics of the human spine. Spine. 1978;3:12-20.
2. White AA, Panjabi MM. Clinical Biomechanics of the Spine. Lippincott. 1990.
3. Adams MA, Dolan P. Spine biomechanics. Journal of Biomechanics. 2005;38(10):1972-83.
4. Davis KG, Marras WS. The effects of motion on trunk biomechanics. Clinical Biomechanics. 2000;15:703 - 17.
5. Mayer TG, Kondraske G, Beals SB, Gatchel RJ. Spinal Range of Motion. 1997;22:1976 - 84.
6. Gray H. Gray's anatomy. London: Churchill Livingstone. 1858.
7. Newell N, Little JP, Christou A, Adams MA, Adam CJ, Masouros SD. Biomechanics of the human intervertebral disc: A review of testing techniques and results. Journal of Mechanical Behaviour of Biomedical Materials. 2017;69:420-34.
8. Behrsin J, Briggs C. Ligaments of the lumbar spine: a review. Surgical - Radiologic Anatomy. 1988;10:211 - 9.
9. Panjabi MM. Clinical spinal instability and low back pain. Journal of Electromyography and Kinesiology. 2003;13(4):371-9.
10. Palanca M, Brodano Barbanti G, Cristofolini L. The size of simulated lytic metastases affects the strain distribution on the anterior surface of the vertebra. Journal of biomechanical engineering. 2018.
11. Chen CS, Chen WJ, Cheng CK, Jao SH, Chueh SC, Wang CC. Failure analysis of broken pedicle screws on spinal instrumentation. Medical Engineering & Physics. 2005;27(6):487-96.
12. Nasser R, Yadla S, Maltenfort MG, Harrop JS, Anderson DG, Vaccaro AR, et al. Complications in spine surgery. J Neurosurg Spine. 2010;13(2):144-57.
13. Hicks JL, Singla A, Shen A, Shen FH, Arlet V. Complications of pedicle screw fixation in scoliosis surgery. Spine. 2010;35:E465 - E70.
14. Hallager DW, Gehrchen M, Dahl B, Harris JA, Gudipally M, Jenkins S, et al. Use of Supplemental Short Pre-Contoured Accessory Rods and Cobalt Chrome Alloy Posterior Rods Reduces Primary Rod Strain and Range of Motion Across the Pedicle Subtraction Osteotomy Level: An In Vitro Biomechanical Study. Spine. 2016;41(7):E388-95.
15. Cho W, Cho SK, Wu C. The biomechanics of pedicle screw-based instrumentation. Journal of Bone Joint Surgery. 2010;92-B:1061 - 5.
16. Cammarata M, Aubin CE, Wang X, Mac-Thiong JM. Biomechanical Risk Factors for Proximal Junctional Kyphosis. Spine. 2014;39(8):E500-7.
17. Cho SK, Shin JI, Kim YJ. Proximal junctional kyphosis following adult spinal deformity surgery. European spine journal. 2014;23(12):2726-36.
18. Nguyen NL, Kong CY, Hart RA. Proximal junctional kyphosis and failure-diagnosis, prevention, and treatment. Current reviews in musculoskeletal medicine. 2016;9(3):299-308.
19. Kim HJ, Lenke LG, Shaffrey CI, Van Alstyne EM, Skelly AC. Proximal junctional kyphosis as a distinct form of adjacent segment pathology after spinal deformity surgery: a systematic review. Spine. 2012;37(22 Suppl):S144-64.
20. Ruspi ML, Faldini C, Cristofolini L. In vitro experimental studies and numerical modeling investigate the biomechanical effects of surgical interventions on the spine. Critical Reviews in Biomedical Engineering. 2019;47(4):295-322.
21. Yerby SA, Ehteshami JR, McLain RF. Loading of Pedicle Screws within the Vertebrae. Journal of Biomechanics. 1997;30:951 - 4.
22. Prasad KN, Cole WC, Hasse GM. Health Risks of Low Dose Ionizing Radiation in Humans: A Review. Experimental Biology and Medicine. 2004:378-82.
23. Cappozzo A, Della Croce U, Leardini A, Chiari L. Human movement analysis using stereophotogrammetry. Part 1: theoretical background. Gait Posture. 2005;21(2):186-96.

24. Kärrholm J. Roentgen stereophotogrammetry: Review of orthopedic applications. Acta Orthopaedica Scandinavica. 2009;60(4):491-503.
25. Fong DT, Chan YY. The use of wearable inertial motion sensors in human lower limb biomechanics studies: a systematic review. Sensors. 2010;10(12):11556-65.
26. Teyhen DS, Flynn TW, Bovik AC, Abraham LD. A New Technique for Digital Fluoroscopic Video Assessment of Sagittal Plane Lumbar Spine Motion. Spine. 2005;30:E406--E13.
27. Papi E, Koh WS, McGregor AH. Wearable technology for spine movement assessment: A systematic review. Journal of Biomechanics. 2017;64:186-97.
28. Pourahmadi MR, Takamjani IE, Jaberzadeh S, Sarrafzadeh J, Sanjari MA, Bagheri R, et al. Kinematics of the Spine During Sit-to-Stand Using Motion Analysis Systems: A Systematic Review of Literature. Journal of sport rehabilitation. 2017;28:77-93.
29. O'Connell G, Vreesilovic EJ, Elliott DM. Comparison of Animals Used in Disc Research to Human Lumbar Disc Geometry. Spine. 2007;32:328-33.
30. Cholewicki J, Crisco JJ, Oxland TR, Yamamoto I, Panjabi MM. Effects of posture and structure on three dimensional coupled rotations in the lumbar spine. Spine. 1996;21:2421 - 8.
31. Danesi V, Zani L, Scheele A, Berra F, Cristofolini L. Reproducible reference frame for in vitro testing of the human vertebrae. Journal of Biomechanics. 2014;47(1):313-8.
32. Kettler A, Wilke HJ, Haid C, Claes L. Effects of specimen length on the monosegmental motion behavior of the lumbar spine. Spine. 2000;25:543 - 50.
33. Busscher I, van Dieen JH, Kingma I, van der Veen AJ, Verkerke GJ, Veldhuizen AG. Biomechanical Characteristics of Different Regions of the Human Spine. Spine. 2009;34:2858-64.
34. Freddi A, Olmi G, Cristofolini L. Experimental stress analysis for materials and structures. Stress analysis models for developing design methodologies. Springer. 2015;5:187-212.
35. Brandolini N, Cristofolini L, Viceconti M. Experimental methods for the biomechanical investigation of the human spine: a review. Journal of Mechanics in Medicine and Biology. 2014;14(01):1430002.
36. Sis HL, Mannenb EM, Wonga BM, Cadel ES, Bouxsein ML, Anderson DE, et al. Effect of follower load on motion and stiffness of the human thoracic spine with intact rib cage. Journal of Biomechanics. 2016;49:3252 - 9.
37. Wilke HJ, Jungkunz B, Wenger K, Claes L. Spinal segment range of motion as a function of in vitro test conditions: effects of exposure period, accumulated cycles, angular-deformation rate, and moisture condition. The Anatomical Record. 1998;251:15-9.
38. Cristofolini L, Brandolini N, Danesi V, Juszczyk MM, Erani P, Viceconti M. Strain distribution in the lumbar vertebrae under different loading configurations. The Spine Journal. 2013;13(10):1281-92.
39. Bay BK, Yerby SA, McLain RF, Toh E. Measurement of Strain Distributions Within Vertebral Body Sections by Texture Correlation. Spine. 1999;24:10-7.
40. Palanca M, Brugo TM, Cristofolini L. Use of digital image correlation to investigate the biomechanics of the vertebra. Journal of Mechanics in Medicine and Biology. 2015;15:1-10.
41. Lionello G, Sirieix C, Baleani M. An effective procedure to create a speckle pattern on biological soft tissue for digital image correlation measurements. Journal of the mechanical behavior of biomedical materials. 2014;39:1-8.
42. Yoshimura T, Nakai K, Tamaoki G. Multi-body Dynamics Modelling of Seated Human Body under Exposure to Whole-Body Vibration. Industrial Health. 2005;43:441-7.
43. Shabana AA. Flexible Multibody Dynamics: Review of Past and Recent Developments. Multibody System Dynamics. 1997;1:182-222.
44. Abouhossein A, Weisse B, Ferguson SJ. A multibody modelling approach to determine load sharing between passive elements of the lumbar spine. Computer methods in biomechanics and biomedical engineering. 2011;14(6):527-37.

45. Lopik DW, Acar M. Dynamic verification of a multi-body computational model of human head and neck for frontal, lateral, and rear impacts. J Multi-body Dynamics. 2007;221:199-217.
46. Esat V, Acar M. Viscoelastic finite element analysis of the cervical intervertebral discs in conjunction with a multi-body dynamic model of the human head and neck. J Multi-body Dynamics. 2009;223:249-62.
47. Lopik DW, Acar M. Development of a multi-body computational model of human head and neck. J Multi-body Dynamics. 2007;221:175-96.
48. Schileo E, Taddei F, Malandrino A, Cristofolini L, Viceconti M. Subject-specific finite element models can accurately predict strain levels in long bones. Journal of Biomechanics. 2007;40(13):2982-9.
49. Fagan MJ, Julian S, Mohsen AM. Finite element analysis in spine research. J Engineering in Medicine. 2002;216.
50. Teo EC, Ng HW. Evaluation of the role of ligaments, facets and disc nucleus in lower cervical spine under compression and sagittal moments using finite element method. Medical Engineering & Physics. 2001;23:155-64.
51. Schileo E, Balistreri L, Grassi L, Cristofolini L, Taddei F. To what extent can linear finite element models of human femora predict failure under stance and fall loading configurations? Journal of Biomechanics. 2014;47(14):3531-8.
52. Jones AC, Wilcox RK. Finite element analysis of the spine: towards a framework of verification, validation and sensitivity analysis. Medical Engeneering & Physics. 2008;30(10):1287-304.
53. Dall'Ara E, Schmidt R, Pahr D, Varga P, Chevalier Y, Patsch J, et al. A nonlinear finite element model validation study based on a novel experimental technique for inducing anterior wedge-shape fractures in human vertebral bodies in vitro. Journal of Biomechanics. 2010;43(12):2374-80.
54. Wilke HJ, Neef P, Hinz B, Seidel H, Claes L. Intradiscal pressure together with anthropometric data - a data set for the validation of models. Clinical Biomechanics. 2001;1:S111-S26.
55. Cristofolini L, Schileo E, Juszczyk M, Taddei F, Martelli S, Viceconti M. Mechanical testing of bones: the positive synergy of finite - element models and in vitro experiments. Philosophical Transactions of The Royal Society. 2010;368:2725 - 63.
56. Panjabi MM, Oxland TR, Yamamoto I, Crisco JJ. Mechanical behaviour of the human lumbar and lumbosacral spine as shown by three-dimensional load displacement curves. The Journal of Bone and Joint Surgery. 1994;76:413-24.
57. Quint U, Wilke HJ, Shirazi-Adl A, Parnianpour M, Loer F, Claes LE. Importance of the Intersegmental Trunk Muscles for the Stability of the Lumbar Spine. Spine. 1998;23:1937 - 45.
58. Wilcox RK. The biomechanics of vertebroplasty: a review. J Engineering in Medicine. 2004;218.
59. Danesi V, Faldini C, Cristofolini L. Methods for the characterization of the long-term mechanical performance of cements for vertebroplasty and kyphoplasty: critical review and suggestions for the test methods. Journal of Mechanics in Medicine and Biology. 2017;17:1-33.
60. Oxland TR. Fundamental biomechanics of the spine - What we have learned in the past 25 years and future directions. Journal of Biomechanics. 2016;49(6):817-32.
61. Pintar FA, Yoganandan N, Myers T, Elhagediab A, Sances A. Biomechanical properties of human lumbar spine ligaments. Journal of Biomechanics. 1992;25:1351 - 6
62. Hukins DWL, Kirby MC, Sikoryn TA, Aspden RM, Cox AJ. Comparison of structure, mechanical properties, and functions of lumbar spinal ligaments. Spine. 1990;15(8):787-95.
63. Dickey JP, Bednar DA, Dumas GA. New Insight Into the Mechanism of the Lumbar Interspinous Ligament. Spine. 1996;21:2720 - 7.
64. Yoganandan N, Kumaresan S, Pintar FA. Geometric and mechanical properties of human cervical spine ligaments. Journal of biomechanical engineering. 2000;122:623-9.
65. Grimes PF, Massie JB, Garfin SR. Anatomic and Biomechanical Analysis of the Lower Lumbar Foraminal Ligaments. Spine. 2000;25:2009 - 14.

66. Yoganandan N, Kumaresan S, Pintar FA. Biomechanics of the cervical spine Part 2. Cervical spine soft tissue responses and biomechanical modeling. Clinical Biomechanics. 2001;16:1-27.
67. Li Y, Shen Z, Huang M, Wang X. Stepwise resection of the posterior ligamentous complex for stability of a thoracolumbar compression fracture: An in vitro biomechanical investigation. Medicine. 2017;96(35):e7873.
68. Corse MR, Renberg WC, Friis EA. In vitro evaluation of biomechanical effects of multiple hemilaminectomies on the canine lumbar vertebral column. American Journal of Veterinary Research. 2003;64:1139-45.
69. Hindle RJ, Pearcy MJ, Cross A. Mechanical function of the human lumbar interspinous and supraspinous ligaments. Scientific and Technical Record. 1989;12:340-4.
70. Gillespie KA, Dickey JP. Biomechanical Role of Lumbar Spine Ligaments in Flexion and Extension: Determination Using a Parallel Linkage Robot and a Porcine Model. Spine. 2004;29:1208 - 16.
71. Panjabi MM, Hausfeld JN, White AA. A biomechanical study of the ligamentous stability of the thoracic spine in man. Acta Orthopaedica Scandinavica. 1981;52(3):315-26.
72. Panjabi MM, Pearson AM, Ito S, Ivancic PC, Gimenez SE, Tominaga Y. Cervical Spine Ligament Injury during Simulated Frontal Impact. Spine. 2004;29:2395-403.
73. Brolin K, Halldin P. Development of a Finite Element Model of the Upper Cervical Spine and a Parameter Study of Ligament Characteristics. Spine. 2004;29:376-85.
74. Ng HW, Teo EC, Lee KK, Qiu TX. Finite Element Analysis of Cervical Spinal Instability Under Physiological Loading. Journal of Spinal Disorders & Techniques. 2003;16:55-65.
75. Guan Y, Yoganandan N, Zhang J, Pintar FA, Cuisk JF, Wolfla CE, et al. Validation of a clinical finite element model of the human lumbosacral spine. Medical & Biological Engineering & Computing. 2006;44:633-41.
76. Bresnahan L, Ogden AT, Natarajan RN, Fessler RG. A biomechanical evaluation of graded posterior element removal for treatment of lumbar stenosis. Spine. 2008;34:17-23.
77. Iorio JA, Jakoi AM, Singla A. Biomechanics of Degenerative Spinal Disorders. Asian spine journal. 2016;10(2):377-84.
78. Shah JS, Hampson WGJ, Jayson MIV. The distribution of surface strain in the cadaveric lumbar spine. The Journal of Bone and Joint Surgery. 1978;60-B:246-51.
79. Hongo M, Abe E, Shimada Y, Murai H, Ishikawa N, Sato K. Surface Strain Distribution on Thoracic and Lumbar Vertebrae Under Axial Compression. Spine. 1999;24:1197 - 202.
80. Moisi M, Fisahn C, Tkachenko L, Tubbs RS, Ginat D, Grunert P, et al. Unilateral Laminotomy with Bilateral Spinal Canal Decompression for Lumbar Stenosis: A Technical Note. Cureus. 2016;8(5):623.
81. Cardoso MJ, Dmitriev AE, Helgeson M, Lehman RA, Kuklo TR, Rosner MK. Does Superior-Segment Facet Violation or laminectomy destabilize the adjacent level in lumbar transpedicular fixation? Spine. 2008;33:2868 - 73.
82. Quint U, Wilke HJ, Löer F, Claes L. Laminectomy and functional impairment of the lumbar spine: the importance of muscles forces in flexible and rigid instrumented stabilization - a biomechanical study in vitro. European Spine Journal. 1998;7:229 - 38.
83. Baisden J, Voo LM, Cusick JF, Pintar FA, Yoganandan N. Evaluation of Cervical Laminectomy and Laminoplasty. Spine. 1999;24:1283 - 189.
84. Tai CL, Hsieh PH, Chen WP, Chen LH, Chen WJ, Lai PL. Biomechanical comparison of lumbar spine instability between laminectomy and bilateral laminotomy for spinal stenosis syndrome - an experimental study in porcine model. BMC Musculoskelet Disord. 2008;9:84.
85. Lee MJ, Bransford RJ, Bellabarba C, Chapman JR, Cohen AM, Harrington RM, et al. The Effect of Bilateral Laminectomy Versus Laminectomy on the Motion Stiffness of the Human Lumbar Spine. Spine. 2010;35:1789 - 93.

86. Oda I, Abumi K, Cunningham BW, Kaneda K, McAfee PC. An In Vitro Human Cadaveric Study Investigating the Biomechanical Properties of the Thoracic Spine. Spine. 2002;27:E64-E70.
87. Hong-Wan N, Ee-Chon T, Qing-Hang Z. Biomechanical Effects of C2–C7 Intersegmental Stability due to Laminectomy With Unilateral and Bilateral Facetectomy. Spine. 2004;29(16):1737-45.
88. Lee KK, Teo EC, Qiu TX, Yang K. Effect of Facetectomy on Lumbar Spinal Stability Under Sagittal Plane Loadings. Spine. 2004;29:1624-31.
89. Teo EC, Lee KK, Qiu X, Ng HW, Yang K. The Biomechanics of Lumbar Graded Facetectomy Under Anterior-Shear Load. Biomedical engineering. 2004;51.
90. Zander T, Rohlmann A, Klockner C, Bergmann G. Influence of graded facetectomy and laminectomy on spinal biomechanics. European Spine Journal. 2003;12(4):427-34.
91. Bydon M, Macki M, Abt NB, Sciubba DM, Wolinsky JP, Witham TF, et al. Clinical and surgical outcomes after lumbar laminectomy: An analysis of 500 patients. Surgical neurology international. 2015;6(Suppl 4):S190-3.
92. Vaccaro AR, Moe RL, Hurlbert RJ, Lehman RA, Harrop JS. Surgical decision making for unstable thoracolumbar spine injuries: results of a consensus panel review by the spine trauma study group. Journal Spinal Disorders Technology. 2006;19:1 - 10.
93. Tian NF, Huang QS, Zhou P, Zhou Y, Wu RK, Lou Y, et al. Pedicle screw insertion accuracy with different assisted methods: a systematic review and meta-analysis of comparative studies. European spine journal. 2011;20(6):846-59.
94. Gaines RW. The use of pedicle-screw internal fixation for the operative tratment of spinal disorders. The Journal of Bone and Joint Surgery. 2000;82-A:1458 - 76.
95. Xie T, Qian J, Lu Y, Chen B, Jiang Y, Luo C. Biomechanical comparison of laminectomy, hemilaminectomy and a new minimally invasive approach in the surgical treatment of multilevel cervical intradural tumour: a finite element analysis. European Spine Journal. 2013;22(12):2719-30.
96. Palanca M, Tozzi G, Cristofolini L. The use of digital image correlation in the biomechanical area: a review. International Biomechanics. 2015;3:1-21.
97. Faldini C, Chehrassan M, Perna F, Ruspi ML, Palanca M, Cristofolini L. The Use of Digital Image Correlation to Analyse Functional Spinal Units in Porcine Model. SRS. 2017.
98. Baldoni J, Lionello G, Zama F, Cristofolini L. Comparison of different filtering strategies to reduce noise in strain measurement with digital image correlation. The Journal of Strain Analysis for Engineering Design. 2016;51(6):416-30.
99. Ruspi ML, Palanca M, Faldini C, Cristofolini L. Full-field in vitro investigation of hard and soft tissue strain in the spine by means of Digital Image Correlation. Muscles,Ligaments and Tendons Journal. 2017;7:538 - 45.
100. Lau D, Clark AJ, Scheer JK, Daubs MD, Coe JD, Paonessa KJ, et al. Proximal junctional kyphosis and failure after spinal deformity surgery. Spine. 2014;39.
101. Heuer F, Schmidt H, Claes L, Wilke HJ. A new laser scanning technique for imaging intervertebral disc displacement and its application to modeling nucleotomy. Clin Biomech (Bristol, Avon). 2008;23(3):260-9.
102. Danesi V, Erani P, Brandolini N, Juszeczyk MM, Cristofolini L. Effect of the In Vitro Boundary Conditions on the Surface Strain Experienced by the Vertebral Body in the Eastic Regime. Journal of Biomechanical Engeneering. 2016;138.
103. Roberts BC, Perilli E, Reynolds KJ. Application of the digital volume correlation technique for the measurement of displacement and strain fields in bone: a literature review. J Biomech. 2014;47(5):923-34.
104. Palanca M, Cristofolini L, Dall'Ara E, Curto M, Innocente F, Danesi V, et al. Digital volume correlation can be used to estimate local strains in natural and augmented vertebrae: An organ-level study. J Biomech. 2016;49(16):3882-90.

105. Kyaw TA, Wang Z, Sakakibara T, Yoshikawa T, Inaba T, Kasai Y. Biomechanical effects of pedicle screw fixation on adjacent segments. European journal of orthopaedic surgery & traumatology : orthopedie traumatologie. 2014;24 Suppl 1:S283-7.
106. Anasetti F, Galbusera F, Aziz HN, Bellini CM, Addis A, Villa T, et al. Spine stability after implantation of an interspinous device: an in vitro and finite element biomechanical study. J Neurosurg Spine. 2010;13(5):568-75.
107. Cristofolini L. In vitro evidence of the structural optimization of the human skeletal bones. J Biomech. 2015;48(5):787-96.
108. Anderson AL, McIff TE, Asher MA, Burton DC, Glattes RC. The Effect of Posterior Thoracic Spine Anatomical Structures on Motion Segment Flexion Stiffness. Spine. 2009;34:441-6.
109. Lanyon IE. Bone remodelling, mechanical stress, and osteoporosis. Osteoporosis. 1980:129-38.
110. Gustafson H, Siegmund G, Cripton P. Comparison of Strain Rosettes and Digital Image Correlation for Measuring Vertebral Body Strain. Journal of biomechanical engineering. 2016;138(5):054501.
111. Danesi V, Tozzi G, Palanca M, Cristofolini L. Application of digital volume correlation (DVC) to investigate the strain distribution in vertebral body. AIAS. 2014.
112. Palanca M, Marco M, Ruspi ML, Cristofolini L. Full-field strain distribution in multi-vertebra spine segments: an in vitro application of digital image correlation. Med Eng Phys. 2017:1-8.
113. Spera D, Genovese K, Voloshin A. Application of Stereo-Digital Image Correlation to Full-Field 3-D Deformation Measurement of Intervertebral Disc. Strain. 2011;47:e572-e87.
114. Busscher I, Ploegmakers JJ, Verkerke GJ, Veldhuizen AG. Comparative anatomical dimensions of the complete human and porcine spine. European spine journal. 2010;19(7):1104-14.
115. Ruspi ML, Cristofolini L. The effect of loading rate on the full-field strain distribution on intervertebral discs. under revision. 2020.
116. Ranu HS. Measurement of pressures in the nucleus and within the annulus of the human spinal disc: due to extreme loading. Proceedings of the Institution of Mechanical Engineers Part H, Journal of engineering in medicine. 1990;204(3):141-6.
117. Thoreson O, Ekstrom L, Hansson HA, Todd C, Witwit W, Sward Aminoff A, et al. The effect of repetitive flexion and extension fatigue loading on the young porcine lumbar spine, a feasibility study of MRI and histological analyses. Journal of experimental orthopaedics. 2017;4(1):16.
118. Fennel AJ, Jones AP, Hukins DWL. Migration of the nucleus pulposus within the intervertebral disc during flexion and extension of the spine. Spine. 1996;21:2753-5757.
119. Fung YC. Biomechanics: Mechanical properties of living tissues. Springer. 1981.
120. Iatridis JC, Weidenbaum M, Mow VC. Is the nucleus pulposus a solid or a fluid? Mechanical behaviors of the nucleus pulposus of the human intervertebral disc. Spine. 1996;21:1174-84.
121. Race A, Broom ND, Robertson PA. Effect of Loading Rate and Hydration on the Mechanical Properties of the Disc. Spine. 2000;25:662 9.
122. Chan SC, Ferguson SJ, Gantenbein-Ritter B. The effects of dynamic loading on the intervertebral disc. European spine journal. 2011;20(11):1796-812.
123. Adams MA, McNally DS, Dolan P. Stress distributions inside intervertebral discs - the effect of age and degeneration. 1996;78-B:965 - 72.
124. Kasra M, Parnianpour M, Shirazi-Adl A, Wang JL, Grynpas MD. Effect of strain rate on tensile properties of sheep disc anulus fibrosus. Technology and Health Care. 2004;12(4):333-42.
125. Galante JO. Tensile Properties of the Human Lumbar Annulus Fibrosus. Acta Orthopaedica Scandinavica. 2014;38(sup100):1-91.

126. Ochia RS, Tencer AF, Ching RP. Effect of loading rate on endplate and vertebral body strength in human lumbar vertebrae. Journal of Biomechanics. 2003;36(12):1875-81.
127. Pintar FA, Yoganandan N, Voo L. Effect of Age and Loading Rate on Human Cervical Spine Injury Threshold. Spine. 1998;23:1957-62.
128. Nuckley DJ. Effect of Loading Rate on the Compressive Mechanics of the Immature Baboon Cervical Spine. Journal of biomechanical engineering. 2005;128(1):18.
129. Marras WS, Knapik GG, Ferguson S. Loading along the lumbar spine as influence by speed, control, load magnitude, and handle height during pushing. Clin Biomech (Bristol, Avon). 2009;24(2):155-63.
130. Gay RE, Ilharreborde B, Zhao K, Boumediene E, An KN. The effect of loading rate and degeneration on neutral region motion in human cadaveric lumbar motion segments. Clin Biomech (Bristol, Avon). 2008;23(1):1-7.
131. Heuer F, Schmidt H, Wilke HJ. The relation between intervertebral disc bulging and annular fiber associated strains for simple and complex loading. J Biomech. 2008;41(5):1086-94.
132. Jones EMC. A good practices guide for Digital Image Correlation. Internation Digital Image Correlation Society. 2018.
133. Iatridis JC, Setton LA, Weidenbaum M, Mow VC. The viscoelastic behaviour of the non-degenerate human lumbar nucleus polposus in shear. J Biomechanics. 1997;30:1005 - 13.
134. Gregory DE, Callaghan JP. An examination of the influence of strain rate on subfailure mechanical properties of the annulus fibrosus. Journal of biomechanical engineering. 2010;132(9):091010.
135. Sheng SR, Wang XY, Xu HZ, Zhu GQ, Zhou YF. Anatomy of large animal spines and its comparison to the human spine: a systematic review. European Spine Journal. 2010;19(1):46-56.
136. Beckstein JC, Sen S, Schaer TP, Vresilovic EJ, Elliott DM. Comparison of animal discs used in disc research to human lumbar disc. Spine. 2008;33:E166 - E73.
137. Palanca M, Ruspi ML, Cristofolini L, Liebsch C, Villa T, Brayda-Bruno M, et al. The strain distribution in the lumbar anterior longitudinal ligament is affected by the loading condition and bony features: an in vitro full-field analysis. PLOS ONE. 2020;15:1-21.
138. Mercer S, Phty B, Bogduk N. The ligaments and anulus fibrosus of human adult cervical intervertebral discs. Spine. 1999;24:619 - 28.
139. Robertson DJ, Von Forell GA, Alsup J, Bowden AE. Thoracolumbar spinal ligaments exhibit negative and transverse pre-strain. Journal of the mechanical behavior of biomedical materials. 2013;23:44-52.
140. Wilke HJ, TRohlmann A, S. N, Schulthei M, Bergmann G, Graichen F, et al. Is it Possible to Simulate Physiologic Loading Conditions by Applying Pure Moments? Spine. 2001;26:636 - 42.
141. Wilke HJ, Krischak ST, Wenger K, Claes L. Load-displacement properties of the thoracolumbar calf spine: experimental results and comparison to know human data. European spine journal. 1997;6:129 - 37.
142. Tkaczuk H. Tensile properties of human lumbar longitudinal ligaments. Acta Orthopaedica Scandinavica. 2014;39(sup115):1-69.
143. Panjabi MM, Goel VK, Takata K. Physiologic strains in the lumbar spine ligaments: an in vitro biomechanical study. Spine. 1982;7:192-203.
144. Ruspi ML, Palanca M, Faldini C, Cristofolini L. The Use of Digital Image Correlation to Analyse Segments of Spine. BSS. 2017.
145. Wilke HJ, Rohlmann F, Neidlinger-Wilke C, Werner K, Claes L, Kettler A. Validity and interobserver agreement of a new radiographic grading system for intervertebral disc degeneration: Part I. Lumbar spine. European spine journal. 2006;15(6):720-30.

146. Wilke HJ, Wenger K, Claes L. Testing criteria for spinal implants: recommendations for the standardization of in vitro stability testing of spinal implants. European spine journal. 1998;7:148 - 54.
147. Wilke HJ, Schmitt H, Wolf S. A universal spine tester for in vitro experiments with muscle force simulation. European Spine Journal. 1994;3:91-7.
148. Al-Rawahi M, Luo J, Pollintine P, Dolan P, Adams MA. Mechanical function of vertebral body osteophytes, as revealed by experiments on cadaveric spines. Spine. 2011;36(10):770-7.
149. Heuer F, Schmidt H, Klezl Z, Claes L, Wilke HJ. Stepwise reduction of functional spinal structures increase range of motion and change lordosis angle. J Biomech. 2007;40(2):271-80.
150. Heuer F, Schmidt H, Wilke HJ. Stepwise reduction of functional spinal structures increase disc bulge and surface strains. J Biomech. 2008;41(9):1953-60.
151. Neumann P, Keller TS, Ekstrom L, Hansson TH, Spengler DM. Mechanical properties of the human lumbar anterior longitudinal ligament. J Biomechanics. 1992;25:1185 - 94.
152. La Barbera L, Brayda-Bruno M, Liebsch C, Villa T, Luca A, Galbusera F, et al. Biomechanical advantages of supplemental accessory and satellite rods with and without interbody cages implantation for the stabilization of pedicle subtraction osteotomy. European spine journal. 2018.
153. Volkheimer D, Malakoutian M, Oxland TR, Wilke HJ. Limitations of current in vitro test protocols for investigation of instrumented adjacent segment biomechanics: critical analysis of the literature. European spine journal. 2015;24(9):1882-92.
154. Ruspi ML, Palanca M, Cristofolini L, Liebsch C, Villa T, Brayda-Bruno M, et al. Digital Image Correlation (DIC) Assessment of the Non-Linear Response of the Anterior Longitudinal Ligament of the Spine during Flexion and Extension. Materials (Digital/Volume Correlation of Biological Tissues and Biomaterials). 2020;13(2):1-14.
155. Neumann P, Keller TS, Ekstrom L, Hansson T. Effect of strain rate and bone mineral on the structural properties of the human anterior longitudinal ligament. Spine. 1994;15:205-11.
156. Neumann P, Keller TS, Ekstrom L, Hansson TH. Effect of strain rate and bone mineral on the structural properties of the human anterior longitudinal ligament. Spine. 1994;19:205 - 11.
157. Benzel EC. Biomechanically relevant anatomy and material properties of the spine and associated elements. Biomechanics of Spine Stabilization. 2001;Thieme Medical, Publisher:8-10.
158. Schendel MJ, Wood K, Butterman GR, Lewis JL, Ogilvie JW. Experimental measurement of ligament force, facet force, and segment motion in the human lumbar spine. J Biomechanics. 1993;26:427 - 38.
159. Jordan J, Konstantinou K, O'Dowd J. Herniated lumbar disc. Muscoloskeletal disorders. 2009;03:1-34.
160. Graf N. Entwicklung einer Messmethode für biomechanische In-vitro-Untersuchungen am humanen Brustkorb. Thesis of Institut für Unfallchirurgische Forschung und Biomechanik, Universitätsklinikum Ulm. 2009.
161. Kowalski RJ, Ferrara LA, Benzel EC. Biomechanics of the Spine. Neurosurg Q. 2005;15:42-59.
162. Bermel EA, Barocas VH, Ellingson AM. The role of the facet capsular ligament in providing spinal stability. Computer methods in biomechanics and biomedical engineering. 2018;21(13):712-21.

Acknowledgments

"If you can dream it, you can do it" (Walt Disney)

Questa è la frase che mi sono sempre ripetuta più volte: in occasioni diverse, in situazioni più o meno complicate della mia vita.

All'inizio di questo percorso di tre anni avevo un po' paura di non farcela, non sapevo se sarei stata in grado di proseguire o se a metà avrei lasciato perdere tutto. Quando alla parallela dovevo staccare le mani per fare il Tkatchev avevo un po' di timore, timore di staccare troppo presto e di finire sullo staggio, timore di staccare troppo tardi e di non prendere lo staggio cadendo a terra o sullo staggio inferiore, timore di cadere male o di sbattere i talloni sullo staggio. Però lo facevo lo stesso e portavo sempre in gara quell'elemento. Perché? Perché la voglia di riprendere lo staggio con le mani per poi finire l'esercizio era troppo forte, era troppo emozionante "volare" sopra lo staggio, era troppo emozionante dire "ce l'ho fatta di nuovo". Nulla avrebbe potuto fermarmi dallo smettere di fare quel salto alla parallela. E lo stesso vale per la vita, la felicità di raggiugere qualcosa deve essere sempre maggiore della paura di non farcela, la voglia di raggiungere i propri sogni deve sempre vincere sulle parole negative di certe persone che cercano di fermarti solamente perché loro non hanno nemmeno il coraggio di provarci.

E così dopo la laurea magistrale non avrei mai immaginato di trovarmi qui oggi a scrivere queste ultime righe della tesi di dottorato. Chi lo avrebbe mai detto? Io di certo no.

La vita è imprevedibile e chi pensa di sapere già tutto si sbaglia di grosso. La vita va vissuta giorno dopo giorno, ora dopo ora, minuto dopo minuto. Non sono le "grandi" scelte quelle che ti cambiano la vita, non sono i giorni con "appuntamenti importanti" a definire il tuo futuro. Sono le piccole cose a rendere unica una giornata, in pochi secondi si definisce quale strada si intraprenderà, in un attimo tutta la tua vita può cambiare in meglio o in peggio. Può accadere che un giorno tu ti svegli la mattina e dici "questa non è la mia vita". Arriva un giorno in cui apri gli occhi e tutto quello che non riuscivi a vedere prima te lo trovi lì davanti a te, chiaro e limpido come se fosse stato lì da sempre, ma fino al giorno prima neanche te lo immaginavi. Ed è così che all'improvviso la mia vita è cambiata, un piccolissimo dettaglio ha scaturito un universo di cambiamenti.

Sono successe tante cose in questi tre anni… Vorrei ringraziare tutte le persone che mi sono state vicine, che hanno affrontato con me certe situazioni difficili prendendomi per mano e accompagnandomi avanti in questa corsa infinita. Vorrei ringraziare quelle persone che ci sono state anche solo per poco tempo. Vorrei ringraziare i miei colleghi che mi hanno insegnato tanto e con cui siamo cresciuti insieme imparando a lavorare in un team. Vorrei ringraziare anche quelle persone che mi hanno voltato le spalle, che mi hanno trafitto più volte alle spalle pensando di essere furbe. Grazie perché mi avete reso più forte, grazie perché mi avete insegnato ad andare avanti e a non fermarmi alla prima delusione grossa.

Un grandissimo grazie va ai miei genitori. Un grazie che non finirò mai di dirlo perché so che potrò sempre contare su di loro, mi hanno sempre sostenuto e spronato a non arrendermi mai sia nei momenti felici ma ancora di più nei momenti difficili. Sono sempre stati accanto a me anche quando prendevo decisioni sbagliate. Perché si le persone devono sbagliare per imparare, devono sbatterci la

testa contro prima di accorgersi degli errori. Ma è proprio questo che fa crescere e fa evitare di fare altri sbagli.

Un grandissimo grazie va come sempre alla mia passione più grande: la ginnastica. La ginnastica che mi ha dato ma anche tolto tanto, che mi ha insegnato a non arrendermi mai, a credere in un obiettivo e a lottare fintanto che non si raggiunge. Non serve essere geni o talenti per raggiungere qualcosa, serve solo la caparbietà di non mollare e di dare tutto sé stessi per il sogno in cui si crede.

Queste ultime righe che sto scrivendo sono sicuramente le parole conclusive di un ulteriore traguardo della mia vita che ho raggiunto, ma a dire il vero preferisco vederle come le prime righe dell'introduzione di un nuovo capitolo di vita.

E infine voglio ringraziare una persona speciale che ha trasformato un giorno qualunque, di un mese qualunque, di un anno senza senso in un giorno da ricordare.